

Electrochemical Generation of Compounds Bearing a Transition Metal – Group (XIV) Element Bond

Part A: Synthesis and Calculations

Part B: Application as Coating Materials in Batteries

Thesis for obtaining the title of PhD

2010

The presented work was performed under supervision of Asst.-Prof. Christa Grogger and Prof. Frank Uhlig on the Institute of Inorganic Chemistry at the Graz University of Technology



Das Land
Steiermark

**To Rupert
and my grandparents**

Acknowledgement

I would like to thank a lot of people for their help in finishing this work. Therefore I would like to mention that the order, in which they are listed up says nothing about their importance.

The FrECheMaterie program shall be gratefully acknowledged for financial support.

At first I would like to thank Asst.-Prof. Christa Grogger for introducing me to this subject, which is really interesting and gave me insight in many different ways. Furthermore I am deeply grateful for the personal assistance and the help with all my problems no matter if they were personal or private. Thanks!

Prof. Frank Uhlig I would like to thank for the supervision and the possibility to work on this institute.

A special gratitude appertains to Prof. Michaela Flock for help with the calculations, and especially for her patience with me during the last three years. I want to say thank you particularly for the help during the writing of this thesis and for always supporting me when I had either personal or scientific problems. I am really thankful for that.

For the performance of my X-Ray analysis I would like to thank Ao. Prof. Albering and Asst. Prof. Roland Fischer. I am grateful for the time and patience you spent on my structures. Furthermore I would like to especially thank Roland, that he always had time for me and my concerns.

For believing in me and the great opportunity to come to Argonne, I would like to say thanks to PhD Carmen Lopez. Thank you for all the help I obtained from you concerning the field of impedance measurements and the correction of my PhD thesis.

I would like to thank the Argonne National Lab for all the materials they provided for me and the chance to work in the Chemical Science and Engineering Division.

Especially grateful I am for the nice co-workers I had on the Institute for Inorganic Chemistry and the Argonne National Lab.

For the performance of the UV measurements, I would like to thank my student Rita Ambach.

For the financial support and especially for all the help, encouragement and the believing in me I would like to say thank you to my parents. Without you this work would have never been possible. I love you, thank you for everything you did for me.

For all the support, strength and help I obtained from my siblings and grand parents I really want to say thank you too.

I also would like to thank my best friends Birgit, Harald und Regina, who were always there for me, no matter what I needed or when.

Last but not least. Some words of appreciation and gratitude for my boyfriend Rupert. I can not express how important you are for me. You were there for me when I wanted to give up everything, gave me strength and helped me to cope with all the problems I had. I hope you know, how much you mean to me. I love you.

Thank you all!

Abstract

The reaction between iron and ruthenium with chloro compounds of group XIV-elements was investigated. The reaction was performed via electrochemistry and the obtained products were analyzed. The influence of the element (E = Si, Ge, Sn), the substituents on it, and the metal were investigated. The NMR and UV properties of these molecules were also calculated to give further insight in the character of the orbitals, transitions and so on. The experimentally obtained data was compared to the calculated results.

The synthesized compounds were used as coating materials for lithium anodes in coin cells. The influence of these products on the battery was investigated via Impedance measurements and experiments on the cycling behaviour of the cell.

Kurzfassung

Die Reaktion zwischen Ruthenium und Eisen mit verschiedenen Chlor-Verbindungen der Elemente der XIV-Gruppe wurde untersucht. Diese Umsetzung wurde mittels Elektrolyse durchgeführt und die erhaltenen Produkte wurden analysiert. Die Größe des Einflusses vom Metal, dem Element (E = Si, Ge, Sn) und deren Substituenten wurde untersucht.

Die NMR und UV Eigenschaften der Moleküle wurden berechnet um weiteren Einblick in den Charakter der Orbitale, die beteiligten Übergänge und weiteres zu erhalten. Die experimentellen Ergebnisse wurden mit den berechneten verglichen.

Die hergestellten Verbindungen wurden als Beschichtungsmaterialien für Lithiumanoden in Knopfzellen verwendet. Der Einfluß dieser Substanzen auf das Verhalten der Batterien wurde mittels Impedanzspektroskopie und Experimenten zur Zyklisierbarkeit der Zellen untersucht.

Index

Part A: Synthesis and Calculations

Purpose of this Study 1

A 1 Generation of compounds bearing a transition metal - group (XIV) element bond..... 4

A 1.1 Synthesis4
A 1.1.1 Oxidative addition of Si-H and Si-X bonds 4
A 1.1.2 Oxidative addition of other Si - compounds..... 5
A 1.1.3 Methods involving transition metal anions – salt elimination reaction 5
A 1.1.4 Inverted salt elimination method – methods with main group metal silyl compounds 6
A 1.1.5 Condensation reaction 7
A 1.1.6 Silylene transfer 7
A 1.1.7 Photochemical rearrangement reactions 7
A 1.1.8 Thermal rearrangement reactions 8
A 1.1.9 Electrochemical reactions 9

A 1.2 Photochemical stability of Fp-silanes11

A 1.3 Photochemical Stability of Rp-Silanes15

A 1.4 Electrochemical Behavior of Fp-group (XIV) Complexes15

A 2 Results and discussion 17

A 2.1 Mechanistic aspects19

A 2.1.1 Important factors 19
A 2.1.2 Conclusion 22
A 2.1.3 Stepwise reaction – Reaction with dichlorosilanes 22

A 2.2 Calculations24

A 2.2.1 NMR calculations..... 24

A 2.3 UV-experiments: Comparison between calculated and measured results25

A 2.3.1 Results 25
A 2.3.2 Discussion 38
A 2.3.2.1 Influence of the chain length 39
A 2.3.2.2 Influence of the main group element E (E = Si, Ge, Sn) 44
A 2.3.2.3 Influence of the metal 48
A 2.3.3 Molar extinction coefficients..... 51
A 2.3.4 Conclusion 52

A 2.4	X-Ray Structures	53
A 3 Experimental part.....		59
A 3.1	General working techniques	59
A 3.2	The undivided cell.....	63
A 3.2.1	Electrolyses performed in the divided cell	64
A 3.2.2	Work up procedure.....	64
A 3.3	Electrolyses with Fp_2 in the undivided cell.....	66
A 3.3.1	Electrolysis of pure Fp_2	66
A 3.3.2	Electrolyses of Fp_2 with mono chloro silanes	67
A 3.3.2.1	Formation of $FpSiMe_3$	67
A 3.3.2.2	Formation of $FpSiMe_2H$	68
A 3.3.2.3	Formation of $FpSiMe_2Ph$	69
A 3.3.2.4	Formation of $FpSiMePh_2$	70
A 3.3.2.5	Formation of $FpSiPh_3$	71
A 3.3.2.6	Formation of $FpSi_2Me_5$	72
A 3.3.2.7	Formation of $FpSi_6Me_{11}$	73
A 3.3.3	Electrolysis of Fp_2 with other group (XIV) elements	74
A 3.3.3.1	Electrolysis of Fp_2 with Ph_3CCl	74
A 3.3.3.2	Formation of $FpGePh_3$	75
A 3.3.3.3	Formation of $FpSnPh_3$	76
A 3.3.3.4	Electrolysis of Fp_2 with Me_3GeCl	77
A 3.3.3.5	Electrolysis of Fp_2 with Me_3PbCl	78
A 3.3.4	Electrolysis of Fp_2 with dichloro silanes	79
A 3.3.4.1	Electrolysis of Fp_2 with $ClSiMe_2-Ph-SiMe_2Cl$ (1:1).....	79
A 3.3.4.2	Electrolysis of Fp_2 with $ClSiMe_2-Ph-SiMe_2Cl$ (1:2) and subsequent electrolysis with Rp_2	80
A 3.3.4.3	Electrolysis of Fp_2 with Me_2SiCl_2	82
A 3.4	Electrolyses of Rp_2 in the undivided cell.....	83
A 3.4.1	Electrolysis of Rp_2 with Me_3SiCl	83
A 3.4.2	Electrolysis of $Co(CO)_3PPh_3$ with trimethyl chloro silanes in the undivided cell.....	84
A 3.5	Electrolyses in the divided cell.....	85
A 3.6	Calculations	88
A 3.6.1	Introduction	88
A 3.6.2	Experimental Part.....	89
B 1 Coating of lithium electrodes: Introduction and Motivation.....		92
B 2 Experimental part.....		95
B 3 Results and Discussion		97
B 3.1	Cycling behavior	98

B 4 Impedance measurements.....	101
B 4.1 Definition:.....	101
B 4.2 Application.....	106
B 4.2.1 Influence of the different coating compounds.....	108
B 4.2.2 Dependency on dipping time.....	110
B 4.2.3 Dependency on Ageing Time.....	111
B 4.3 Conclusion.....	115

Part C: Appendix (on CD-ROM)

C 1 X-Ray data

C 2 UV-calculations

C 3 Impedance and cycling data

Purpose of this Study

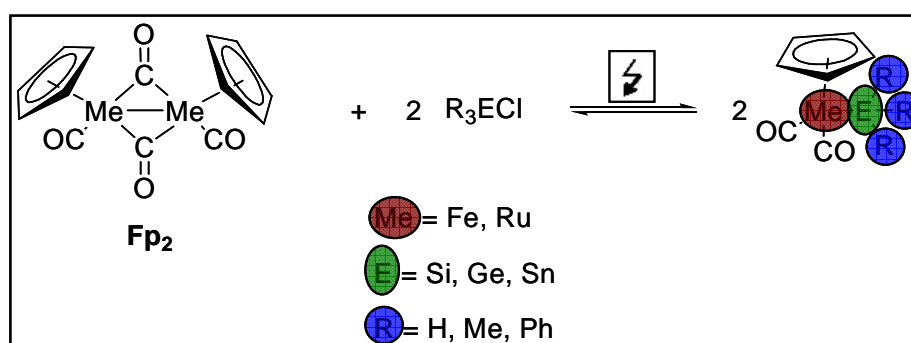
In the last few years, electrolysis has become an important method for synthesizing new and different compounds, with a special emphasis on the generation of C-C, Si-Si, Si-C and Si-Ge bonds.

The development of this area started with the work of Prof. E. Hengge, whose ideas were basis for several dissertations at the Institute of Inorganic Chemistry of the Graz University of Technology,¹ and who devised new methods to generate Si-Si and Si-C bonds via electrolyses.

A number of other working groups, especially Jouikov *et al.*, were or are still performing research in the field of main group electrochemistry.² In addition to working in the field of Si-C³ and Si-Si compounds he extended this work to the generation of Si-Se⁴ bonds and germatranes⁵ and e.g. an approach to the generation of silanones. Of course this list is not complete, a full review of the work done on C-C bond formation can be seen in the PhD thesis of Loidl, B. TU Graz, 2004.

Besides bond generating electrolysis, methods were also developed to functionalize species. Examples include the generation of Si-O-Si bonds⁶ and the appearance of the so called silanones intermediates.⁷

Previous work on the electrochemical generation of Fp-silanes was performed by H. Fallmann.⁸ Based on this work the aim of this PhD thesis was to synthesize and characterize different compounds containing metal-group (XIV) element bonds. The basis reaction for that is:



Scheme 1: General reaction scheme for the formation of the titel compounds

The electrochemical method utilized has one big advantage for generating these types of compounds compared to other synthetic ways: the electrolysis is a one pot reaction and total conversion of the starting materials to the products can be obtained. It was also an important aim to show that the products can not only be synthesized but also isolated and analyzed via single crystal analyses.

¹ See e.g.: Litscher, G. PhD thesis, TU Graz **1977**; Firgo, H PhD thesis TU Graz, **1980**, Kalchauer, W. PhD thesis, TU Graz, **1986**, Grogger, Ch. PhD thesis, TU Graz, **1994**; Stefan, J. PhD thesis, TU Graz, **2007**

² Jouikov, V.; Krasnov, V. *J. Organomet. Chem.* **1995**, 498, 231-219; Jouikov, V.; Grigorieva, L. *Electrochim. Acta* **1996**, 41, 469; Jouikov, V.; Salaheev, G. *Electrochim. Acta* **1996**, 41, 2623

³ Jouikov, V. *ECS Transactions* **2008**, 15, 1, 317-324.

⁴ Jouikov, V. V.; Fattakhova D. S. *J Electrochim. (Grenoble)* **1993**, CA 6.36

⁵ Soualmi, S.; Ignatovich, L.; Lukevics, E.; Ourari, A.; Jouikov, V. *ECS Transactions* **2008**, 13, 24, 63-69

⁶ Voronkov, M. G.; Zosimo-Landolfo, G. *J. Organomet. Chem.* **1998**, 557, 1, 143-155

⁷ Jouikov, V. V. *Current Topics Electrochem.* **2008**, 13, 1-19

⁸ Fallmann, H. PhD-thesis, TU Graz **2001**

Part A: Synthesis and Calculations

Another objective was also to characterize the different compounds via UV spectroscopy to get an insight into the orbitals involved in the transitions.

A second part of the work outlines the application of the generated compounds as coatings on metallic lithium anodes in batteries. Lithium is a great material for electrodes because of its specific properties, like the energy density, great specific capacity and the possibility to use charged or uncharged positive electrode materials.⁹

Nevertheless there are also problems concerning lithium as an electrode material. These are especially safety issues and cycling efficiency during long operation. It is thought that these problems are due to the changes of the lithium surface chemistry and the morphology. These changes result in the observation of so called dendritic growth of lithium on the surface. It is caused by the repeated dissolution and re-plating of lithium on the surface. A general belief is that these dendrites are the reason for the instability of lithium and the cause of lithium anode safety issues because of the high reactivity due to their high surface areas.¹⁰

One way to avoid those problems with lithium as electrode material without the loss of the specific properties of the metal is to functionalize the surface of the electrode with organometallic or inorganic materials like e.g. conductive ceramics made of lithium phosphorus oxynitride¹¹. The materials we used therefore are the compounds obtained from the electrolysis, which were studied previously. By the reaction of these materials with the nucleophilic surface of metallic lithium a functionalization of the surface should be obtained, which increases the cycling stability of the batteries (which means that more cycles can be performed before the battery fails).

⁹ Vincent, C. A. *Solid State Ionics* **2000**, 134, 159; Tarascon, J. M.; Armand, ; *Nature (London)* **2001**, 414, 359; Crowther O. West, A. C. *J. Electrochem. Soc.* **2008**, 155, A806;

¹⁰ Tatsuma, T.; Taguchi, M.; Iwaku, M.; Sotomura, T.; Oyama, N. *J. Electroanal. Chem.* **1999**, 472, 142; Brissot, C.; Rosso, M.; Chazalviel, J.-N.; Lascaud, S. *J. Electrochem. Soc.* **1999**, 146, 4393; Aurbach, D.; Zinigrad, E.; Teller, H.; Dan, P. *J. Electrochem. Soc.* **2000**, 147, 1274

¹¹ United states patent, Bates, J. B.; No. 5,314,765 **1994**

Part A: Electrochemical synthesis of compounds containing a transition metal – group (XIV) element bond

A 1 Generation of compounds bearing a transition metal - group (XIV) element bond

The first compound with an iron silicon bond was FpSiMe_3 and it was prepared by Wilkinson *et al.* in 1956 as an orange compound.¹² With this discovery from 1965 on the field of electron rich, low valent metal-silicon complexes started to grow fast.

There are similar properties of transition-metal silicon compounds to their analogous alkyl derivatives but also some significant differences like the habit that many late transition metal silicon bonds are inert against insertion reactions.¹³ This goes hand in hand with the fact that metal-silicon bonds are often shorter than their, based on the covalent radii, calculated bond. That is due to the fact that there is π -back bonding between the two atoms. Conversely, it has also been seen that silicon-transition metal complexes undergo preferable addition/elimination reactions.

A 1.1 Synthesis

A 1.1.1 Oxidative addition of Si-H and Si-X bonds

Low valent, electron rich complexes with empty coordination sites are the starting materials for these kinds of reactions¹⁴. The general scheme follows (L = ligand, M = metal, X = halogen, R = organic fragment e.g. methyl, phenyl...):



In general Si-H bonds are more reactive versus oxidative addition than Si-X bonds.

This type of reaction is often accompanied by the loss of a small molecule like H_2 or HCl .¹⁵

Si-H bonds can also react with dinuclear metal complexes, e.g., trichlorosilane, to undergo reactions with Fp_2 to give four distinct products. Concerning this reaction, it is not quite clear if the mechanism can be considered as an oxidative addition or just as a metal-metal bond cleavage.¹⁶

¹² Piper, T. S.; Lemal, D.; Wilkinson, G.: *Naturwissenschaften*, **1956**, 43,129

¹³ Tilley, T.D.: *The silicon heteroatom bond*, **1991**, Wiley & Sons, chapter 9, page246-252

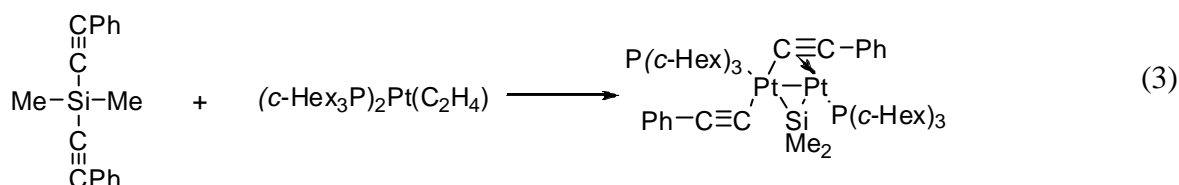
¹⁴ Bentham, J. E.; Craddock, S.; Ebsworth, E. A. V.; *J. Chem. Soc. A* **1971**, 587

¹⁵ Archer, N. J.; Haszeldine, R. N.; Parish, R. V.; *J. Chem. Soc., Chem. Commun.* **1971**, 524; Straus, D. A.; Tilley, T. D., Rheingold, A. L.; Geib, S. J.; *J Am. Chem. Soc.*, **1987**, 109 5872

¹⁶ Jetz, W.; Graham, W. A. G.; *Inorg. Chem.*, **1971**, 10, 1159

A 1.1.2 Oxidative addition of other Si - compounds

Si-C or Si-Si bonds can also be oxidatively added to metal complexes. Although this reaction type is not really of big synthetic use it is rather important for certain transition metal catalyzed reactions.¹⁷ As an example the following reaction is:



The reaction takes place under Si-C bond cleavage and loss of ligated ethylene.¹⁸

A 1.1.3 Methods involving transition metal anions – salt elimination reaction

This type of reaction is one of the most synthetically useful ones. With this method the first compound bearing a Fe-Si bond, FpSiMe_3 , was obtained.¹⁹

The general scheme for this reaction type is (M = metal, X = halogen, R = organic fragment e.g. methyl, phenyl):



In general, the reaction is dependant on the steric and electronic properties of the leaving group on the silicon atom. Organohalosilanes react not as easily as hydridohalosilanes, and triflates and iodides are better leaving groups than the chloride. The problem relating to iodide and bromide is that the possibility of transmetalation reactions is slightly higher.²⁰

Another important factor influencing the reaction is the nature of the solvent. Polar media like e.g. THF provide the possibility, that the nucleophilic attack of the carbonyl oxygen atom on the silicon atom is a likely reaction. As a result Si-O bonded compounds are obtained like e.g. disiloxanes of the

¹⁷ Curtis, M. D.; Epstein, P.S.; *Adv. Organomet. Chem.*, **1981**, 19, 213

¹⁸ Ciriano, M.; Howard, J. A. K.; Spencer J. L. Stone, F. G. A. Wade, H. J. *Chem. Soc. Dalton Trans.*, **1979**, 1749

¹⁹ Piper, T. S.; Lemal, D.; Wilkinson, G. *Naturwissenschaften*, **1956**, 43, 129

²⁰ Aylett, B. J.; Campbell, G. M. *J. Chem. Soc. A*. **1969**, 1910

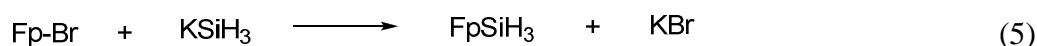
type $O(SiR_3)_2$.²¹ Another problem occurs with cyclic ethers, because they can take part in ring opening reactions initiated by the metal-silicon bond.²²

When using acyclic alkanes, other problems occur. The low solubility of transition metal complexes in alkanes leads to the formation of heterogenous mixtures, which causes longer reaction times.²³

The nucleophilicity of the metalate is also important for a successful reaction. It depends not only on the metal itself but also on the substituents on the metal ($[Co(CO)_4]^- < [Mn(CO)_5]^- < [Mo(CO)_3Cp]^- < [Re(CO)_5]^- < [FeCp(CO)_2]^- < [Fe(CO)_4]^{2-}$ ²⁴). This can be illustrated by the example of substituting one CO-ligand at the metal atom by a PPh_3 group. By that the nucleophilicity is increased and the reaction is processing faster.²⁵ The cause for this behavior lies in the weak π -donating character of the PPh_3 group. The electron density increases on the metal atom because it can not be redistributed to the phosphane ligand.

A 1.1.4 Inverted salt elimination method – methods with main group metal silyl compounds

This reaction type is not extensively used for Fp-Si compounds because it is rather difficult to obtain not only Fp-Br but also unbranched, linear silyl anions.²⁶



On the contrary, for early transition metals, which do not form stable anions, the inverse salt elimination works better than the regular one.²⁷

This reaction works well when using mercury compounds as silylating agents:²⁸



²¹ Curtis, M. D. *Inorg. Chem.*, **1972** 11, 802; Malisch, W. *J. Organomet. Chem.*, **1972**, 38, C28; Jetz, W.; Graham, W. A. G. *J. Organomet. Chem.*, **1974**, 69, 383; Nicholson, B. K.; Simpson, J. *J. Organomet. Chem.*, **1978**, 155, 237

²² Brinkman, K. C.; Gladysz, J. A. *Organometallics*, **1984**, 3, 147

²³ Malisch, W.; Kuhn, M. *Chem. Ber.* **1974**, 107, 979

²⁴ King, R. B. *Acc. Chem. Res.*, **1970**, 3, 417

²⁵ Curtis, M. D. *Inorg. Chem.* **1972**, 11, 802

²⁶ Hamon, J.-R.; Astruc, D.; Michaud, P.; *J. Am. Chem. Soc.* **1981**, 103, 758

²⁷ Kayser, C.; Marschner, C.; *Monatshefte Chem.* **1999**, 130, 203

²⁸ Glockling, F.; Hooton, K. A.; *J. Chem. Soc. A* **1947**, 1066; Seyferth, D.; Cross, R. J.; Prokai, B., *J. Organomet. Chem.* **1967**, 7, P20; Lee, A. G. *J. Organomet. Chem.* **1969**, 16, 321

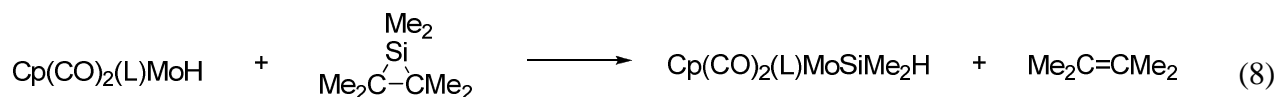
A 1.1.5 Condensation reaction

This method is very rarely used, but it works e.g. for an acidic transition molybdenum hydride under elimination of an amine:²⁹



A 1.1.6 Silylene transfer

Hexamethylsilacyclopropane reacts with a transition metal-hydride (L = CO, PMe₃) via a radical mechanism to the corresponding products.³⁰



It seems that the ring is opened by an radical of Cp(CO)₂(L)Mo·. This leads to the formation of a Cp(CO)₂(L)MoSiMe₂CMe₂CMe₂· radical, from which an alkene is eliminated. The silyl radical obtained abstracts protons from the starting transition metal complex to yield the corresponding product.

A 1.1.7 Photochemical rearrangement reactions

In 1974 Pannell and Rice showed that through photochemical rearrangement reactions, Fe-Si bonds can be obtained:³¹



The same reaction can also be performed with PPh₃ instead of CO-ligands attached to the iron. Another remarkable property of the starting compound is its thermodynamical stability. If the Cp-ligand is changed to an indenyl-ligand no enhancement in stability is observed.. However a reaction to the same product can be observed as under photochemical treatment.³²

²⁹ Cardin, D. J.; Keppie, S. A.; Lappert, M. F. *J. Chem. Soc. A.* **1970**, 2594

³⁰ Berry, D. H.; Mitstifer, J. H. *J. Am. Chem. Soc.* **1987**, 109,3777

³¹ Pannell, K. H.; Rice, J. R. *J. Organomet Chem.* **1974** 78, C35

Both reactions occur under elimination of a carbonyl ligand and a silene transition state. After that a rearrangement reaction takes place. Therefore, the existence of a Si-Si bond in the molecule is important.

A 1.1.8 Thermal rearrangement reactions

Sun et al. reported the following reaction in 1993. It is a thermal rearrangement reaction taking place under reflux. During 24 h the whole amount of the starting material is converted into the following product:³³



Figure 1: Scheme of the metathesis reaction

This is a metathesis reaction between the Fe-Fe and the Si-Si bond. Normally those bonds do not react with each other if they are in separated molecules (intermolecular), but here an intramolecular reaction between the iron and silicon atoms takes place.

The same process also takes place, if a hydrated Indenyl-ligand (IndH₄) is used instead of the Cp-ligand.³⁴

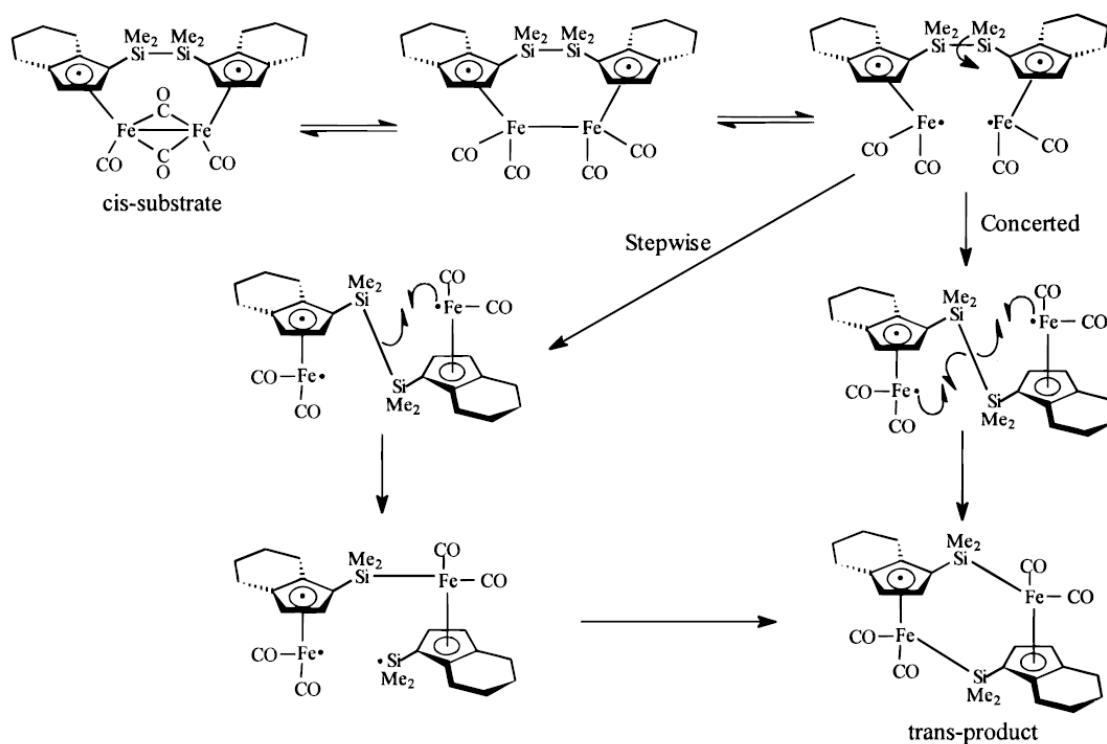
Concerning the mechanism, the reaction starts with a pair wise opening of the CO-bridges. This is followed by the thermal homolysis of the Fe-Fe bond and leads to the presence of two Fe radicals. The next step is a rotation through the Si-Si bond. It is not yet sure if this rearrangement reaction occurs stepwise or concerted, but this step is responsible for the stereoselectivity of the reaction. The driving force for the reaction is the conformation change between the starting material and the product. The starting material has twist conformation and is unsymmetrical whereas the product has a less tensed chair conformation and is symmetrical.

³² Pannell, K. H.; Kobayashi, T.; Kapoor, R. N. *Organomet.* **1992**, 11, 2229

³³ Sun, H.; Xu, S.; Zhou, H. *J Organomet. Chem.* **1993**, 444, C41

³⁴ Wang, B.; Zhang, Y.; Xu, S.; Zhou, X. *Organomet.* **1997**, 16, 4620

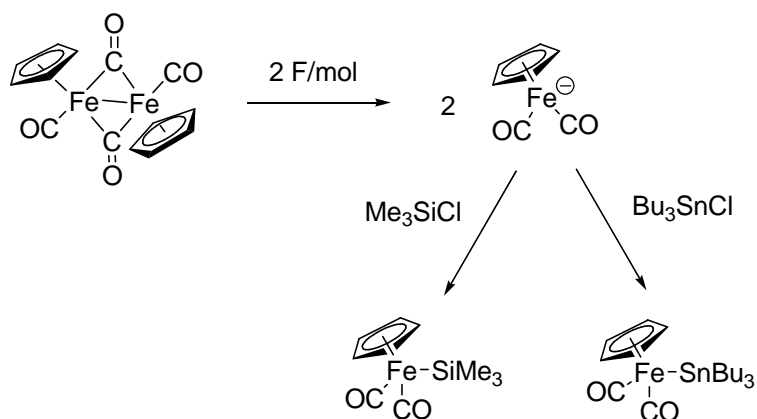
Part A: Synthesis and Calculations



Scheme 2: Reaction mechanism of the thermal rearrangement reaction

A 1.1.9 Electrochemical reactions

Ruiz et al. were the first to report Fp-Si and Fp-Sn bonds via an electrochemical reaction. They reacted Fp_2 under electrolysis conditions with Me_3SiCl and Me_3SnCl and obtained the corresponding products.³⁵ They postulated an anionic mechanism for this reaction: A direct two electron reduction of Fp_2 followed by a nucleophilic attack of the generated Fp^- on the chlorosilane or -stannane



Scheme 3: Reaction mechanism for the electrochemical conversion of Fp_2

³⁵ Ruiz, J.; Serein-Spirau, F.; Atkins, P.; Astruc, D. *C. R. Acad. Sci., Ser. IIb: Mec., Phys., Chim., Astron.* **1996**, 323, 851

Part A: Synthesis and Calculations

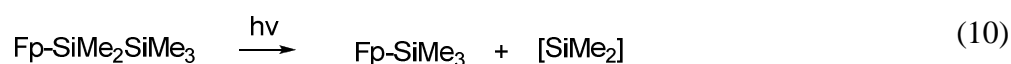
A 1.2 Photochemical stability of Fp-silanes³⁶

Monosilanes attached to iron or a transition metal do not show photochemical reactions, they are stable. But when a disilane or higher silane is attached to e.g. iron an activation of the silicon-silicon bond takes place and photochemical rearrangement reactions occur.

The first compound with a transition metal and a silicon-silicon bond was synthesized using a salt elimination procedure in 1969.³⁷ The chemistry of such compounds changes dramatically. There is an activation of the Si-Si bond, induced by the transition metal. Most of these compounds are stable against oxidation and thermal reactions, but they are very sensitive to photochemical degradation.

Two different reaction types occur under photochemical irradiation:³⁸

- Stepwise degradation of the silicon-silicon backbone under loss of silylene units.
- Isomerization reactions which follow or accompany the degradation process.



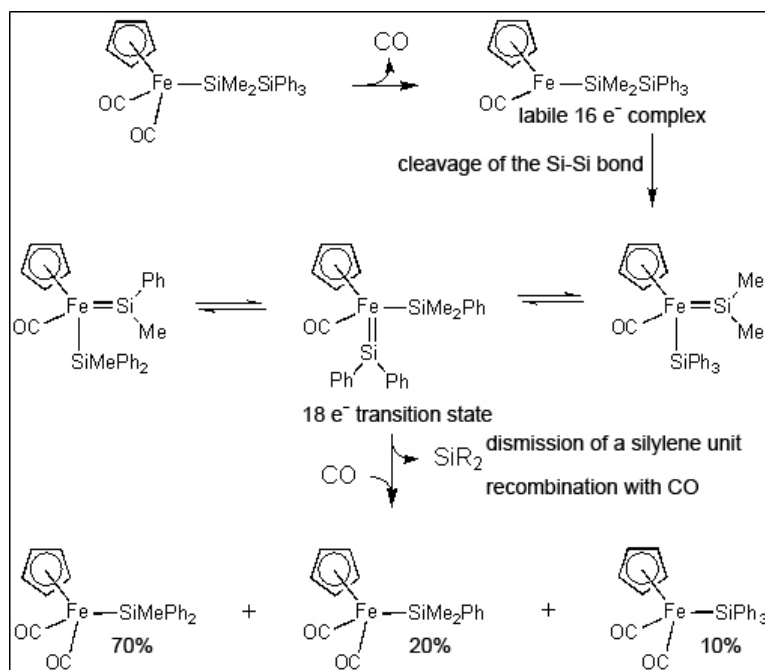
It seems that the reaction is independent of the type of substituents on the silicon atom. At least a mixture of methyl and phenyl rests $\text{FpSi}_2\text{Me}_n\text{Ph}_{5-n}$ always gives the same result: 20% FpSiMe_2Ph , 70% FpSiMePh_2 and 10% FpSiPh_3 .

The following mechanism was proposed for the photochemical degradation reaction:³⁹

³⁶ Sharma, H. K.; Pannell, K. H. *Chem. Rev.* **1995**, 95, 1351-1374

³⁷ King, R. B.; Pannell, K. H.; Bennett, C. R.; Ishag, M.; *J. Organomet. Chem.* **1969**, 19, 327

³⁸ Pannell, K. H., Rice, J. R. *J. Organomet. Chem.* **1974**, 78, C35; Pannell, K. H.; Cervantes, J.; Hernandez, C.; Cassias J.; Vincenti, S. *Organometallics* **1986**, 5, 1056; Pannell, K. H.; Rozell, J. M.; Hernandez, C. *J. Am. Chem. Soc.* **1989**, 111, 4482; Jones, K. L.; Pannell, K. H. *J. Am. Chem. Soc.* **1993**, 115, 11336; Hernandez, C.; Sharma, H. K.; Pannell K. H. *J. Organomet. Chem.* **1993**, 462, 259



Scheme 4: Reaction mechanism for the photochemical degradation

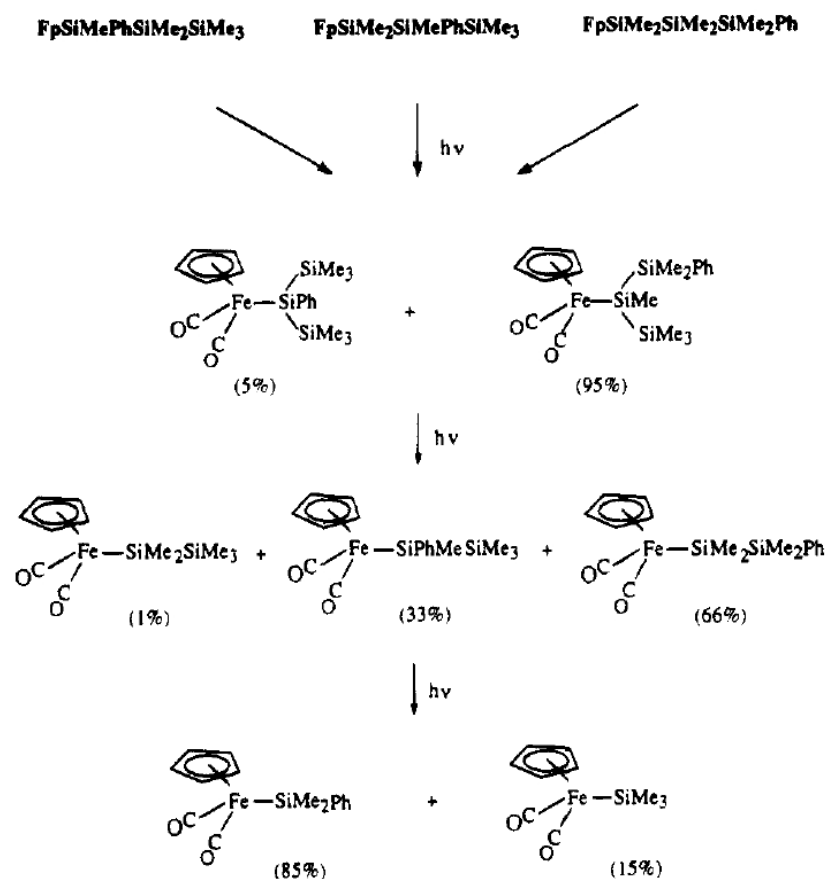
The reaction includes a starting step, in which a carbonyl group is eliminated. This leads to a labile 16 electron complex. Under cleavage of the silicon-silicon bond in this molecule an 18 electron transition state including a silylene bond is generated. At this step three structures are in equilibrium with each other by 1,3-alkyl and aryl migration. The equilibration is fast. From this transition state a silylene unit is dismissed and a carbonyl group is re-coordinated.

Performing the experiment with other aryl groups like $\text{Fp-Si}_2\text{Me}_4\text{Ar}$ ($\text{Ar} = \text{C}_6\text{H}_4\text{X}$, $\text{X} = \text{H}$, $m\text{-CF}_3$, $o\text{-Me}$, $p\text{-Me}$, $p\text{-NMe}_2$) suggests that electron donating groups stabilize the transition state $\text{CpFe(CO)}_2\text{(=SiMeAr)(SiMe}_3\text{)}$ ⁴⁰. This can be seen from the product distribution. The stabilization of this transition state and not $\text{Fp(=SiMe}_2\text{)(SiMe}_2\text{Ar)}$, suggests that the bond between iron and silicon in the silylene transition state is highly polarized like: $\text{Fe}=\text{Si} \leftrightarrow \text{Fe}^--\text{Si}^+$ ⁴¹.

Iron trisilyl complexes $\text{FpSi}_3\text{Me}_6\text{R}$ are also photochemically unstable. Linear starting materials react under isomerization and subsequent silylene loss.

⁴⁰ Jones, K. L.; Pannell, K. H. *J. Am. Chem. Soc.* 1993, 115, 11336;

⁴¹ Ueno, K.; Tobita, H.; Shimoi, M.; Ogino, H. *J. Am. Chem. Soc.* 1988, 110, 4092; Tobita, H.; Ueno, K.; Shimoi, M.; Ogino, H. *J. Am. Chem. Soc.* 1990, 112, 3415

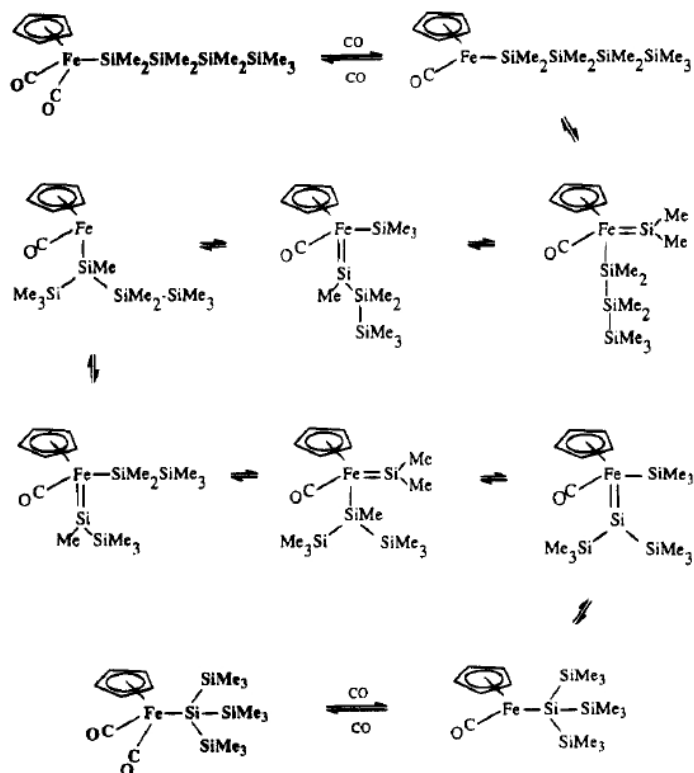
Scheme 5: Photochemical reaction for linear Fp-trisilanes⁴²

Tetra-, penta- and hexasilanes attached to an Fp-group show different photochemical behavior. They preferably isomerize under methyl and silyl migration to the more stable isomer. The deoligomerisation of the silicon backbone is not very likely for these molecules. But during isomerization intermediate states can occur in which silyl compounds are in equilibrium.⁴³

⁴² Hernandez, C.; Sharma, H. K.; Pannell, K. H. *J. Organomet. Chem.* **1993**, 462, 259

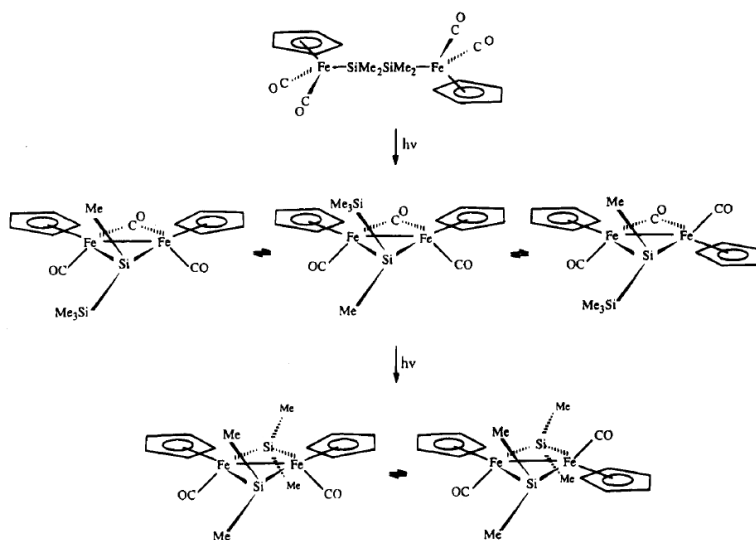
⁴³ Ueno, K.; Tobita, H.; Ogino, H. *Chem. Lett.* **1990**, 369

Part A: Synthesis and Calculations



Scheme 6: Mechanistic aspects to the photochemical degradation of Fp-tetrasilanes

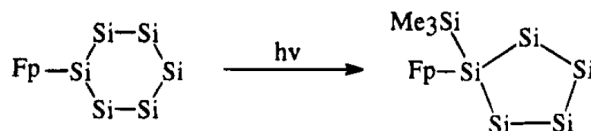
Bimetallic complexes have also been shown to undergo photochemical conversions, e.g. the Fp-(SiMe₂)₂-Fp compound shows transition states with silylene intermediates. The reaction results in a mixture of *cis* and *trans* products.⁴⁴



Scheme 7: Photochemical reaction for the Fp-(SiMe₂)₂-Fp compound

⁴⁴ Pannell, K. H.; Sharma, H. *Organometallics* **1991**, 10, 954; Ueno, K.; Hamashima, N.; Ogino, H. *Organometallics* **1991**, 10, 959; Ueno, K.; Hamashima, N.; Ogino, H. *Organometallics* **1992**, 11, 1435

Cyclic silane compounds attached to cyclopentadienyl iron dicarbonyl (Fp) groups also undergo photochemical reactions. For example if a permethylated six membered silicon ring is attached to the Fp group, the following reaction takes place under photochemical treatment:⁴⁵



Scheme 8: Photochemical reaction of the Fp-permethylated silicon six membered ring Fp-cycloSi₆Me₁₁

Notably this reaction proceeds without silylene elimination. This is different from the photochemical reaction of the unsubstituted permethylated cyclohexasilane which reacts under loss of silylene units first to the five and then to the four-membered ring.⁴⁶

A 1.3 Photochemical Stability of Rp-Silanes

In contrast to Fp-silanes the corresponding ruthenium compounds are stable against photochemical treatment. They do not show isomerization or degradation processes. For instance, RpSi_nMe_{2n+1} is thermally and photochemically stable under these conditions. This may be due to the low quantum yield in the starting ejection process of carbon monoxide. When this first step does not occur all following reactions can not take place, because the 16 e⁻ transition state is not generated. This implies that the photochemistry occurring at the Fp-silanes is not really photochemistry of the Si-Si bond.⁴⁷ This can also be shown when the disilane rest is attached to the Cp-ring and not directly to the iron atom. Then also no photochemical reaction occurs.⁴⁸

A 1.4 Electrochemical Behavior of Fp-group (XIV) Complexes⁴⁹

Analyzing the reduction potentials of FpSiR₃ with R = Me₃, MePh₂, Ph₃ it can be shown that the influence of the substituent is not significant. All three compounds show a reversible, single electron wave, while the carbonyl group attached to the iron has more influence. If this one is replaced either by PPh₃ or AsPh₃ the electrochemical reduction behavior changes a lot.

For the germanium compounds FpGeR₃ with R = Ph₃, Et₃ a similar behavior can be observed. All the compounds show a reduction wave at around -2V (vs. SCE). The same is given for FpSnPh₃. The

⁴⁵ Pannell, K. H.; Wang, L.-J.; Rozell, J. M. *Organometallics* **1989**, 8, 550

⁴⁶ Ishikawa, M.; Kumada, M. J.; *Chem. Soc. Chem. Commun.* **1970**, 712; Ishikawa, M.; Kumada, M. *J. Organomet. Chem.* **1972**, 42, 325

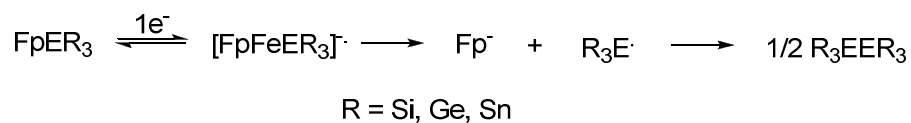
⁴⁷ Pannell, K. H.; Rozell, J. M.; Tsai, W.-M. *Organometallics* **1987**, 6, 2085

⁴⁸ Pannell, K. H.; Cervantes, J.; Parkanyi, L.; Cervantes-Lee, F. *Organometallics* **1992**, 11, 3139

⁴⁹ Combes, C.; Corriu, R. J. P.; Dabosi, G.; Henner, B. J. L.; Martineau, M. *J. Organomet. Chem.* **1984**, 141-150

Part A: Synthesis and Calculations

fact that just one reduction potential can be seen indicates that all those compounds undergo the same reduction mechanism:



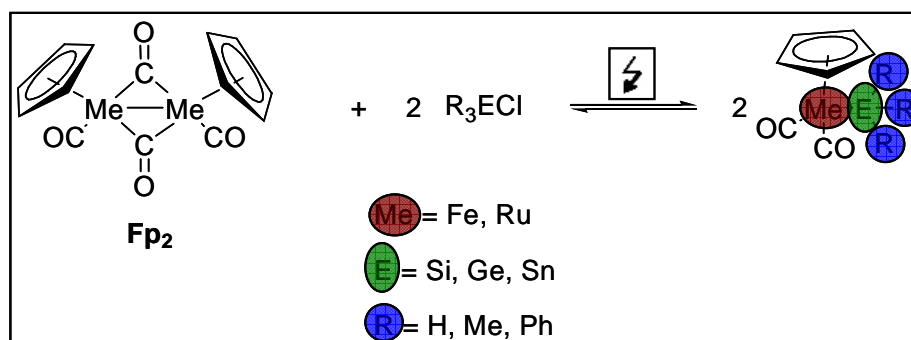
Scheme 9: Reaction mechanism for the electrochemical behavior of Si-, Ge- and Sn - compounds

During the electrochemical reduction the bond between Fe-E is broken and the Fp^- anion is generated. Another fact is that the reduction is slightly easier for the tin compounds and takes place in the following order: $\text{Sn} > \text{Ge} > \text{Si}$

If there is an additional bond to a chlorine atom, e.g. Sn-Cl , in the molecule this bond is easier to reduce than the Fe-Sn one. The obtained radical dimerises to generate a distannane.

A 2 Results and discussion

Based on the results Fallmann obtained in his PhD thesis, the following reaction was performed electrochemically using a divided cell, with a magnesium sacrificial anode and a surrounding stainless steel cathode. As electrolyte a 0.2 M solution of Bu_4NBr in THF was used.



Scheme 10: Reaction performed electrochemically

In the beginning of the electrolysis, the voltage level was watched for the first ten minutes. Afterwards every thirty min the progress of the electrolysis was monitored via ^{29}Si -NMR or IR. Especially IR spectroscopy is a very useful method because the diminishing of the corresponding band belonging to the bridging CO ligands at 1784 cm^{-1} of the Fp_2 starting material can be followed easily (see figure 2).

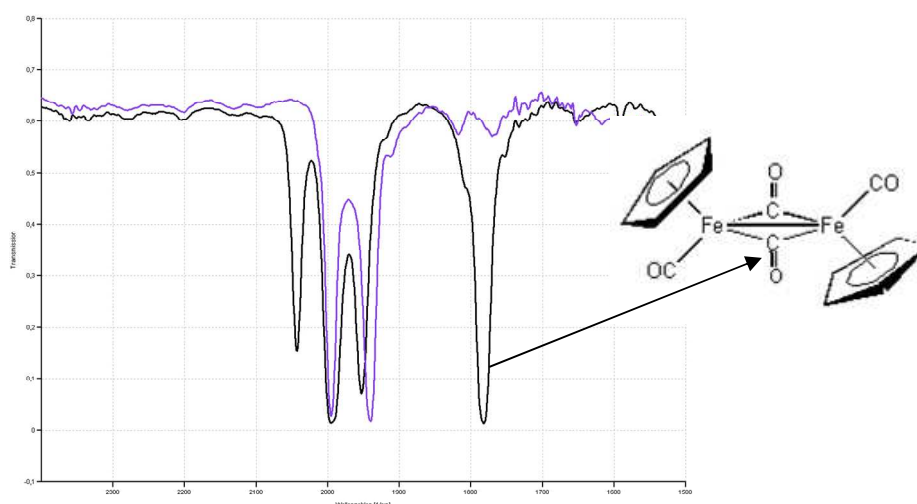


Figure 2: Diminishing of the IR band for the bridging CO ligands during electrolysis (black line: starting solution, violet line: solution after electrolysis)

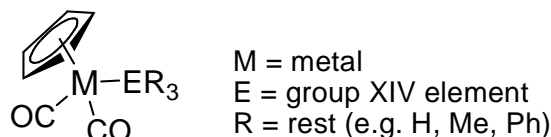
During the synthesis different observations were made which give further information concerning the reaction mechanism. First of all, the reaction does not proceed without application of an ultrasonic bath. Otherwise no product formation takes place. Secondly the reaction is dependent on magnesium

Part A: Synthesis and Calculations

as an electrode material. And last but not least the necessary time is shorter than calculated. This effect is dependent on the substituent on the silicon moiety.

The reaction is also an equilibrium reaction and Fp_2 is always built back until the product is available with no impurities. Only in very pure form the product is stable in solution.

The following products could be isolated using column chromatography and following a multiple step work up procedure:



Scheme 11: General product scheme

Table 1: Synthesized products

Product	Number	X-Ray
FpSiMe_2H (Cyclopentadienyl iron dicarbonyl dimethyl silane)	1	y
FpSiMe_3 (Cyclopentadienyl iron dicarbonyl trimethyl silane)	2	y
FpSiMe_2Ph (Cyclopentadienyl iron dicarbonyl dimethyl phenyl silane)	3	y
FpSiMePh_2 (Cyclopentadienyl iron dicarbonyl methyl diphenyl silane)	4	y
FpSiPh_3 (Cyclopentadienyl iron dicarbonyl triphenyl silane)	5	y
FpGePh_3 (Cyclopentadienyl iron dicarbonyl triphenyl germane)	6	y
FpSnPh_3 (Cyclopentadienyl iron dicarbonyl triphenyl stannane)	7	y
RpSiMe_3 (Cyclopentadienyl ruthenium dicarbonyl trimethyl silane)	8	y
FpSi_2Me_5 (Cyclopentadienyl iron dicarbonyl pentamethyl disilane)	9	y
$\text{FpSi}_6\text{Me}_{11}$ (Cyclopentadienyl iron dicarbonyl undecamethyl cyclopentasilane)	10	y
$\text{Fp}-(\text{SiMe}_2)_2\text{-Fp}$ ((dimethylsilyl)- cyclopentadienyl iron dicarbonyl) dimer)	11	y
$\text{Fp-SiMe}_2\text{-Ph-SiMe}_2\text{-Fp}$ 1,4- (cyclopentadienyl iron dicarbonyl dimethylsilyl) benzene	12	n
$\text{Fp-SiMe}_2\text{-Ph-SiMe}_2\text{-Rp}$ 1-(cyclopentadienyl iron dicarbonyl dimethylsilyl), 4-(cyclopentadienyl ruthenium dicarbonyl dimethylsilyl) benzene	13	n

The compounds **1** and **2** could just be crystallized by the use of an OHCD laser, because they are liquid at room temperature.

Two of the isolated products (**6** and **7**) are not really air sensitive and could be crystallized without using inert atmosphere.

All products are yellowish or orange.

To get further information on the reaction mechanism the reaction of Fp_2 with Me_3SiCl was also performed in a divided cell.

A 2.1 Mechanistic aspects

Ruiz *et al.* were the first ones to generate iron-silicon bonds electrochemically (foot note 35). They proposed that the reaction proceeds via a direct two electron reduction of Fp_2 to Fp^- followed by a nucleophilic attack on the chlorosilane. They performed the experiments just on NMR scale. After scaling up the synthesis and isolating the corresponding products, we observed different things that show that another mechanism is needed to explain the observations.

A 2.1.1 Important factors

1. Reaction time

The reaction proceeds electro catalytically. This means less time is necessary than theoretically calculated. The percentage of time needed varies a lot and it seems that it is dependent on the substituents on the silicon atom, but no general trend can be observed. The reaction times are shown in the following table:

Table 2: Reaction time in percentage of the theoretically needed time

Compound	Time [%]
Me_3SiCl	14.7
Me_2HSiCl	18.7
Me_2PhSiCl	5.7
MePh_2SiCl	16.3
Ph_3SiCl	85.4
$\text{Si}_6\text{Me}_{11}\text{Cl}$	93.3
Ph_3GeCl	3.0
Ph_3SnCl	25.9
$\text{ClSiMe}_2\text{-Ph-SiMe}_2\text{Cl}$	72.7
Me_2SiCl_2	66.5

Regarding the silyl compounds, it can be suggested that bigger substituents like three phenyl groups or the six membered permethylated ring influence the reaction time. This is not the case for the germanium- (**6**) and tin compound (**7**). So it seems that not only the substituents are important concerning the reaction time but also the element to which they are attached.

It is also remarkable that compound **6** was generated extremely fast and that the dichlorosilanes (corresponding to the products **11**, **12**, **13**) reacted slower than the others. But this is not really comparable because the theoretical needed time is calculated for the substitution of one Fp fragment and not two.

Comparing the Fp-SiMe₃ compound **2** to the Rp-SiMe₃ **8**, the ruthenium compound reacts much slower (50.52% of the theoretical needed time) than the iron one.

2. Reaction without electrolysis

Additional evidence for an electrocatalytic effect was seen when the reaction also took place with no applied current on. It was observed to proceed very slowly and need days.⁵⁰

3. Dependency on Mg as electrode material

The reaction was also found to be dependent on magnesium as electrode material. With other sacrificial anodes the reaction is a regular two electron reduction but with no electrochemical activation observed. The cathode material is not critical. It is e.g. possible to exchange the stainless steel with a second magnesium electrode without change of reaction time or product yield (see footnote 50).

4. Activation

It seems that some kind of activation of the electrolysis is necessary e.g. the use of the ultrasonic bath. Performing the syntheses just with a stirrer does not show the same effect than the ultrasonic bath. Maybe the reason for that is that the passivation layer on the magnesium has to be destroyed before the reaction can take place.

5. Divided Cell

The corresponding product could never be obtained by using the divided cell although different reaction conditions were chosen. Which parameters were varied can be seen from the following table (marked are the parameters varied):

Table 3: Parameters, which were changed in the performing of the electrolyses

Supporting salt solution	Anode	Cathode	Membrane	Compartments	Results
0.2 M Bu ₄ NBr in THF	Mg-rod	Stainless steel	MA 3475	Fp ₂ just in one compartment	No current flow in the cell
0.75 g Bu₄NBr und je 1.3 g LiCl und MgCl₂ in 80 mL THF	Mg-rod	Stainless steel	MA 3475	Fp ₂ just in one compartment	Low current flow, but no wanted product

⁵⁰ PhD thesis, Fallmann, H. 2001

Supporting salt solution	Anode	Cathode	Membrane	Compartments	Results
0.75 g Bu ₄ NBr und je 1.3 g LiCl und MgCl ₂ in 80 mL THF	Mg-rod	Stainless steel	MA 7000	Fp ₂ just in one compartment	Low current (8mA) flow, but no wanted product
0.75 g Bu ₄ NBr und je 1.3 g LiCl und MgCl ₂ in 80 mL THF	Mg-rod	Stainless steel	Glass frit	Fp ₂ just in one compartment	Low current) flow, but no wanted product
0.75 g Bu ₄ NBr und je 1.3 g LiCl und MgCl ₂ in 80 mL THF	Mg-rod	Stainless steel	MA 7000	Fp ₂ just in one compartment, excess of Me₃SiCl	Low current (15 mA) flow, but no wanted product
0.75 g Bu ₄ NBr und je 1.3 g LiCl und MgCl ₂ in 80 mL THF	Pt/H₂	silver	MA 7000	Fp ₂ just in one compartment,	Low current (5 mA) flow, but no wanted product
0.75 g Bu ₄ NBr und je 1.3 g LiCl und MgCl ₂ in 80 mL THF	Mg-rod	Stainless steel	MA 7000	Fp ₂ just in both compartment,	Low current (12 mA) flow, put no wanted product
0.6 g Bu ₄ NBr	Mg-rod	Stainless steel	MA 3475	Fp₂ just in one compartment and no chloro compound	The resistance was too high, no current flow.

6. Electrolysis of Fp₂

Several attempts were also made to study the reactivity of Fp₂ on its own without any chloro compound in the electrolysis cell. This reaction did not work, as it was observed that the current dropped and no electrolyses took place. We also attempted an activation of the electrode with the ultrasonic bath but it did not lead to the desired electrolysis. Intriguingly, as soon as a chloro compound (e.g. triphenyltin chloride) was added to the electrolysis solution the reaction started immediately.

7. Equilibrium reaction

The reaction is an equilibrium reaction. Until the product is not isolated in pure form, Fp₂ is always reformed. This means that the product is not stable in solution as long as impurities are available with which to react.

A 2.1.2 Conclusion

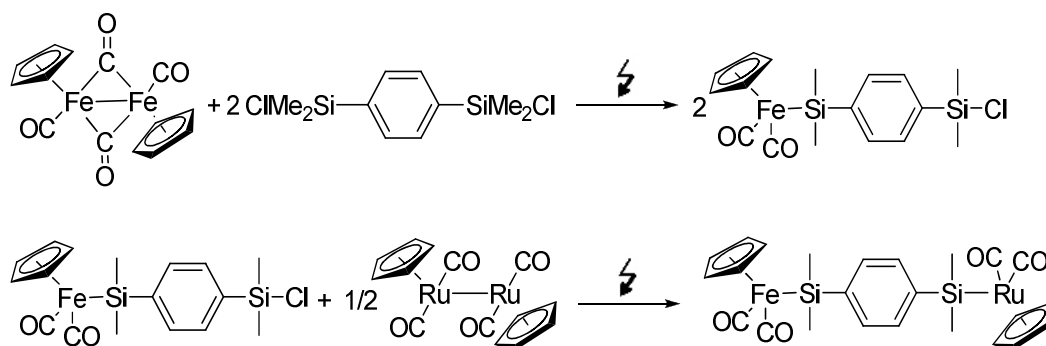
Several different observations have been made, including.

- that the electrolysis is depending on Mg as sacrificial anode,
- just works by the use of an ultra sonic bath,
- does not work in a divided cell and so on.

That suggest that the reaction does not proceed via a two electron reduction step followed by a nucleophilic attack on the chloro compound. but via Grignard like intermediates. Most likely, the applied current in combination with ultrasonic treatment acts as sort of activator for the formation of FpMgX salts. Although these were not isolated in this study, similar compounds have been published in literature.⁵¹

A 2.1.3 Stepwise reaction – Reaction with dichlorosilanes

In the following scheme the stepwise reaction of first Fp₂ with a dichlorosilane yields a product that than reacts with R_p₂. The intermediate was not isolated. This is because monochlorinated products are not stable during the work up procedure. They degrade during isolation by column chromatography.



Scheme 12: Stepwise reaction

The obtained product is a mixture of the di-iron compound and the bimetallic compound with iron and ruthenium on the same molecule. The ratio is 9:1 for the bi-iron compound. Fallmann reported in his PhD thesis, that the reaction of e.g. Fp₂ with dichloro tetramethyl disilane is a stepwise reaction. This means that at first one chlorine atom is substituted by an Fp-complex, and than this reaction will take place quantitatively before the second chlorine atom is substituted.⁵²

⁵¹ McVicker, G. B. *Inorg. Chem.* **1975**, 14, 9, 2087; Burlitch, J. M.; Ulmer, S. W. *J. Organomet. Chem.* **1969**, 19, 21-23; Felkin, H.; Knowles, P. J.; Meunier, B. *J. Organomet. Chem.* **1978**, 146, 151

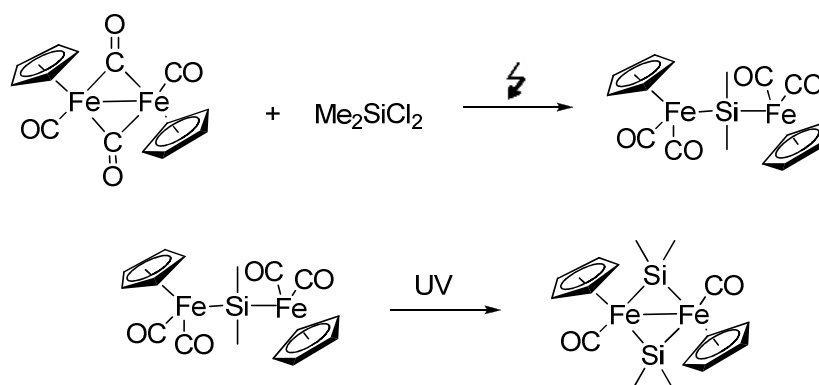
⁵² Fallmann, H. PhD thesis **2001**, TU Graz

Part A: Synthesis and Calculations

Based on this result, we performed the electrolysis under the assumption that after all the bridging carbonyl groups had reacted, just monosubstituted product is available. This only works if the monosubstitution takes place completely. So the observation of the timeline of the reaction e.g. via NMR would give a chance for further optimization of the reaction and for better yields in the dimetalated compound.

Nevertheless in our case we were able to show that the reaction does not proceed totally stepwise. It can be seen from the product distribution that in most of the cases the second chlorine atom reacts with Fp_2 , so that both are substituted by Fp. Just a small part of the product molecules are compounds in which only one chlorine atom reacted with Fp and the other one with the corresponding Rp.

Another reaction performed with a dichlorosilane is shown here:



Scheme 13: Reaction of Fp_2 with dichlorodimethylsilane

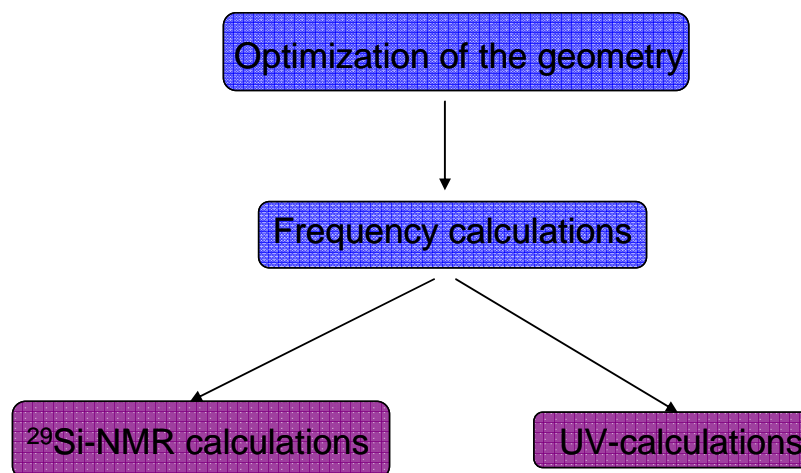
It led to an unexpected result. We expected the formation of Fp_2SiMe_2 and could prove its existence via NMR (^{29}Si -NMR: 98.5 ppm (THF, D_2O)⁵³). But the obtained crystal structure was completely different. Since, the initially formed Fp_2SiMe_2 is very sensitive to UV light, when light gets into the sample a photochemical reaction occurs, leading to the formation of a SiMe_2 dimerized material. A possible mechanism is that starting from the first product one CO is dismissed out of the molecule (it is a common start for photodegradation reaction of Fp-compounds), next the 16 e^- silylene transition state-dimerizes to the final product, whose structure we obtained by X-Ray analysis. The product is already known in literature as a photodegradation product of $\text{Fp-SiMe}_2\text{SiMe}_2\text{-Fp}$ ⁵⁴ but no X-Ray structure was obtained before.

⁵³ According to the ^{29}Si -NMR database used on the institute

⁵⁴ Zhang, Y.; Cervantes-Lee, F.; Pannell, K. H. *Organometallics* **2003**, 22, 2517-2524

A 2.2 Calculations

Calculations were performed following this scheme:



Scheme 14: Flow chart for the calculations

For further details to the methods and basis sets used see the experimental part of this work.

A 2.2.1 NMR calculations

Very little ^{29}Si -NMR data had been published for these types of molecules when this work started. Therefore, calculations were performed to ensure that the measured values correspond to the products expected. In the table below the experimental values are compared with the calculated ones. The calculations were performed with Gaussian03 mPW1PW91/6-311G**; referenced to tetramethylsilane (Si-value: 340.66 ppm). The measurements were performed in THF with D_2O as standard.

Table 4: Comparison of the calculated to the experimental values for ^{29}Si -NMR data

	$\Delta^{29}\text{Si}_{\text{calc.}}$ [ppm]	$\Delta^{29}\text{Si}_{\text{exp.}}$ [ppm]	Difference
Me₃SiFp	49.48	41.06	8.42
Me₂HSiFp	29.73	21.90	7.83
Me₂PhSiFp	45.66	35.91	9.75
MePh₂SiFp	44.90	35.10	9.80
Ph₃SiFp	50.06	36.31	13.76
FpSi₂Me₅	16.20; -11.50	11.37; -18.70	4.83; 7.2

It can be seen that the numbers differ in their absolute value but their relative difference is always around 8-10 ppm. So the general trend is well reproduced. The difference is within the method's

range and keeping in mind that the silicon NMR spectrum has a range of around 300 ppm, accepted the results are very good. A comparison of these values with the experimental results showed that the values for both methods are in consistent with each other, and therefore it was very likely that the obtained products were the ones wanted.

The only compound which shows a result with a larger than normal error is the triphenylated compound. This can be due to the fact that different conformers of FpSiPh_3 exist because of the mobility of the phenyl – rings. Therefore calculations of the different conformeres should be performed. The results can be weighted with a gauss function.

A 2.3 UV-experiments: Comparison between calculated and measured results

The UV spectra were measured as well as calculated and the orbitals involved were visualized to identify those most important ones for the transitions.

A 2.3.1 Results

The HOMO-LUMO transition, calculated for the different compounds, is involved in the following UV bands:

Table 5: Comparison between the calculated HOMO-LUMO transitions in the different molecules

λ ... calculated wavelength [nm]

f ... caclulated oscillator strength

	λ [nm]	f	transition	Percentage of the transition %
FpSiMe₂H	397.79	2.41e-03	HOMO → LUMO	38.8
	341.39	1.78e-03	HOMO → LUMO	28.1
FpSiMe₃	397.95	2.38e-03	HOMO → LUMO	29.4
	342.32	2.15e-03	HOMO → LUMO	36.1
FpSiMe₂Ph	346.13	1.65e-03	HOMO → LUMO	34.4
FpSiMePh₂	298.70	1.51e-01	HOMO → LUMO	53.3
FpSiPh₃	305.93	1.27e-01	HOMO → LUMO	72.1
FpGePh₃	306.30	1.46e-01	HOMO → LUMO	73.3
FpSnPh₃	315.03	1.80e-01	HOMO → LUMO	75.5
RpSiMe₃,	314.02	3.43e-04	HOMO → LUMO	93.0
FpSi₂Me₅	395.41	2.18e-03	HOMO → LUMO	29.0
	348.07	3.38e-03	HOMO → LUMO	21.7

Part A: Synthesis and Calculations

	323.10	2.56e-03	HOMO → LUMO	21.3
FpSi₆Me₁₁	294.28	1.64e-01	HOMO → LUMO	32.7

Comparing the molecules FpSiMe₂H and FpSiMe₃ the HOMO-LUMO transition in both molecules is part of nearly the same UV bands. Even the percentage of the transition is nearly the same. These are bands at the upper end of the spectrum, where the intensity of the experimental spectrum is not high. The oscillator strength of these transitions is also low. Also the transition takes place in two different excitations with nearly the same percentage. To this result also the transition from HOMO to LUMO for FpSiMe₂Ph fits. This compound also shows an excitation at 346 nm with a similar oscillator strength.

But the compound FpSiMePh₂ shows a different behavior. In this compound two bands have HOMO-LUMO participation and the most important one has remarkably lower wave lengths than in the other compounds. The transition at 298.7 nm has a very high percentage of HOMO-LUMO participation and high oscillator strength. So this band can be assigned as the most important and most probable one in this spectrum. This is the same for the Fp-ring compound. It also shows similar wavelengths and high oscillator strength.

Another compound, which shows different behavior is the Fp-disilane. There the HOMO-LUMO transition is involved in three bands with nearly the same percentage. They all have high wavelengths and small oscillator strengths.

It seems that when silicon is attached to a methyl group, the HOMO-LUMO orbitals are involved in more than one transition. This is true for FpSiMe₂H, FpSiMe₃, FpSiMe₂Ph, FpSiMePh₂ and FpSi₂Me₅. In all these compounds there is not only one band which can be attached to the HOMO-LUMO transition.

The other compounds show similar behavior. They all have a band at a wavelength around 310 nm in which the HOMO-LUMO transition is involved. This excitations are involved in the most intense transitions, which can be seen in the spectra.

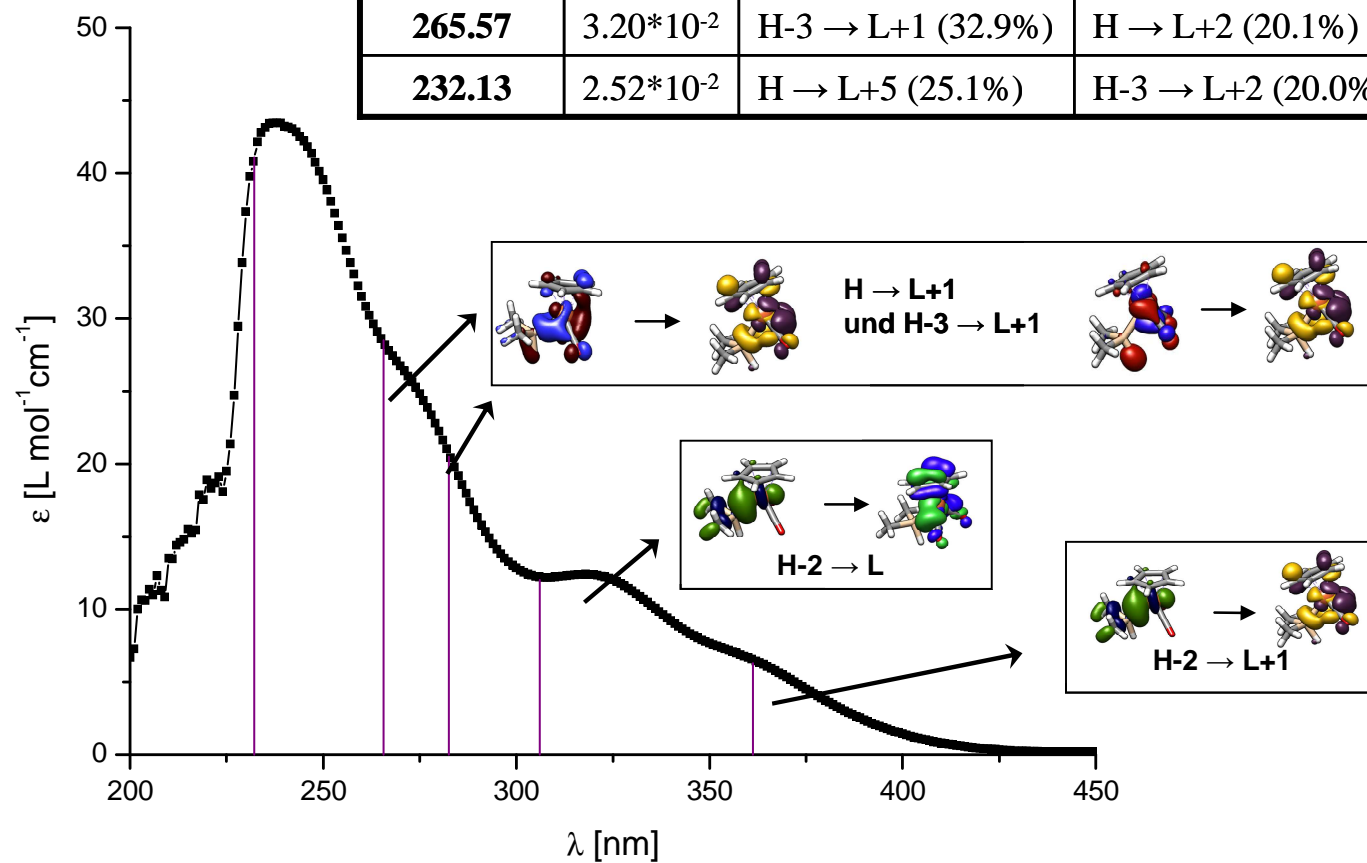
In general it is remarkable that the HOMO-LUMO band is always at high wavelengths, but it is not in all the cases the most probable one.

The results are shown in the following figures. The vertical lines, included in the experimental spectra, indicate the calculated transitions (Calculations were performed with TurboMole and TZVP base set). The corresponding orbitals are shown as well.

Most of the calculated UV bands exist of more than one excitation. They mainly consist of two or three main transitions from which the most probable two ones are listed up.

Results for Me₂HSiFp

λ_{calc} [nm]	f_{calc}	transition	transition	λ_{exp} [nm]
361.16	$1.12 \cdot 10^{-2}$	H-2 \rightarrow L+1 (52.3%)	H \rightarrow L+1 (35.5%)	363
305.99	$3.13 \cdot 10^{-3}$	H-2 \rightarrow L (64.7%)	H \rightarrow L (15.3%)	315
282.47	$4.12 \cdot 10^{-2}$	H \rightarrow L+1 (28.5%)	H-2 \rightarrow L+1 (28.5%)	277
265.57	$3.20 \cdot 10^{-2}$	H-3 \rightarrow L+1 (32.9%)	H \rightarrow L+2 (20.1%)	
232.13	$2.52 \cdot 10^{-2}$	H \rightarrow L+5 (25.1%)	H-3 \rightarrow L+2 (20.0%)	

Figure 3: UV-Results for FpSiMe₂H; λ = wave length [nm], f = oscillator strength

Results for Me_3SiFp

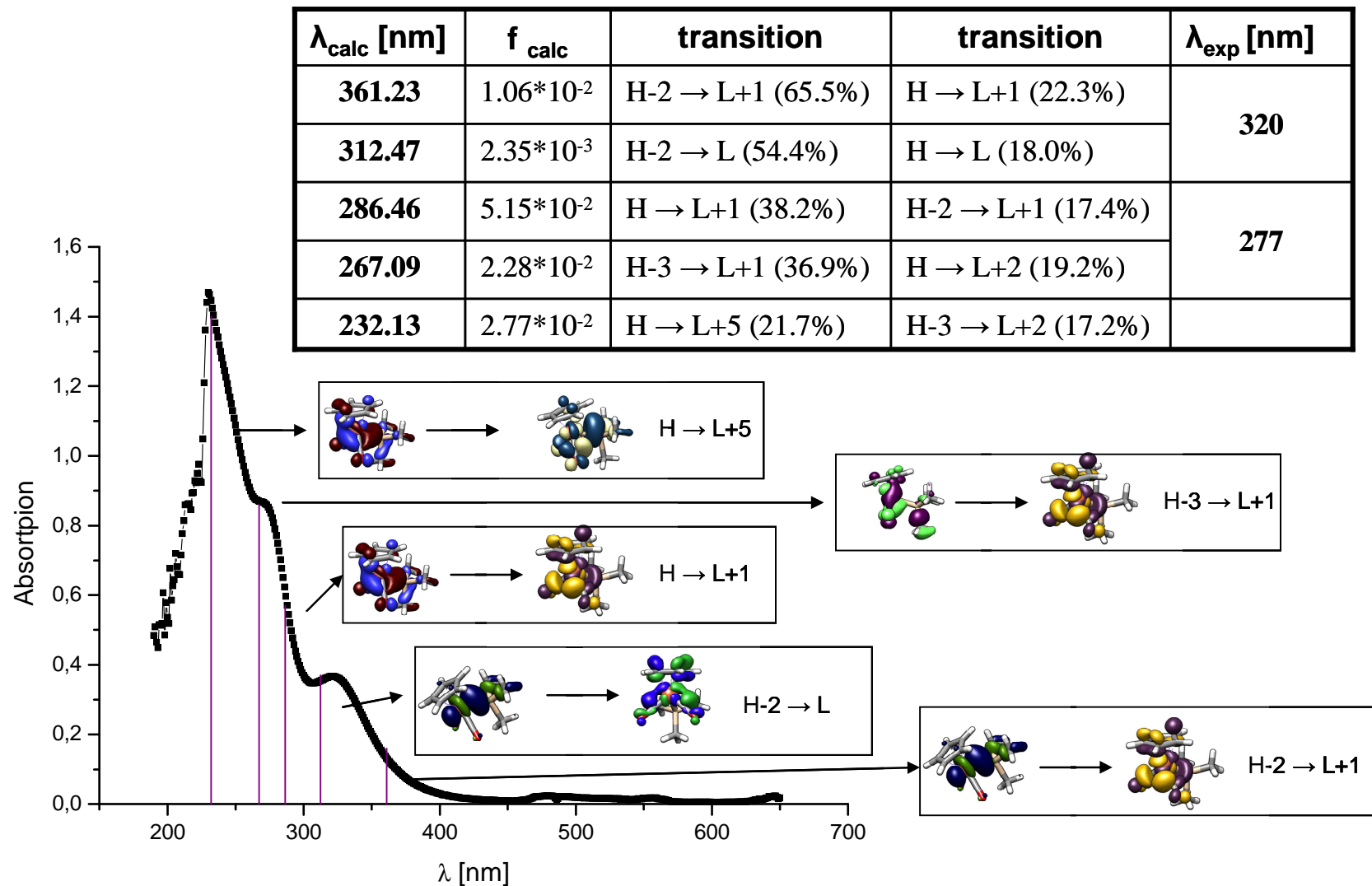
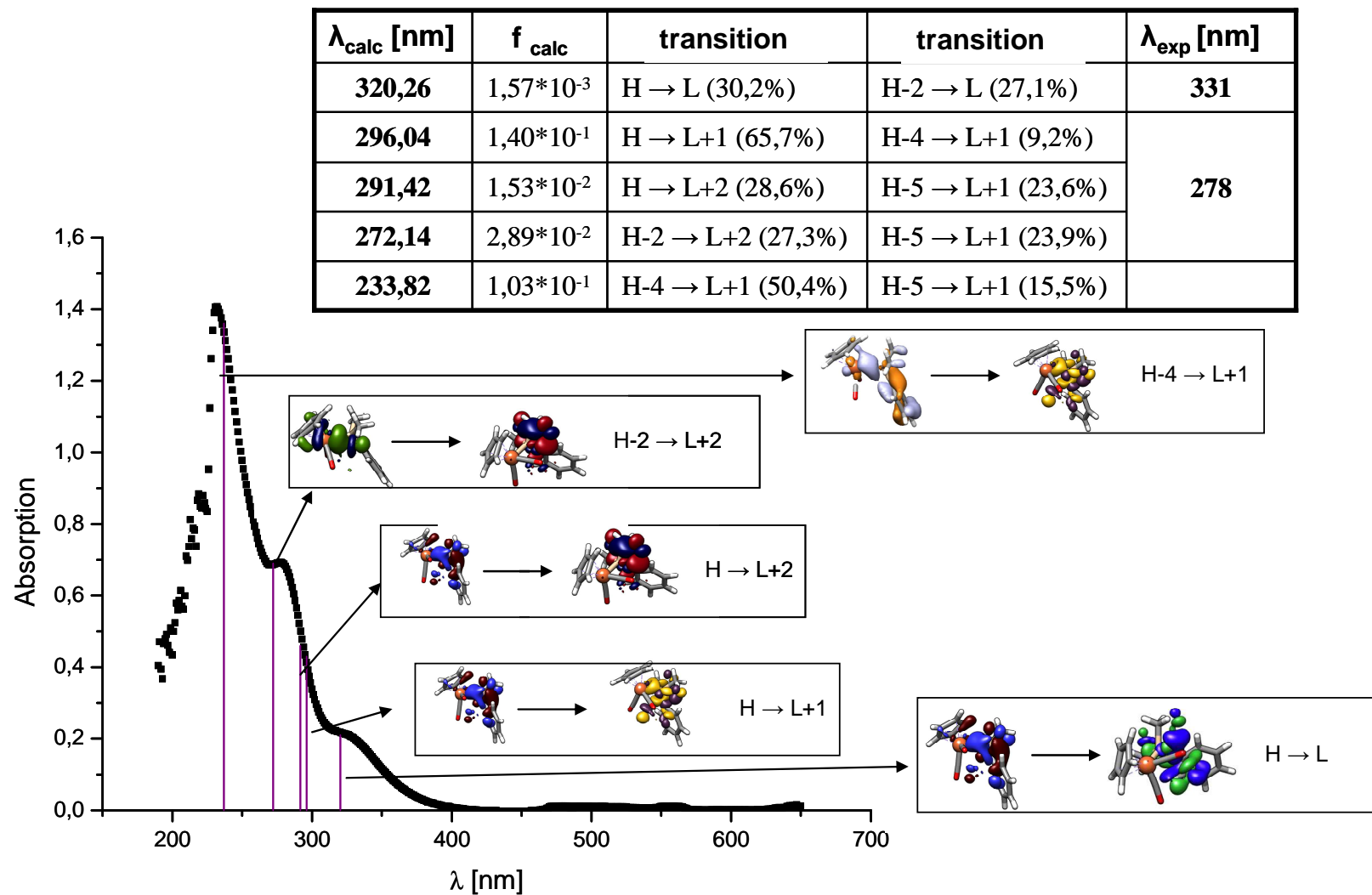
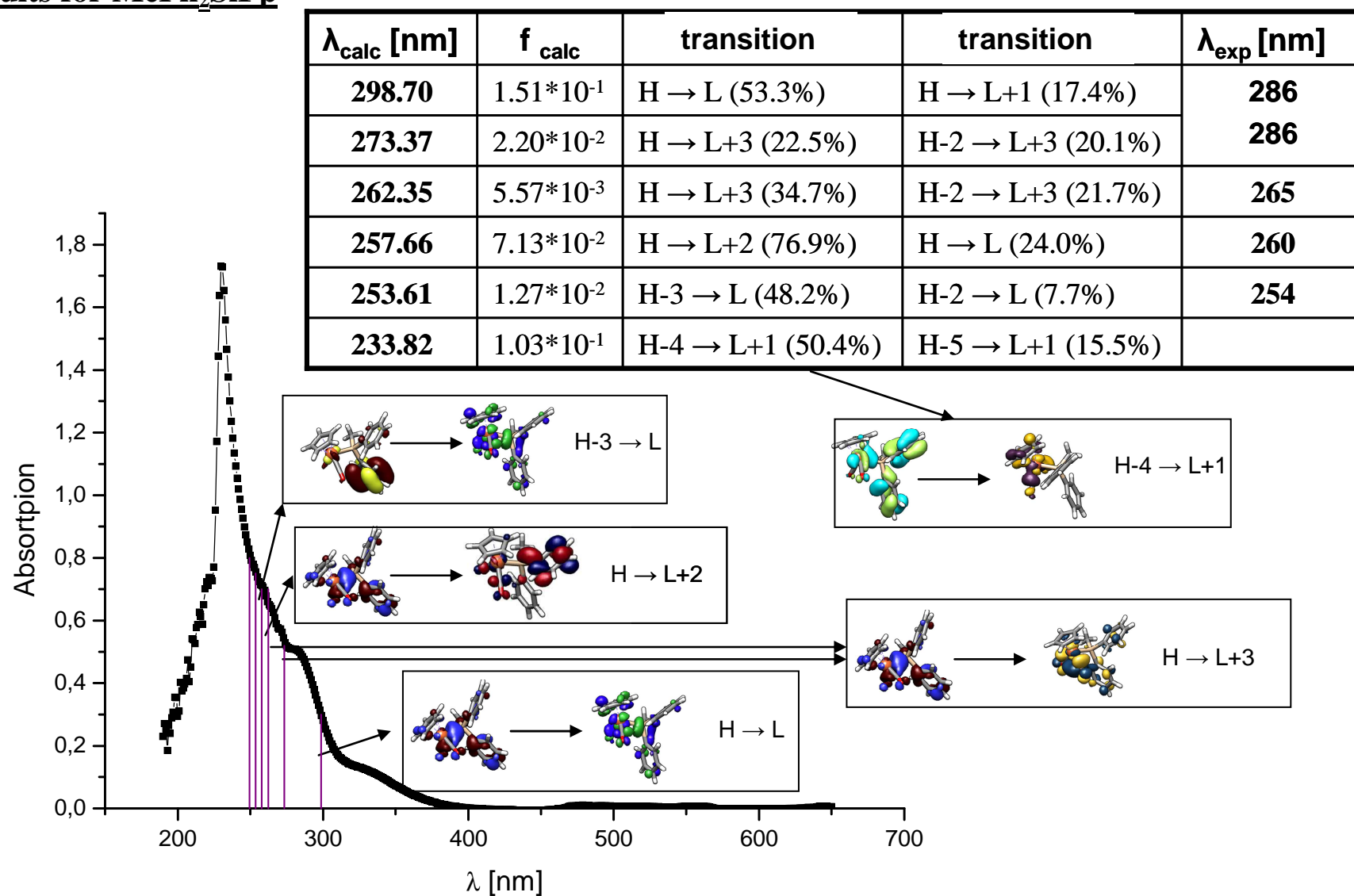
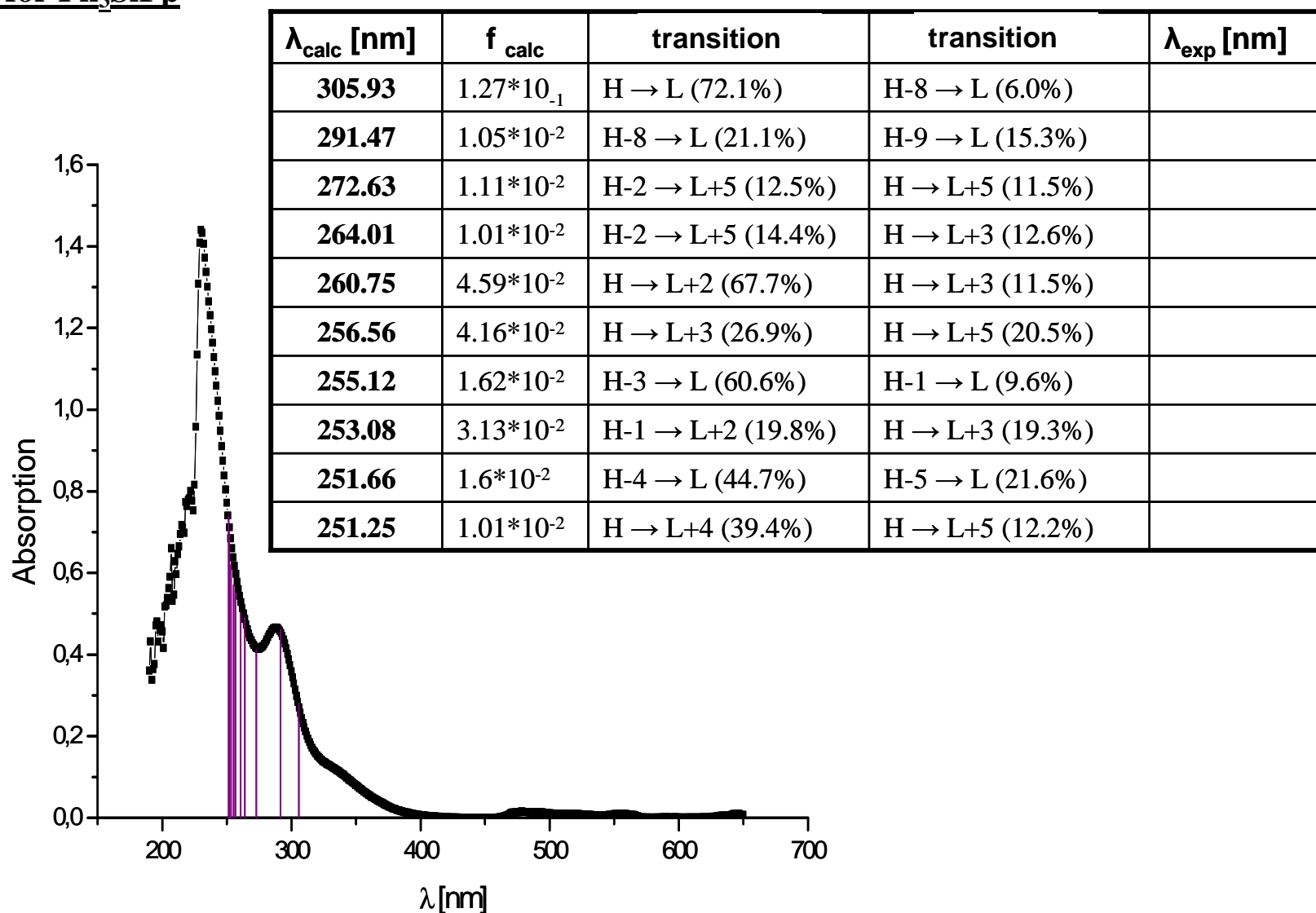


Figure 4: UV-Results for FpSiMe_3 ; λ = wave length [nm], f = oscillator strength

Results for Me₂PhSiFpFigure 5: UV-Results for FpSiMe₂Ph; λ = wave length [nm], f = oscillator strength

Results for MePh₂SiFpFigure 6: UV-Results for FpSiMePh₂; λ = wave length [nm], f = oscillator strength

Results for Ph_3SiFp Figure 7: UV-Results for FpSiPh_3 ; λ = wave length [nm], f = oscillator strength

The following orbitals are involved in the transitions in Ph_3SiFp :

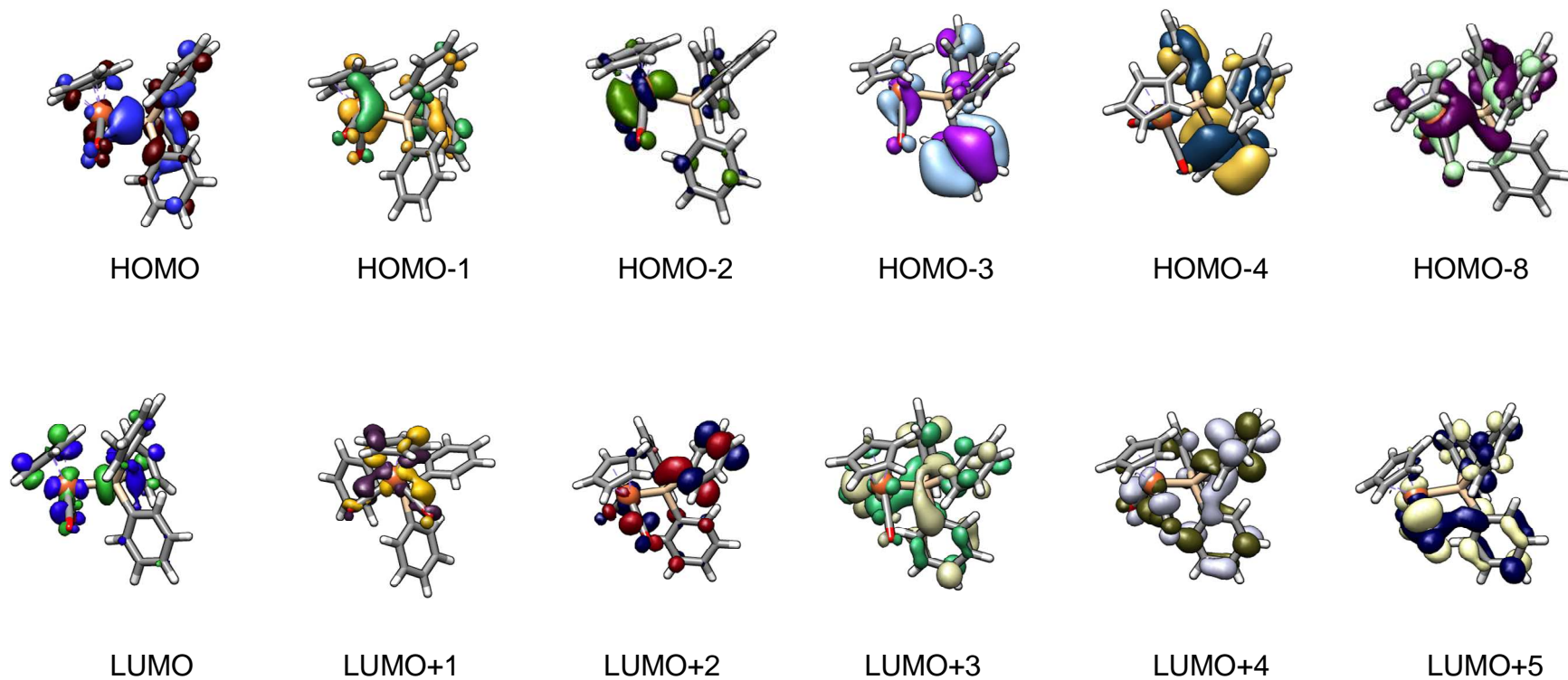
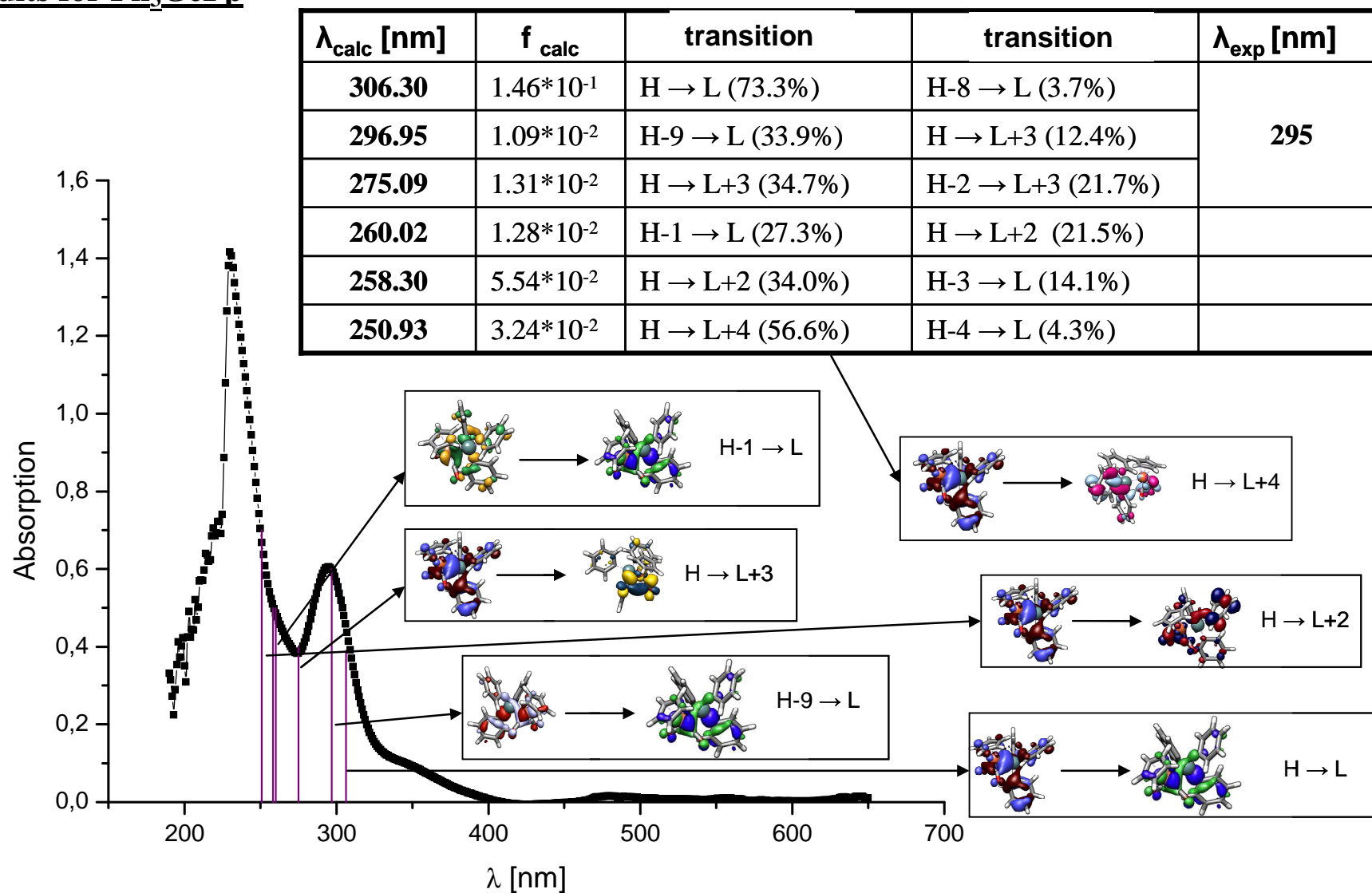
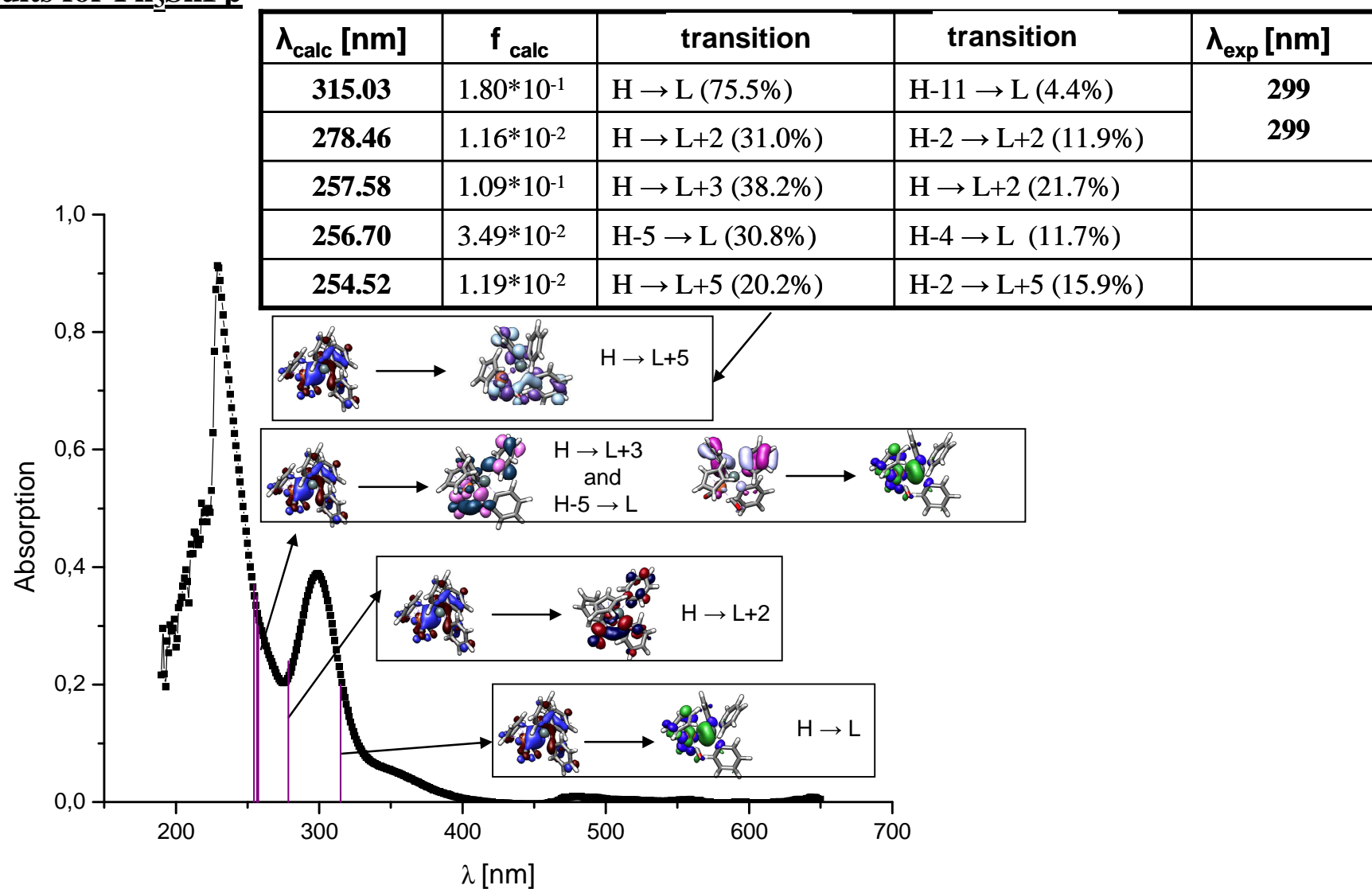
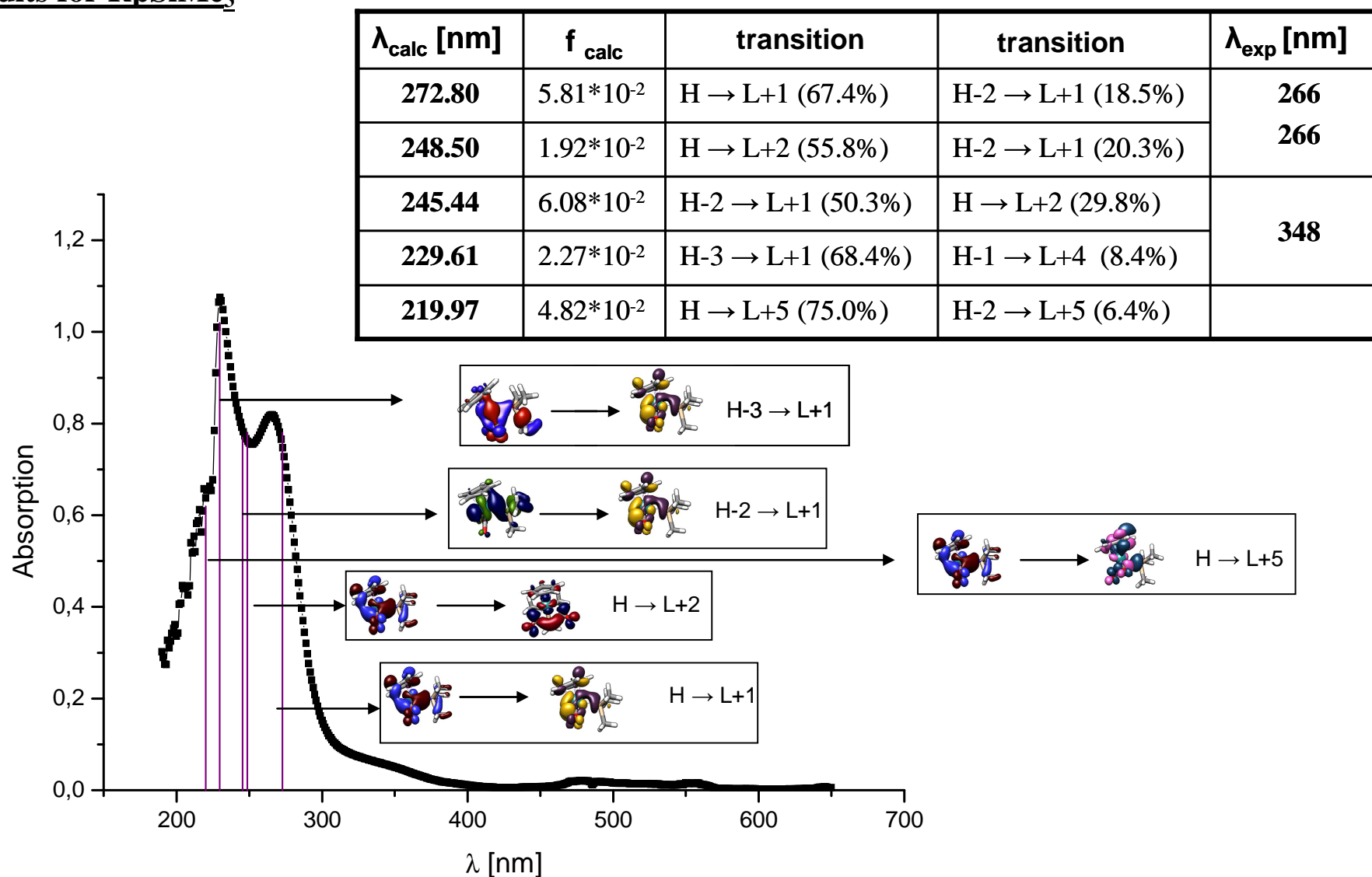
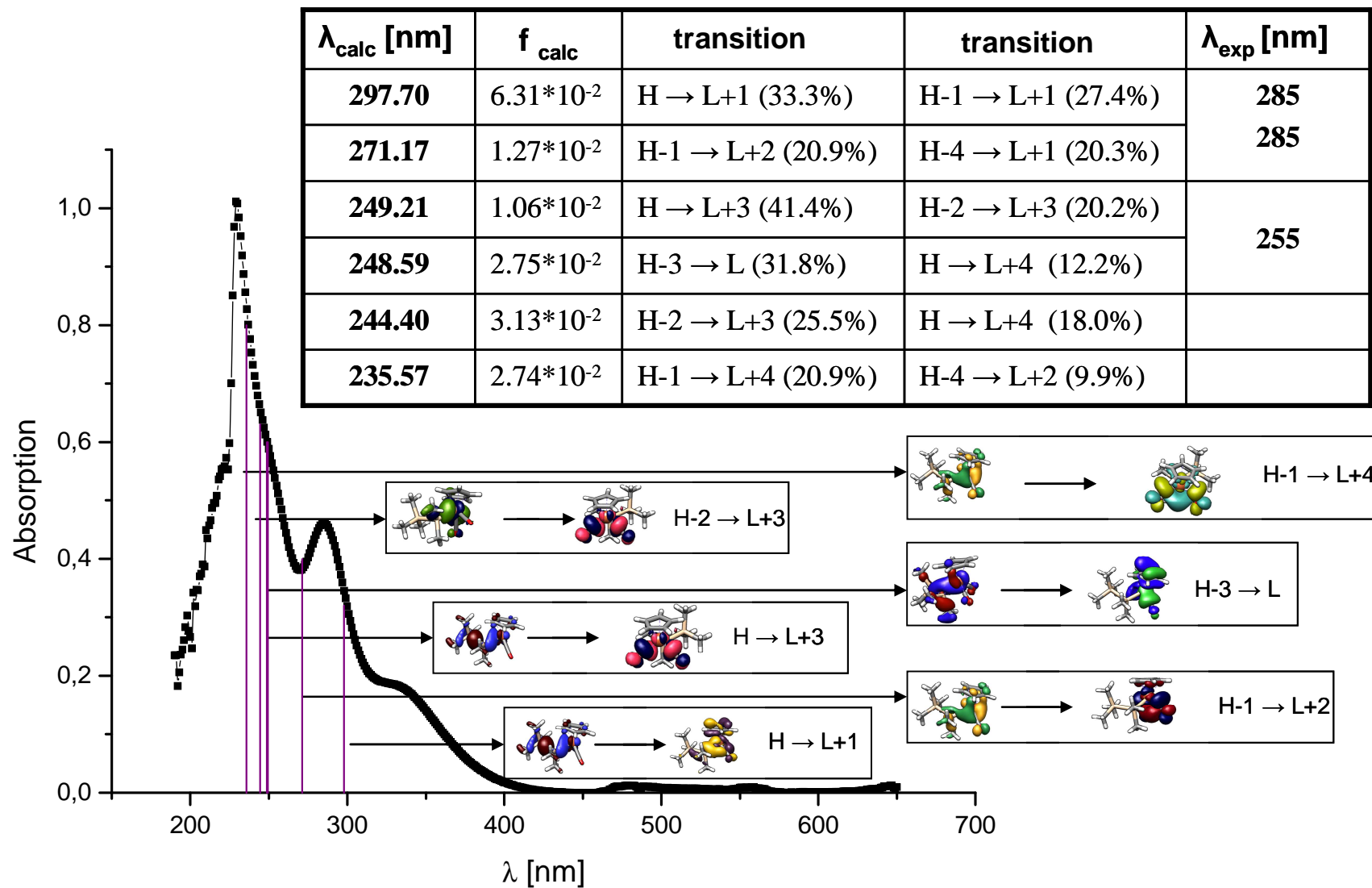


Figure 8: UV-Results for FpSiPh_3 ; orbitals involved in the transitions

Results for Ph_3GeFp Figure 9: UV-Results for FpGePh_3 ; λ = wave length [nm], f = oscillator strength

Results for Ph_3SnFp Figure 10: UV-Results for FpSnPh_3 ; λ = wave length [nm], f = oscillator strength

Results for RpSiMe₃Figure 11: UV-Results for RpSiMe₃; λ = wave length [nm], f = oscillator strength

Results for $\text{FpSiMe}_2\text{SiMe}_3$ Figure 12: UV-Results for $\text{FpSiMe}_2\text{SiMe}_3$; λ = wave length [nm], f = oscillator strength

Results for $\text{FpSi}_6\text{Me}_{11}$

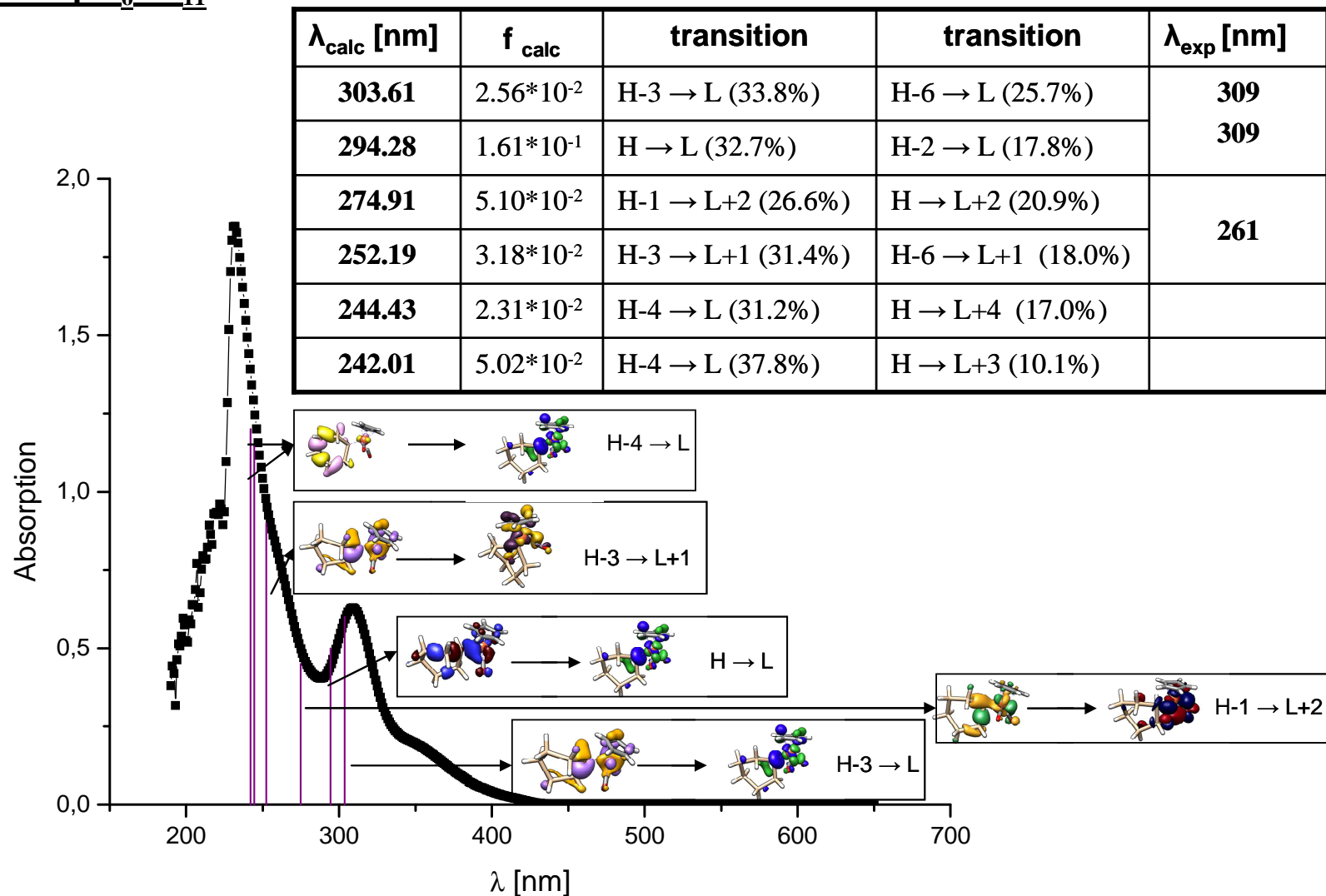


Figure 13: UV-Results for $\text{FpSi}_6\text{Me}_{11}$; λ = wave length [nm], f = oscillator strength

A 2.3.2 Discussion

For the smallest molecule we studied, FpSiMe_2H , the calculated and experimental wave lengths are in good agreement. For the other molecules the calculated results differ more, but reproduce the trends observed.

Further improvement of the theoretical results may be expected if more sophisticated methods such as CC2 or CASSCF/CASPT2 are applied. However, both of these methods are computationally quite demanding.

It is remarkable that the transition from HOMO to LUMO is not the most probable one. The transitions arise not only from HOMO to LUMO or from HOMO-1 to LUMO-1 but also from other orbitals. One reason is the transition metal, which produces orbitals very similar in energy.

As a general trend it can be said that the transition metal is very important for the UV transitions, because in nearly all the excitations the Fp group is involved.

Due to the solvent, dichloromethane, in which all the compounds were measured, it is not possible to measure reliably below wavelengths of 230 nm. Nevertheless, this solvent is the best compromise between solubility of the compounds and behavior in the UV-VIS area.

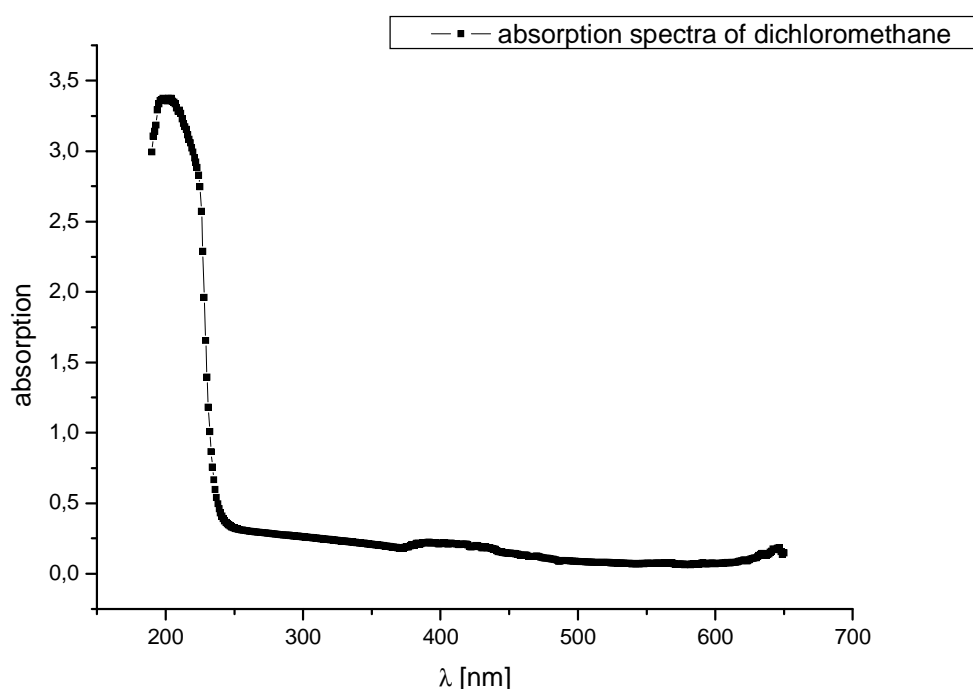


Figure 14: UV-VIS spectrum of dichloromethane

The Fp_2 spectrum is shown here, to see if substituents attached change the spectrum and shift them to higher or lower wavelengths.

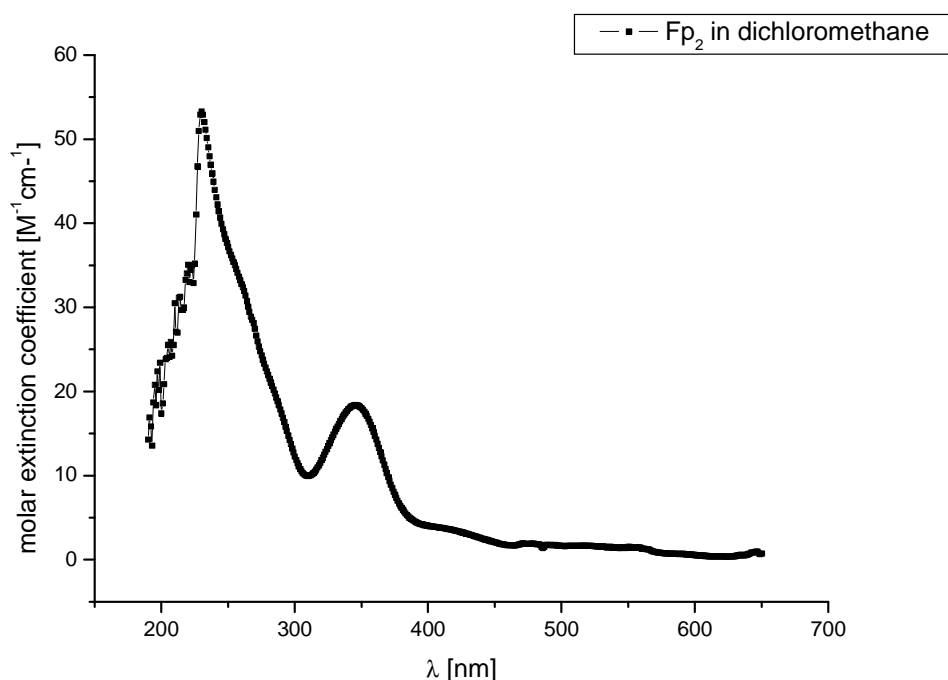


Figure 15: UV-VIS spectrum of Fp_2 in dichloromethane

The corresponding molar extinction coefficients were calculated from the spectra:

Table 6: molar extinction coefficients for Fp_2 in CH_2Cl_2
 ϵ ... molar extinction coefficients [$M^{-1}cm^{-1}$]
 λ ... wave length [nm]

CH_2Cl_2	ϵ [$M^{-1}cm^{-1}$]	λ [nm]
Peak 1	55.0	229
Peak 2	18.4	346
Peak 3	4.0	420

The different Fp -compounds in comparison to Fp shift the peaks to lower wavelengths. In Fp_2 the most distinctive peak is at around 346 nm and in the different Fp -compounds (see e.g. figure 16) it is around 300-310 nm.

A 2.3.2.1 Influence of the chain length

The size of the silicon substituent has a remarkable influence on the spectra. This is demonstrated in the following figure:

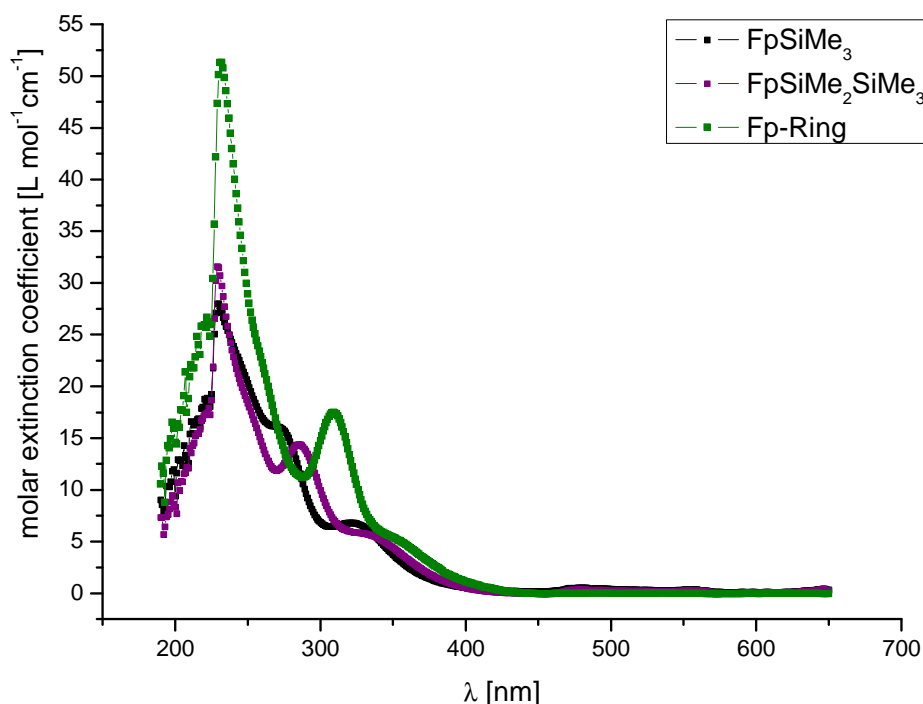


Figure 16: Comparison of the UV-VIS spectra of FpSiMe₃, FpSi₂Me₅ and FpSi₆Me₁₁

The longer the elongated silicon chain the more the observed peaks shift towards higher wavelengths – red shifting. Additionally the peak at around 350 nm is decreases with the size of the substituent. In all cases the calculations reproduce this trend very well.

The peak at around 300 nm was chosen to discuss the differences between the three compounds. Table 7 shows which orbitals are involved in giving this peak intensity.

Based on the performed calculations the influence of the different orbitals can be obtained. The transition between HOMO and LUMO+1 is important for all three molecules concerning the UV band at around 300 nm. Therefore these orbitals and their energies are discussed in the following table. The calculated orbitals important for this transition are shown. The wavelengths obtained with the two methods are combined and the calculated oscillator strengths are listed up.

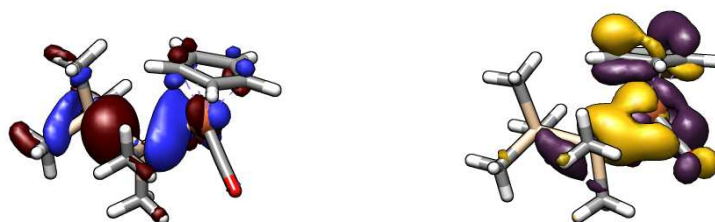
Table 7: Orbitals involved in the band at around 300 nm; The experimental data is given in square brackets.

FpSiMe₃



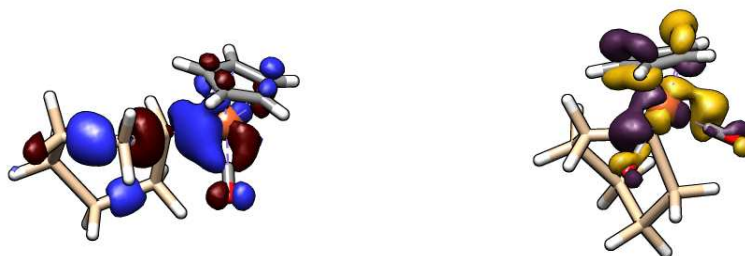
H → L+1 (38.2%); 286.46 nm; f = 5.15*e-02; [277 nm]

FpSi₂Me₅



H → L+1 (33.3%); 297.70 nm, f = 6.31*e-02; [285 nm]

FpSi₆Me₁₁



H → L+1 (41.7%); 311.64 nm; f = 3.57*e-03; [309 nm]

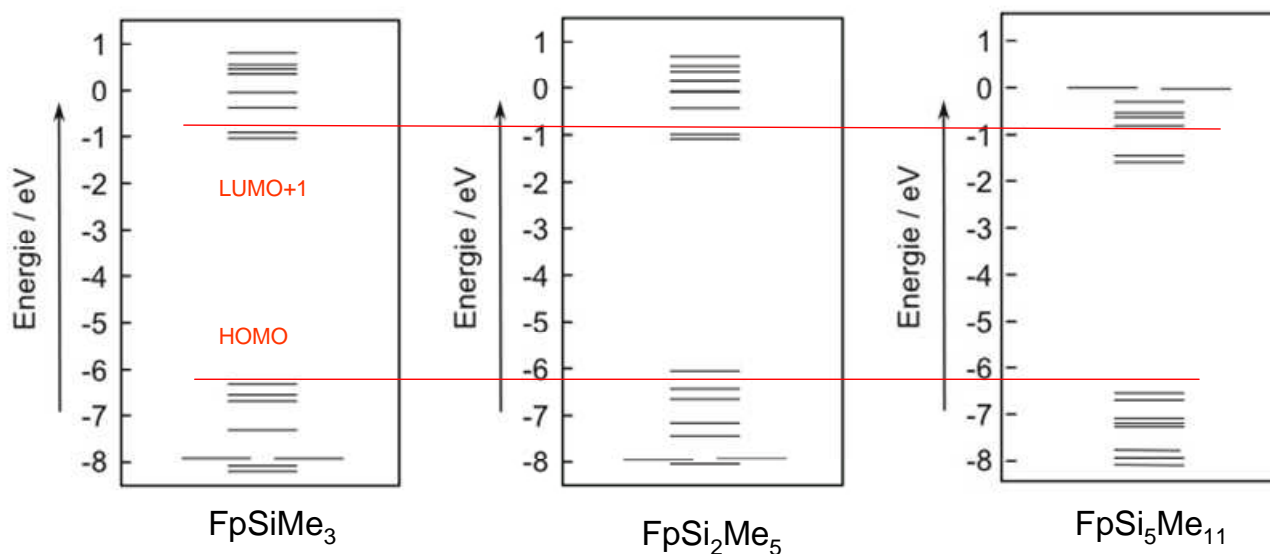
The measured and calculated wavelengths are in good agreement. The calculated ones are just slightly higher than the experimental ones.

It is obvious that the bigger the substituent the smaller the oscillator strength becomes for the transition. The calculations also fit to the experimental spectrum concerning the wavelength of the transition of HOMO to LUMO+1. It increases with the size of the substituent.

Part A: Synthesis and Calculations

Concerning the orbitals it seems that the transition mainly is a charge transfer one, because the starting molecular orbital is distributed all over the molecule. In contrast to that the orbital into which the excitation happens is mostly localized on the Fp-fragment.

In all three compounds the transition between HOMO-LUMO+1 is important, although not the only one involved. This energy gap for the three compounds and the corresponding orbital energies are shown in the following figure:



Scheme 15: Comparison of the orbital energies for FpSiMe₃, FpSi₂Me₅ and FpSi₆Me₁₁ (Energy for the gap between HOMO and LUMO+1: FpSiMe₃ + 5.39 eV; FpSi₂Me₅: + 5.06 eV; FpSi₆Me₁₁: +5.10 eV)

The highest energy difference between HOMO and LUMO+1 exists for FpSiMe₃. It is remarkable that the energy for the LUMO+1 decreases with the size of the substituent. To investigate the character of the transition between HOMO and LUMO+1 differential electron density calculations were performed. The results can be seen in the following pictures.

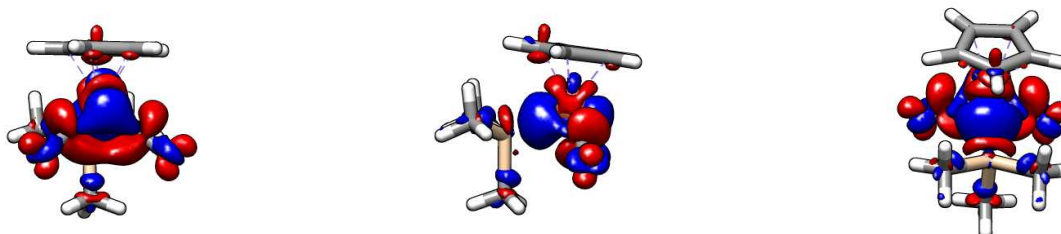


Figure 17: Calculated differential electron density for FpSiMe₃ (red: increasing electron density, blue: decreasing electron density)

Part A: Synthesis and Calculations

The main electron density is distributed on the Fp-ligand. Electron density from the Fe-Si bond is removed and is placed on the iron atom. Therefore, it could be possible to detect a lengthening of the bond between iron and silicon. Electron density is also put into the orbitals of the carbonyl carbon and oxygen atoms. The electron density is redistributed between the different orbitals. Conversely it seems that the Cp-ring does not have big influence. There is just a small amount of electron density brought into the π -orbitals of the carbonyl groups. In total it is an iron centered excitation.

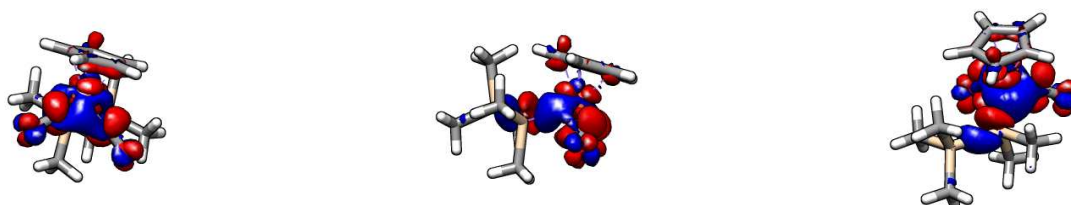


Figure 18: Calculated differential electron density for FpSi_2Me_5 (red: increasing electron density, blue: decreasing electron density)

In the excitation of the disilane it is again a matter of an iron centered transition. Around the iron atom most of the electron density is redistributed. The biggest influence comes from the Fp-Ligand, in which the Cp-ring plays just a subordinated role. Just a small amount of electron density is brought into the π -orbitals of the carbonyl groups. It seems that during the excitation electron density is removed from the Si-Si bond and from the Si-Fe bond, when compared to FpSiMe_3 the electron density distribution on the iron atom is also different.

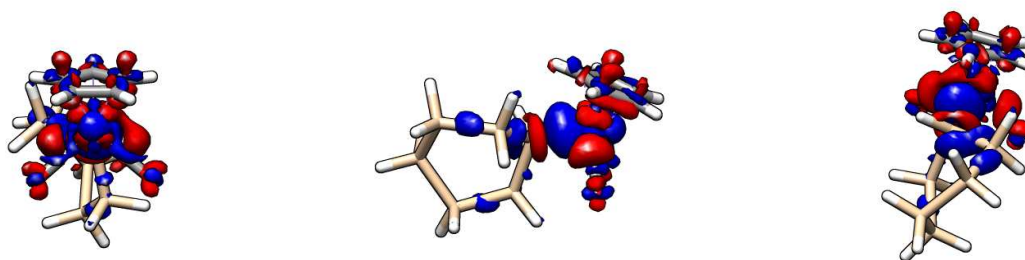


Figure 19: Calculated differential electron density for $\text{FpSi}_6\text{Me}_{11}$ (red: increasing electron density, blue: decreasing electron density)

The differences may result from the observation that the calculations resulted in a twist conformation of the Fp-Ring, but the X-Ray structure of the product showed that a chair conformation is observed. Further calculations with different conformers should be performed to clarify the situation.

In general it is also an excitation which mostly influences the orbitals on the Fp-substituent. In this case the influence of the Cp-ring is bigger, in that it seems that more electron density is transferred into the π -orbitals of the carbonyl group. There is also electron density taken from the nearest Si-Si bonds and put on the Si-Fe bond. It can be concluded that the calculations support a charge transfer transition..

A 2.3.2.2 Influence of the main group element E (E = Si, Ge, Sn)

The influence of the element E (E = Si, Ge, Sn) on the spectra is rather small, as seen in the Figure 20. Just the intensity of the peak changes and there is a slight red shift.

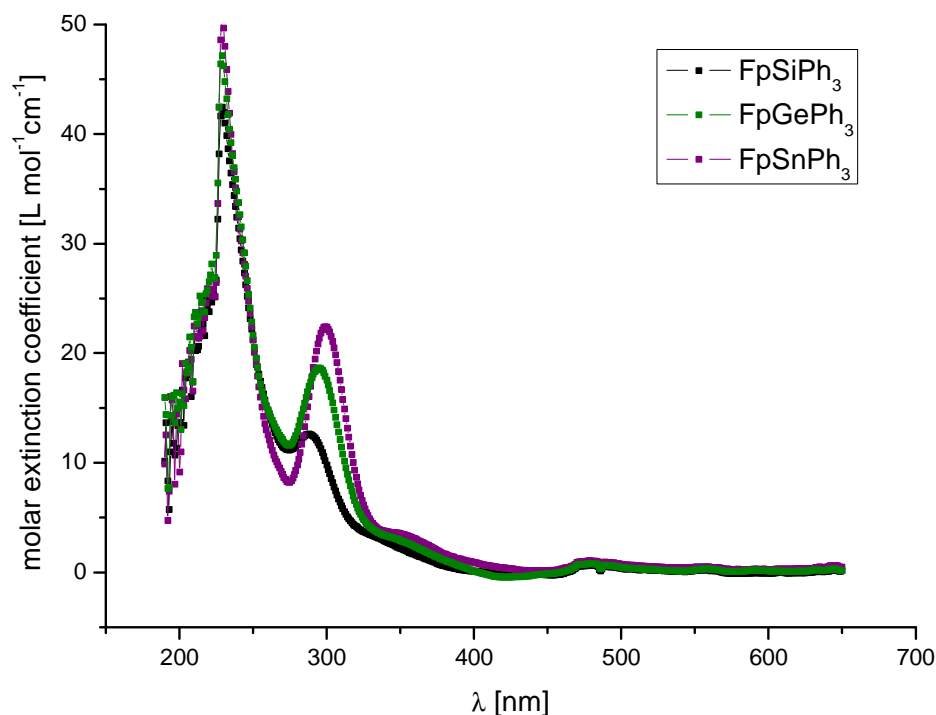
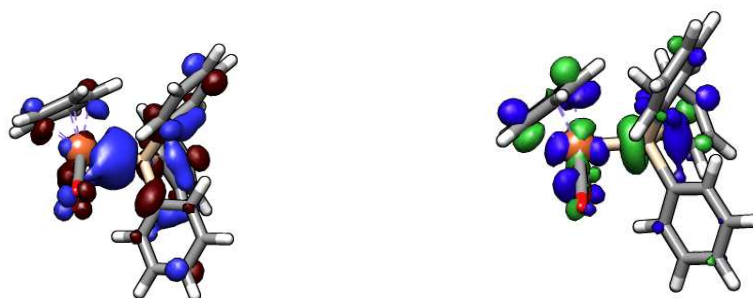


Figure 20: Comparison between the UV-Vis spectra of FpSiPh₃, FpGePh₃ and FpSnPh₃

As discussed earlier the peak around 300 nm mainly involves the HOMO and LUMO orbitals.

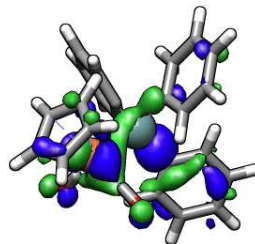
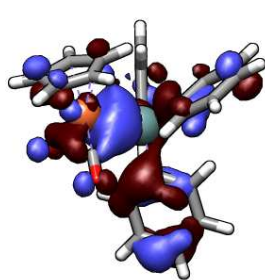
Table 8: Orbitals involved at the band around 300 nm. The experimental data is given in square brackets.

FpSiPh₃



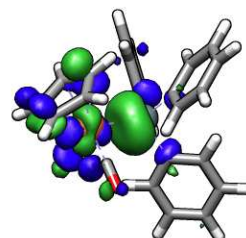
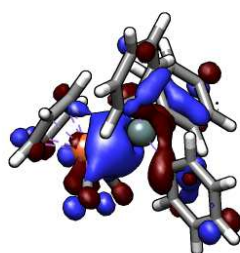
H → L (72,1%); 305.93 nm; f = 1.27*e-01; [288 nm]

FpGePh₃



H → L (73.3%); 306.30 nm, $f = 1.46 \cdot 10^{-1}$; [295 nm]

FpSnPh₃



H → L (75.5%), 315.03 nm; $f = 1.80 \cdot 10^{-1}$; [299 nm]

There is good agreement between the calculated and the experimental wavelengths with a difference just about 15 nm. This is within the methods normal error range.

The size of the HOMO-LUMO gap determines the wavelength of the transition. The gap decreases from silicon to tin. Therefore the peak should be slightly shifted in the spectrum to higher wave lengths. This trend agrees with experimental spectra. Also the increase of the intensity of the peak is mirrored in the growing oscillator strength going from Si to Sn.

The orbitals concerned are very similar for the three different molecules. The transition seems to correspond to an electron excitation from a $\sigma_{\text{Fe-Si}}$ to the $\sigma^*_{\text{Fe-Si}}$ orbital.

Part A: Synthesis and Calculations

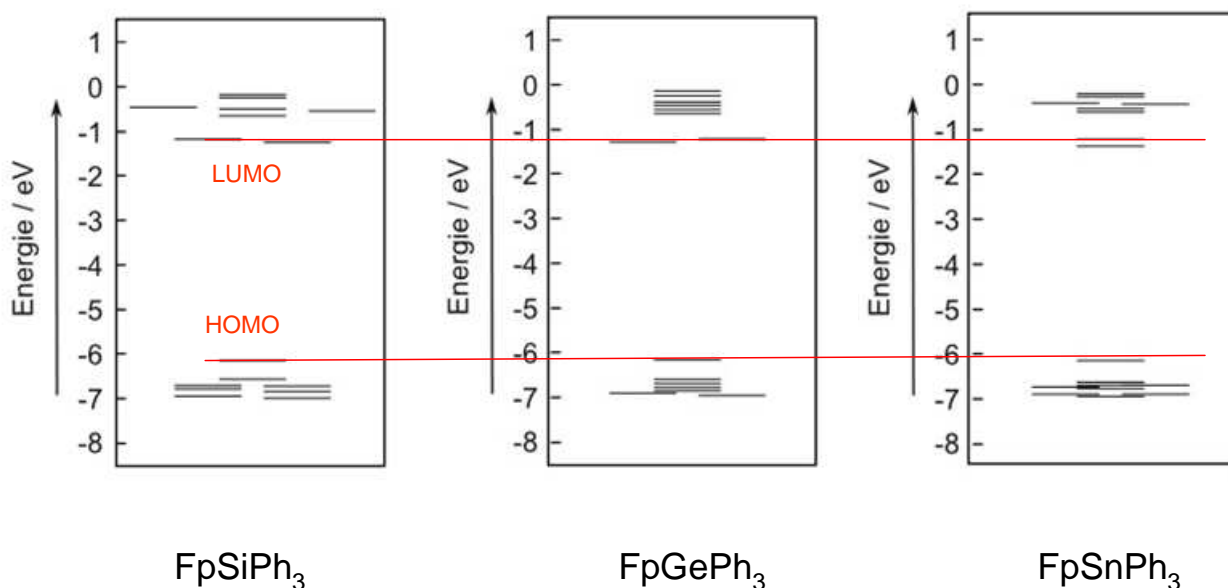


Figure 21: Comparison of the orbital energies for FpSiPh₃, FpGePh₃ and FpSnPh₃ (Energy for the HOMO-LUMO gap: FpSiPh₃: +4.92 eV; FpGePh₃: +4.89 eV; FpSnPh₃: +4.76 eV)

The energy of the HOMO is nearly the same for all three molecules, but the one for the LUMO is slightly decreasing.

The differential electron density calculations showed the following results:

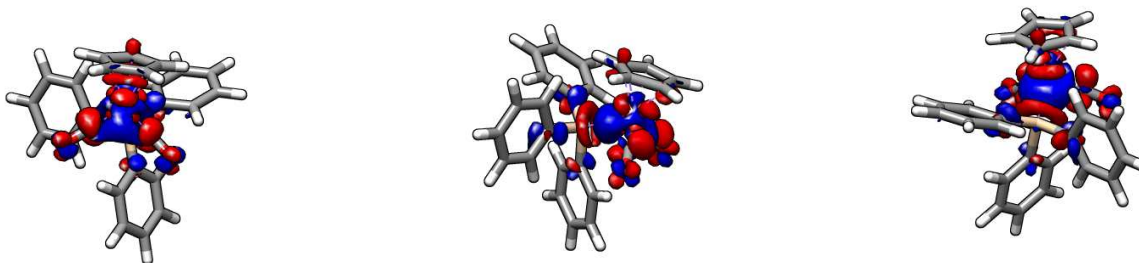


Figure 22: Calculated differential electron density for FpSiPh₃ (red: increasing electron density, blue: decreasing electron density)

In agreement with the $\sigma_{\text{Fe-Si}}$ to the $\sigma^*_{\text{Fe-Si}}$ transition the electron density between Fe-Si decreases and it increases on the iron and silicon atoms. In the rest of the molecule a distribution of electron density between the iron and the Fp-Rest takes place.

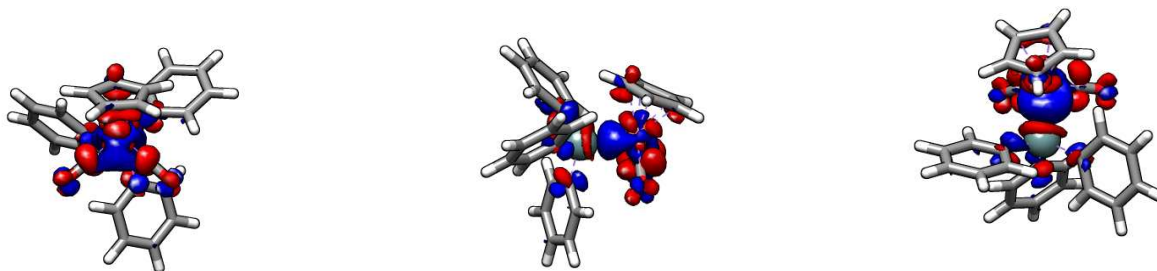


Figure 23: Calculated differential electron density for FpGePh₃ (red: increasing electron density, blue: decreasing electron density)

The orbitals involved in this excitation are the same than for the compound FpSiPh₃. It is also a mainly iron centered transition. It is possible that the decrease on the electron density at the Fe-E bond is smaller for the germanium compound than for the silicon compound.

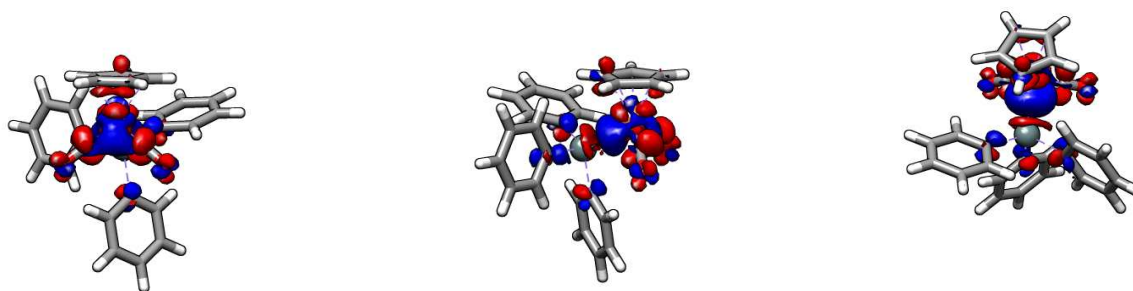


Figure 24: Calculated differential electron density for FpSnPh₃ (red: increasing electron density, blue: decreasing electron density)

For this molecule the same orbitals and changes in electron density can be seen as for FpSiPh₃ and FpGePh₃. It is remarkable that the electron density difference in the orbitals comprising the Si-Fe bond is even smaller than for the germanium compound. But this difference is just very small. All the other changes are the same.

The HOMO and LUMO orbitals both cover the whole molecule, although they are centered on the iron and carbonyl groups. Additionally the calculation of the electron density showed that it seems to be an excitation which is spread all over the molecule except the phenyl rings. For this excitation it can be seen that the transition from the $\sigma_{\text{Fe-Si}}$ to the $\sigma^*_{\text{Fe-Si}}$ is important.

For all three molecules it appears that electron density is transferred from the $\sigma_{\text{Fe-Si}}$ to the $\sigma^*_{\text{Fe-Si}}$ orbital. This means that the energy density is getting more localized on the atoms than on the bond. It was also seen that the electron density changes mostly on the Fp-group, especially on the iron and carbonyl functionalities.

A 2.3.2.3 Influence of the metal

At last the influence of the metal on the spectrum is examined.

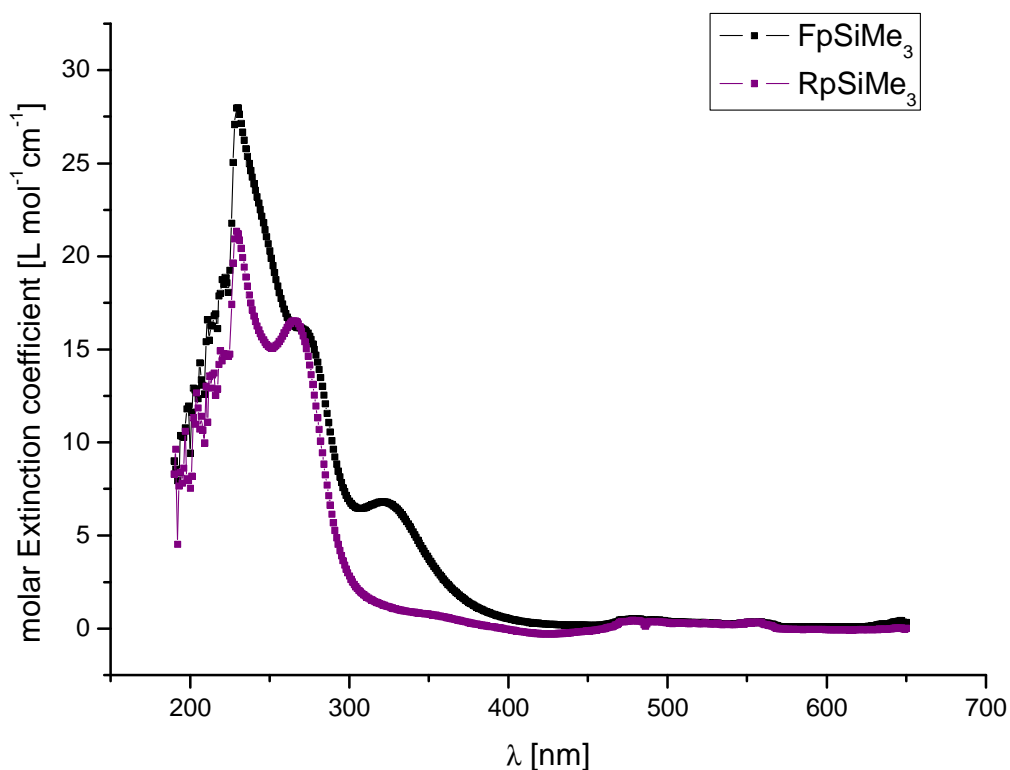


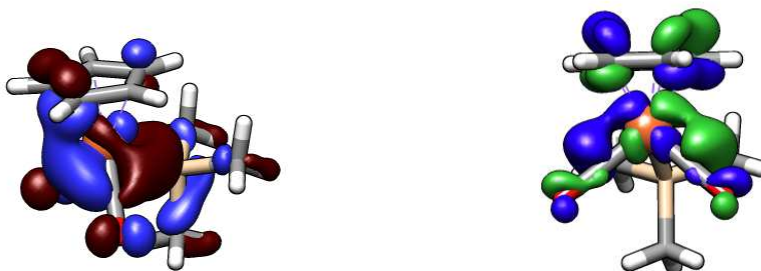
Figure 25: Influence of the metal on the UV-VIS spectra: RpSiMe_3 and FpSiMe_3

In this case the peak at around 320 nm is discussed. It is rather small in the experimental spectrum of the ruthenium compound but rather distinctive for the iron one.

The following orbitals/transitions are involved:

Table 9: Orbitals involved at the transition at around 320 nm. The experimental data is given in square brackets.

FpSiMe_3



$\text{H} \rightarrow \text{L}$ (36.1%); 342.32 nm; $f = 2.15 \cdot 10^{-3}$; [321 nm]

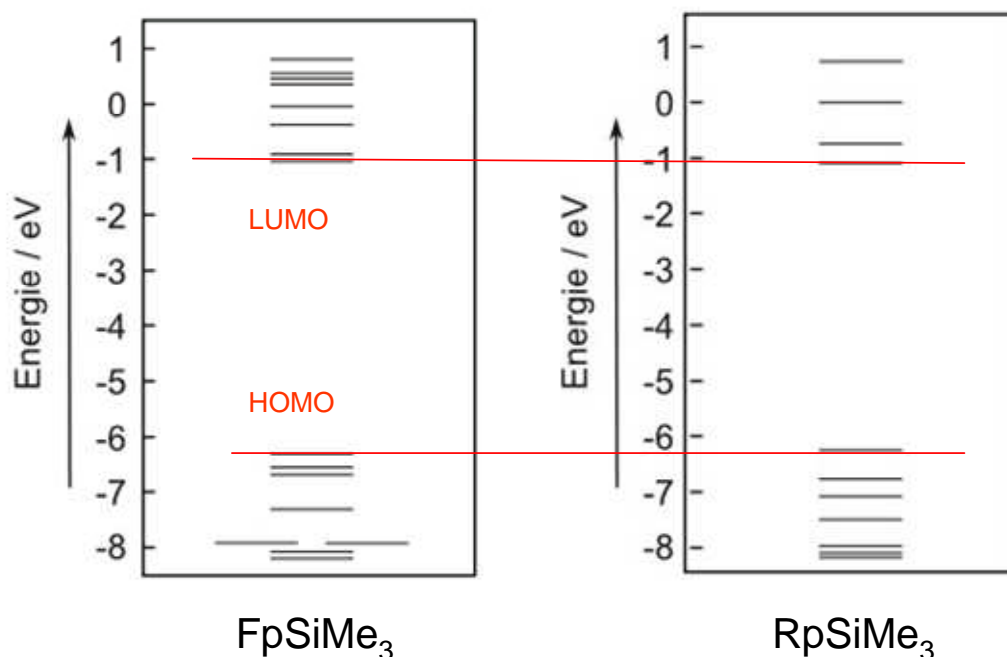
RpSiMe₃



H → L (93.0%); 314.02 nm, $f = 3.43 \cdot 10^{-4}$; [~ **348 nm**]

Calculations show that the transition from HOMO to LUMO is the most important for both molecules in this band.

The orbitals look very similar and it is very likely that the transition is a charge transfer between the orbitals on the silicon and the iron atom.



Scheme 16: Comparison of the orbitals between FpSiMe₃ and RpSiMe₃ (The gap between HOMO and LUMO is: FpSiMe₃: +5.27 eV; RpSiMe₃: +5.17 eV)

It is important to note that the oscillator strength for the transition is much higher for the iron compound than for the ruthenium one. This is in good agreement with the experiment, although in the spectrum the exact peak position is difficult to determine. It seems that this transition gets lost under the noise of the spectrum. It was also noted that the corresponding spectrum of pure dichloromethane has a slightly higher base line in this area.

Part A: Synthesis and Calculations

Also remarkable is that the unoccupied orbitals for the ruthenium compound have, in general, higher energies and they are further apart from each other than in the iron compound.

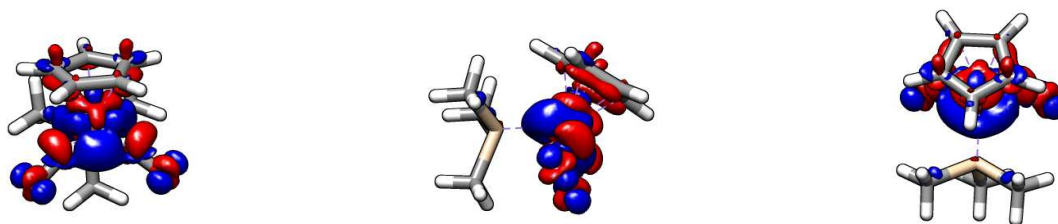


Figure 26: Calculated differential electron density for FpSiMe_3 (red: increasing electron density, blue: decreasing electron density) for the transition between HOMO and LUMO

The whole electron density centered at the Fp-Rest of the molecule. It is obvious that the silicon substituent is not really involved in this transition. This corresponds mostly to a local electron excitation on the Fp-fragment.

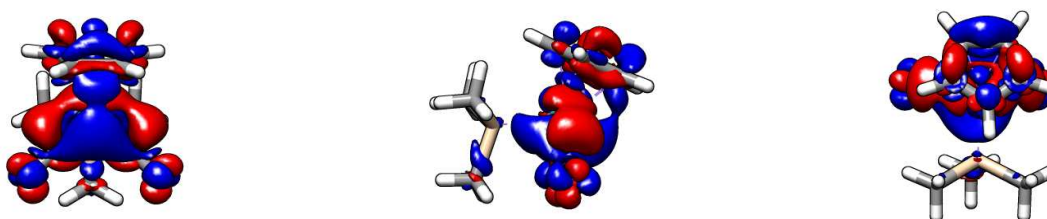


Figure 27: Calculated differential electron density for RpSiMe_3 (red: increasing electron density, blue: decreasing electron density) for the transition between HOMO and LUMO

In this case the electron density change is also localized on the Rp-Rest of the molecule. There are electron density changes on the Cp-Ring. Also a transfer of the density in the orbital along the bond between ruthenium and silicon into the orbitals vertical to the ruthenium center takes place.

In general it seems that in this case the main excitation is located at the Rp-fragment.

A 2.3.3 Molar extinction coefficients

The molar extinction coefficients were calculated out of the measured spectra:

Table 10: calculated molar extinction coefficients

ϵ ... molar extinction coefficients [$M^{-1}cm^{-1}$]

λ ... wave length [nm]

FpSiMe₃	ϵ [$M^{-1}cm^{-1}$]	λ [nm]
Peak 1	29	229
Peak 2	15.2	277
Peak 3	6.8	321-322

FpSiMe₂Ph	ϵ [$M^{-1}cm^{-1}$]	λ [nm]
Peak 1	39.4	230
Peak 2	19.2	278
Peak 3	5.1	331

FpGePh₃	ϵ [$M^{-1}cm^{-1}$]	λ [nm]
Peak 1	45.2	229
Peak 2	18.2	295
Peak 3	2.8	349

FpSnPh₃	ϵ [$M^{-1}cm^{-1}$]	λ [nm]
Peak 1	46.8	229
Peak 2	19.9	299
Peak 3	2.6	353

FpSiMePh₂	ϵ [$M^{-1}cm^{-1}$]	λ [nm]
Peak 1	12.3	229
Peak 2	3.5	253.7
Peak 3	3.2	259.6
Peak 4	2.9	265.3
Peak 5	2.6	271.4
Peak 6	2.2	286.5
Peak 7	1.5	333

FpSi₆Me₁₁	ϵ [$M^{-1}cm^{-1}$]	λ [nm]
Peak 1	55.2	229
Peak 2	21.5	261.5
Peak 3	17.5	309
Peak 4	4.7	356

FpSiPh₃	ϵ [$M^{-1}cm^{-1}$]	λ [nm]
Peak 1	40.2	230
Peak 2	12.7	288
Peak 3	3.2	337

RpSiMe₃	ϵ [$M^{-1}cm^{-1}$]	λ [nm]
Peak 1	22.1	229
Peak 2	16.9	266
Peak 3	1.1	348

FpSiMe₂H	ϵ [$M^{-1}cm^{-1}$]	λ [nm]
Peak 1	40.4	231
Peak 2	24.5	277
Peak 3	13.4	315
Peak 4	6.3	363

Disilane	ϵ [$M^{-1}cm^{-1}$]	λ [nm]
Peak 1	37.3	229
Peak 2	16.4	255
Peak 3	14.4	285
Peak 4	5.6	338

A 2.3.4 Conclusion

The experimental and calculated results are in good agreement with each other. The nature and the character of the transitions obtained in the experiment can be explained using the results of the calculations. Both methods, the experimental and quantumchemical one, showed similar results concerning the wavelengths of the obtained peaks and also the oscillator strength respectively the intensity of the peak in the experimental spectrum.

Information concerning the energy of the orbitals involved in the excitations, the differential electron density, and the nature of the orbitals could be obtained out of the performed calculations. Also it could be explained if the transition is more likely to be a charge transfer or a local one.

A 2.4 X-Ray Structures

Finally, after optimizing the work up procedure the products could be isolated and single crystal X-Ray structures could be obtained of the products **1-10**:

From the structures it was shown that the reaction does not only work for silicon compounds with different substituents but also for other elements of the XIV - group. Also it could be successfully shown that it is not limited to iron as the metal.

The whole data concerning the X-Ray structures (e.g. the R/R_w factors) can be found in the appendix (Part C 1) but selected results will be discussed here.

The crystal structures obtained are shown here:

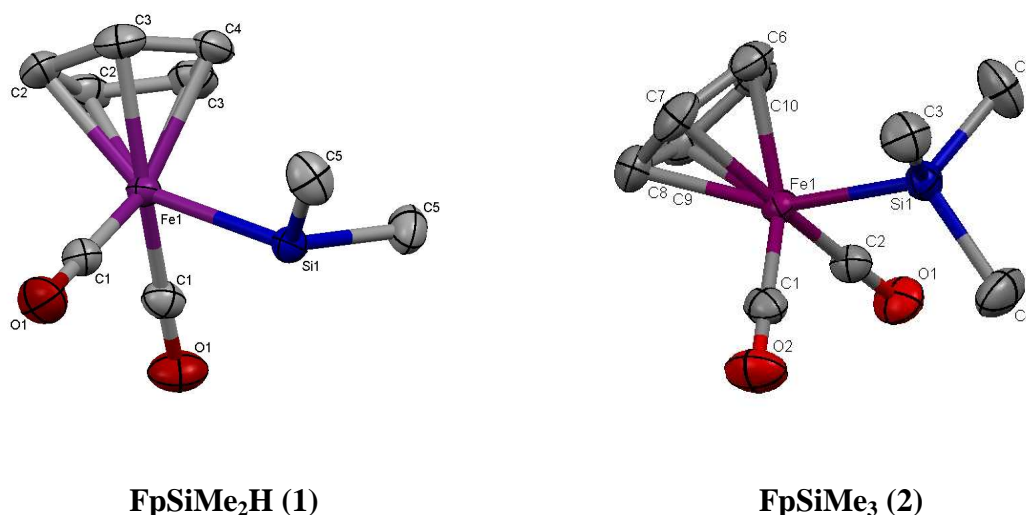


Figure 28: Crystal structures of FpSiMe₂H and FpSiMe₃

It is noteworthy that FpSiMe₂H (1) crystallizes in the hexagonal space group P6₃/m. The molecule is located at the mirror plane perpendicular to the hexagonal axis.

Part A: Synthesis and Calculations

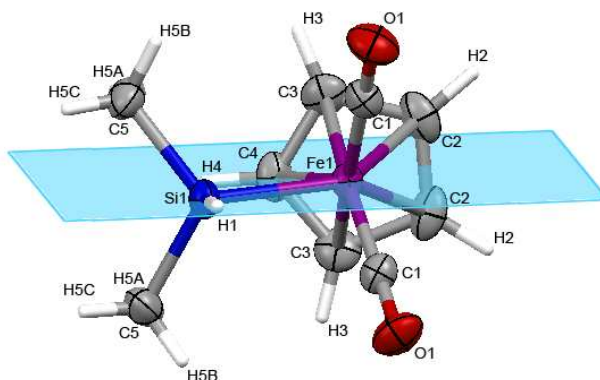


Figure 29: Crystal structure of FpSiMe_2H

The crystal structure of FpSiMe_3 (compound **2**; monoclinic - $C2/c$) is also remarkable because it shows that there is a not negligible interaction between the carbonyl oxygen and the hydrogen of the Cp-ring. The distance between those two atoms is just 2.686 Å.

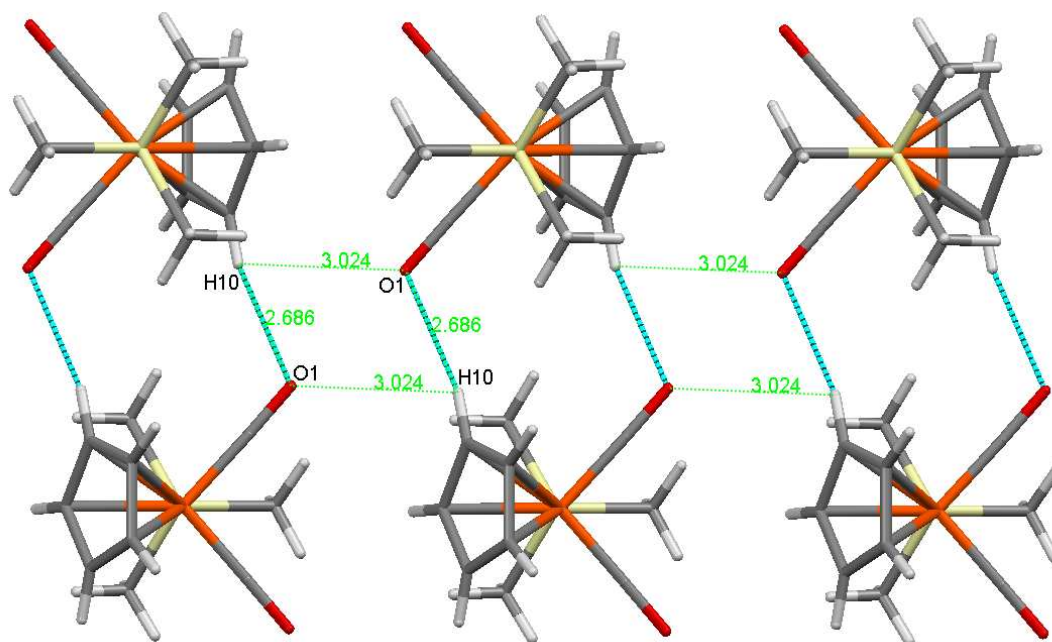


Figure 30: Intermolecular interaction between the carbonyl oxygen and a Cp-hydrogen

The crystal structures obtained for the molecules with mixed substituents of methyl and phenyl groups are shown in the following figure:

Part A: Synthesis and Calculations

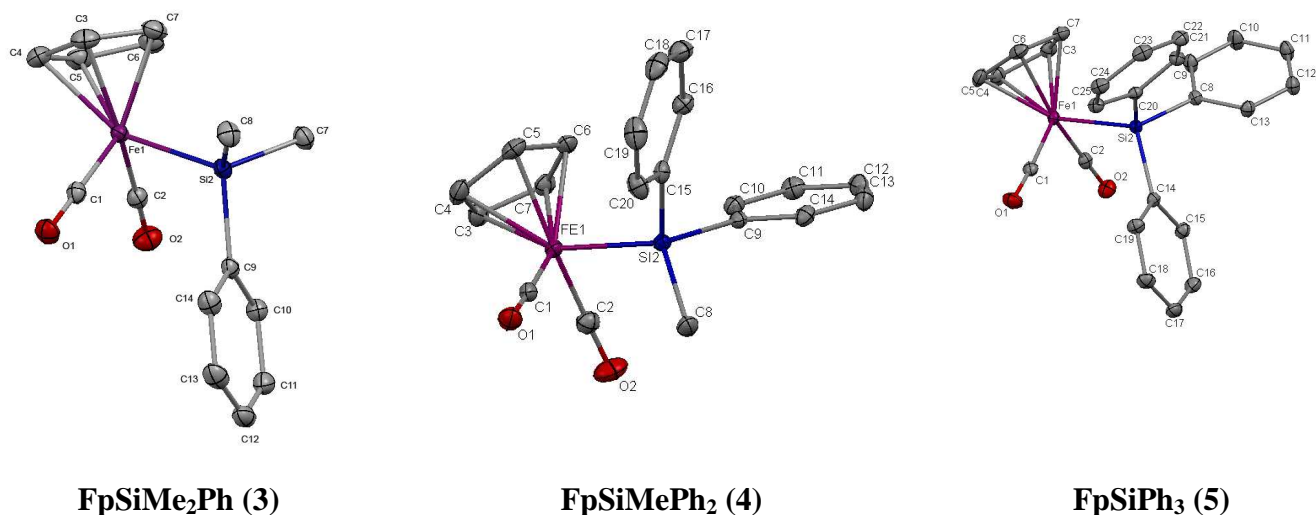


Figure 31: Crystal structures of FpSiMe₂Ph, FpSiMePh₂ and FpSiPh₃

For these three molecules the compounds could be crystallized in the following forms with the determined space group:

FpSiMe₂Ph: monoclinic – Pn

FpSiMePh₂: orthorhombic - P2₁2₁2₁

FpSiPh₃: monoclinic - P2(1)/n

To compare the different structures, those of FpGePh₃ and FpSnPh₃ are shown in the next figure:

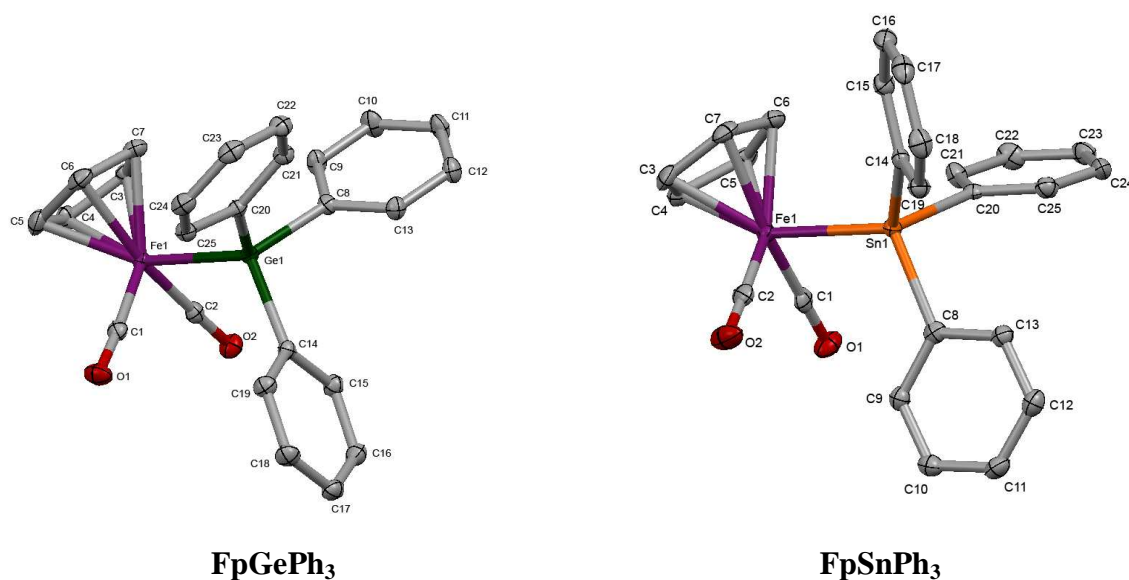


Figure 32: Crystal structures of FpGePh₃ and FpSnPh₃

A comparison between the different triphenylated compounds FpSiPh₃ (5), FpGePh₃ (compound 6; monoclinic - P2₁/n) and FpSnPh₃ (compound 7; monoclinic - P2₁/c) shows that the germanium and the silicon compound are isotopic. This means they have identical atomic coordinates, unit cells and molecular symmetries, which is shown for the germanium compound in the following figure.

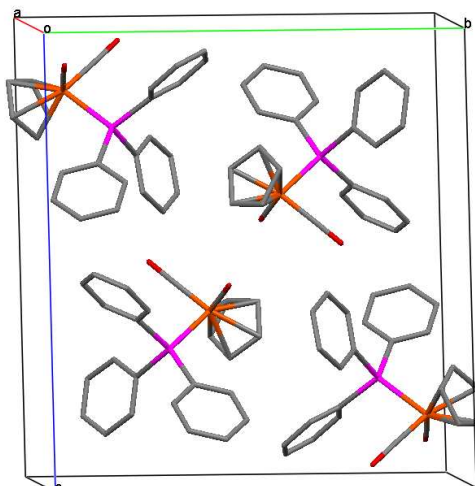


Figure 33: Unit cell of $FpGePh_3$

In comparison the tin compound is slightly different. Two of the three lattice constants are comparable but the third one (the monocline b-axis) is doubled, which is caused by a slight deviation in the packing of the molecules (see figure 31). In the unit cell of the tin compound two independent molecules are arranged in the asymmetric unit whereas in the corresponding silicon and germanium compounds only one symmetry independent molecule is included.

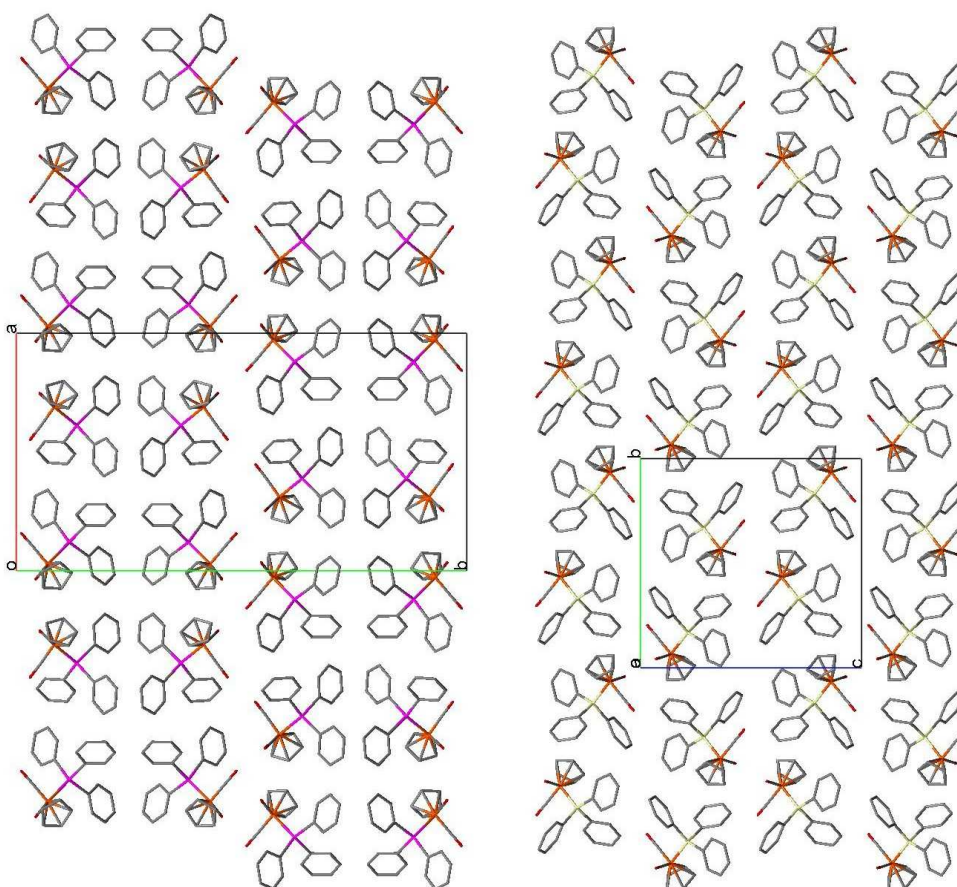
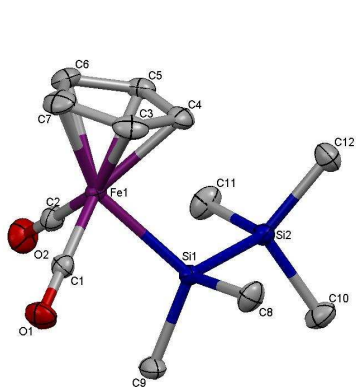
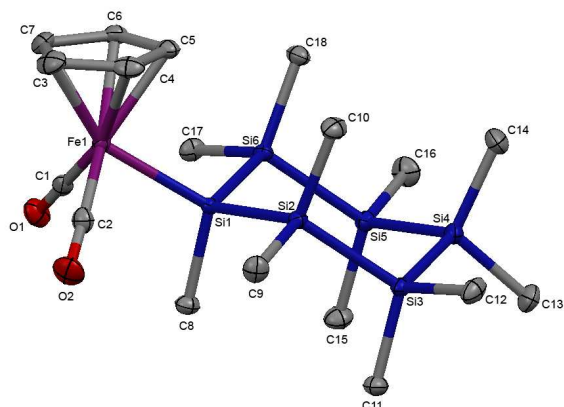


Figure 34: Packing of the Sn-compound (left) and of the Si (Ge) compound (right)

Part A: Synthesis and Calculations



FpSi_2Me_5



$\text{FpSi}_6\text{Me}_{11}$

The Fp-disilane (9) and the compound bearing the ring (10) both crystallize in a monoclinic crystal system with the space group $P2_1/n$.

The packing is shown for the crystals of 10.

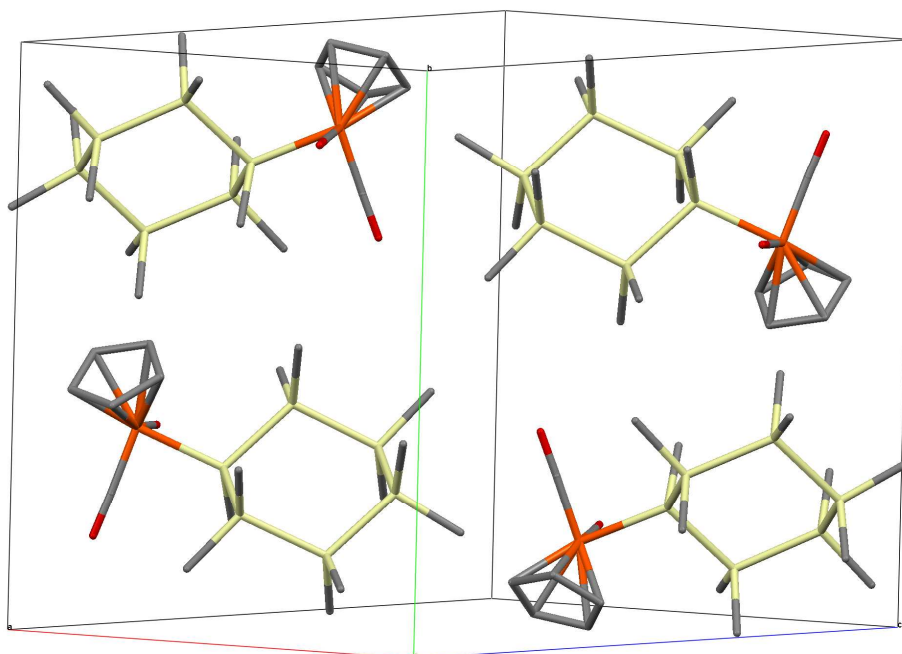


Figure 35: Packing of $\text{FpSi}_6\text{Me}_{11}$ molecules

Comparing the FpSiMe_3 compound (2) to the RpSiMe_3 (8) it was noted that the iron compound crystallized in a triclinic and the ruthenium one monoclinic C-centered space group. The unit cell of RpSiMe_3 has two independent molecules, which can be transferred into each other by the inversion center of the space group $P-1$.

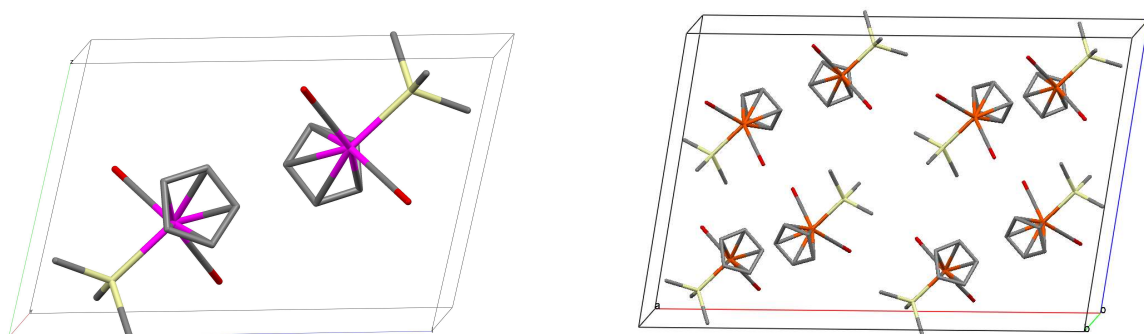


Figure 36: Unit cell for RpSiMe_3 (left) and FpSiMe_3 (right)

Table 11 lists the different measured iron-silicon bond lengths of the products compared to those calculated with mPW1PW91/6-311G**.

Table 11: Comparison between calculated and experimental Fe-Si bond lengths

Product	Fe-Si _{exp} [Å]	Fe-Si _{calculated} [Å]
FpSiMe ₂ SiMe ₃	2.3412	2.3747
FpSiPh ₃	2.3289	2.3741
FpSiMePh ₂	2.3263	2.3619
FpSiMe ₂ Ph	2.3199	2.3607
FpSiMe ₃	2.3164	2.3598
FpSiMe ₂ H	2.3119	2.3401

In this case the tendency is again well produced. Compared with the Fe-Si bond lengths in Fp-Hypersilyl (at 2.398 Å it is one of the longest Fe-Si bonds) these bonds are remarkably shorter. This is due to the fact that silicon substituents cause longer bonds evoked by electronic properties and steric effects. The slightly withdrawing effect of the phenyl group causes the bond length grows from the compound **2** to **5**.

A comparison of the Fe-E bonds with E = Si, Ge, Sn is shown in Table 12:

Table 12: Comparison of Fe-E (E = Si, Ge, Sn) bond lengths

Product	Fe-E _{exp} (E = Si, Ge, Sn) [Å]
FpSiPh ₃	2.3289
FpGePh ₃	2.3748
FpSnPh ₃	2.5330

Because of the low melting point of FpSiMe₃ and FpSiMe₂H these compounds were crystallized *in situ* on the diffractometer by zone-melting using an IR laser system.

A 3 Experimental part

A 3.1 General working techniques

Electrical equipment

For IR spectrums the Perkin Elmer 883 infrared grid spectrometer was used. The samples were put in an IR cell, in which the sample could be kept under nitrogen.

Nuclear magnetic resonance NMR measurements were done with a VARIAN 300 MHz machine. (^1H : 300 MHz, ^{13}C : 75.5 MHz, ^{29}Si : 59.6 MHz, ^{119}Sn : 111.9 MHz). As internal standard tetramethylsilane and as external one deuterated solvents were used. Depending on the sample either single pulse programs or measurements with INEPT (insensitive nuclei enhanced by polarization transfer⁵⁵) pulse sequences were performed.

Gas chromatographic – mass spectrometric GC-MS measurements were performed with devices from Agilent Technologies: 7890A GC System and a 5975C VL MSD System. The GC has a polysiloxane column with a length of 30 m, an inner diameter of 0.250 mm and a film of 0.25 μm .

Ultra violet UV measurements were performed by using a Perkin Elmer Lambda 35 UV/VIS spectrometer. The measurements were performed in dichloromethane and for the calculation of the molar extinction coefficient the concentration was taken, which gave absorption under 1.5 so that the Lamber Beersche Law is fulfilled.

X-Ray structures were performed by Prof. Jörg Albering or Asst. Prof. Roland Fischer. The X-Ray structures of samples that are liquids at room temperature could be obtained by using the so called OHCD (optical heating and crystallization device) laser. This is a focused IR laser which cools down the sample and slowly melts it up again zone wise. The advantages of this procedure are that the crystals grow from bottom to top can be optical observed, the capillary cannot be broken by mechanical damage, heat and position can be easily controlled and there is a high temperature gradient⁵⁶.

Single crystal X-ray diffraction data were collected on a Bruker KAPPA APEX II CCD diffractometer using graphite-monochromated $\text{MoK}\alpha$ radiation ($\lambda = 0.71073 \text{ \AA}$) and combination of 0.5° ω - and ϕ -frames covering the complete sphere of the reciprocal space with $\Theta = 29.84^\circ$. The crystal was cooled at 100 K using an OXFORD CRYOSTREAM. After data integration with the SAINT program a multi-scan absorption correction was performed with the program SADABS. Both programs are integrated in the Bruker APEX2⁵⁷ software package. The structure was solved by direct

⁵⁵ Helmer, B. J.; West, R.; *Organometallics*; **1982**, 1, 877-879

⁵⁶ Prof. Roland Böse; www.ohcd-system.com

⁵⁷ Bruker programs: APEX2, version 2008.3-0, Bruker AXS Inc., Madison, WI, **2008**

Part A: Synthesis and Calculations

methods, expanded with Fourier syntheses and refined on F2 with the program suite SHELX97⁵⁸. All non-hydrogen atoms were refined anisotropically, the hydrogen atoms were located on difference Fourier syntheses, assigned with isotropic displacement factors and included in the final refinement using the geometrical constraints of the HFIX command.

General working conditions

All reactions were performed under nitrogen atmosphere. The nitrogen was purified using a copper catalyst and phosphorus pentoxide.

Conventional Schlenk technique was applied during working.

The solvents were all taken from the solvent distillation apparatus, in which they were purified over ion exchange materials and used as obtained.

The electrolysis cell, all flasks, in which products or product solutions were put, and also the column used for column chromatography were wrapped in aluminum foil, because most of the products are sensitive against light, especially in solution.

Electrodes

H₂/Pt (hydrogen)-anode⁵⁹

With the help of a small tube, hydrogen is bubbled on a platinum net, thus surrounding the net with H₂. The platinum net is connected as the anode in the electrical circuit and therefore the hydrogen is oxidized to protons directly at the platinum net. This electrode was already successfully used for the generation of Si-C-bonds.

Magnesium anode

A magnesium rod was used as a sacrificial anode. The electrodes surface was etched (in an acid solution containing HCl), when already black and dried or was just polished with sandpaper when it was not so dirty. Afterwards it was dried with cellulose. The clean and shiny electrode was assembled in the electrolysis cell as fast as possible. The magnesium was contacted directly.

⁵⁸ G. M. Sheldrick, SHELX97: Program System for Crystal Structure Determination, University of Göttingen, Göttingen, Germany, **1997**

⁵⁹Patent: DE102004029258, 2006-01-12. Popp; A.; Weidner, R.; Stueger, H; Grogger C.; Loidl B.

Part A: Synthesis and Calculations

Silver cathode

A silver ounce was used as a cathode. It was also polished with sandpaper and dried with cellulose before using it. For electrolyses the silver was contacted with a copper wire.

Stainless steel cathode

For the divided cell different geometries of the stainless steel cathodes were used. Each of the electrodes was etched, dried, polished and dried again before using it. They were all contacted with a copper wire which must not touch the solution.

In the undivided cell cylindrical cathodes were used.

Supporting salt solution

A solvent for electrolysis must be aprotic, electrochemically stable and nonreactive versus reactants and products, especially versus generated anions. Also the starting materials, products and supporting salts should be soluble in the solvent. Therefore THF is a good choice because it fulfills all these wanted properties.

The supporting salt should also be electrochemically stable and soluble in the solvent. It must provide good electrical conductivity and should not react with the products formed during electrolysis (e.g. fluorinated compounds can make a halogen exchange with chlorinated products⁶⁰).

Tetrabutylammonium bromide is especially useful as supporting salt. Therefore we used it either alone as a 0.02 M THF solution or in combination with lithium chloride and magnesium chloride.

The supporting salt was always added to an evacuated and with nitrogen flushed flask and heated afterwards three times under vacuum until it started melting. After cooling down the THF was added.

Galvanostatic electrolysis

All electrolysis were performed in galvanostatic mode. This means that the current is set to a fixed value and the voltage regulates itself to the value of the easiest reducible compound in the solution.

This mode has the advantage that the electrolysis can be performed without a reference electrode and that the current yield can be easily calculated.

It is important to know how much current flowed through the electrolysis cell during the time the electrolysis is actively running in order to calculate the current yield.

The theoretical possible amount of substance yield can be expressed as:

⁶⁰ PhD Thesis, Fallmann, H.; 2001

Part A: Synthesis and Calculations

$$n = \frac{I * t}{z * F} \quad (12)$$

n ... amount of substance [mol]

I ... current [A]

t ... time of the electrolysis [s]

z ... number of transferred electrons

F ... Faraday constant = 96485.3399 [C/mol=As/mol]

With the same equation the time necessary for transferring all the starting materials to the wanted products can also be calculated.

The current yield can then be described as:

$$cy = \frac{n_{practical} * 100}{n_{theoretical}} = \frac{n_{practical} * F * z * 100}{I * t} \quad (13)$$

cy... current yield [%]

$n_{practical}$... obtained amount of substance [mol]

$n_{theoretical}$... theoretically possible amount of product [mol]

I ... current [A]

t ... time of the electrolysis [s]

z ... number of transferred electrons

F ... Faraday constant = 96485.3399 [C/mol=As/mol]

In general it can be said that if the resistance in the cell is too high, the current regulates itself to a lower value. That means that the current flow is not constant. Therefore an average value was estimated for the current flowing through the cell. The high resistance in the cell can have different reasons e.g. that there is no conversion of the starting materials or no products are created.

A 3.2 The undivided cell

The undivided electrolysis cell has just one compartment and no anion exchange membrane. Five openings are on the upper part of the cell: two for the electrodes and one for taking out the samples. The two left are for a siloxen faucet and a bubbler.

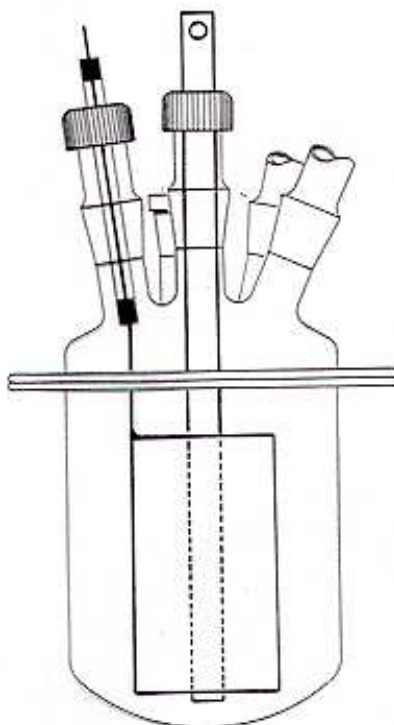


Figure 37: Undivided electrolysis cell⁶¹

The magnesium anode was always placed in the middle of the surrounding cylindrical cathode to obtain a uniform potential distribution. Given a fixed current density, the current which flows through the cell and the amount of substance converted is depending on the surface of the cathode. The bigger the surface of the cathode the more substance is reacted at the same current density. Therefore, the placing of the sacrificial anode in the center of the surrounding cathode is a good way to assemble the cell.

⁶¹ PhD thesis Fallmann, H.; 2001

A 3.2.1 Electrolyses performed in the undivided cell

General procedure

In a prepared flask (heated under vacuum, flushed with nitrogen) with stirrer 0.6 g Bu₄NBr (mw = 322.38 g/mol, n = 1.86 mol) were heated slightly under vacuum without melting it. After cooling down to room temperature 80 mL dry THF were put into the flask and the mixture was stirred, till all of the supporting salt was dissolved (mostly over night). After that the metal containing substance and the corresponding chloro compound were added in a molar ratio of 1:2 and stirred until totally dissolved.

The cell was assembled like shown in Figure 37, then heated under nitrogen flow and left for cooling down three times at least.

After immersing the electrolyte the whole cell is adjusted in an ultrasonic bath which provides effective rearrangement throughout the whole electrolysis. To prevent warming up, the ultrasonic bath must be cooled.

The reaction was started at fixed 10 mA. Depending on the voltage flowing through the cell the current was adjusted to it. After starting the reaction, in most cases an increase of the voltage could be observed. If the resistance in the cell at 10 mA was too high the reaction was stopped for a short time but the ultra sonic bath kept on running. After 1-2 hours the voltage should be stable and the reaction could be started again. If this was not the case the cell was kept without applied current and no ultrasound over night before starting it again on the next day.

When the electrolysis was running stable, the progress of the reaction was checked every 30 minutes preferably by IR measurements. To perform ²⁹Si-NMR on the reaction solution was not that easy, because of the metals and salts in the solution.

After the electrolysis was finished the always very dark brown solution was worked up.

A 3.2.2 Work up procedure

After transfer to a flask most of the solvent was removed by using a condensation bridge. The residual product mixture should not by any means dry out; there should always be around 5-10 mL solution left. (It is a hard and long job to dissolve the dry residue again!)

To the rest of the solution 50 mL of dry pentane and 30 mL of dry toluene were added. (If the mixture is not completely dissolved, 3-5 mL THF can be added)

The solution is filtrated over dry celite. A dark brown residue is staying on the celite.

After that a column with a Y-piece, siloxen faucet and stop plug was prepared according to figure 34.

Part A: Synthesis and Calculations

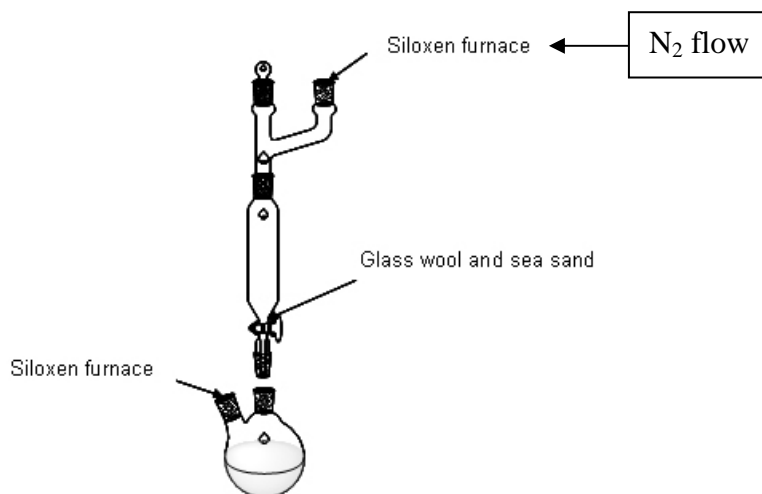


Figure 38: used column

Before using it, the silica gel should be dried at least one night in an oven. The still warm silica was transferred to a dried out two necked flask, and then evacuated. To the cooled down silica gel dry toluene was added until all the silica gel was mixed up with toluene and no bubbles were in the mixture. When adding toluene the solution warms up a bit. After that the mixture was transferred into the column. After some time the silica gel sets down and the toluene was emptied till just two millimeters of toluene were left over the surface of the compact silica gel.

The reaction mixture was concentrated to 5-10 mL and was transferred to the column with a syringe. The different products eluted with toluene can be easily recognized by their color. The reaction mixture is deep brown, the product yellow-orange and not reacted or re-reacted Fp_2 is red.

A by-product found in all electrolysis is ferrocene. It has an orange color and the fraction elutes after the product. On top of the column always a deep brown, nearly black residue stayed, which probably consists of different silicon-polymers. They could never be identified with certainty.

After that the product fractions were concentrated by using a condensation bridge and put into a refrigerator for crystallization.

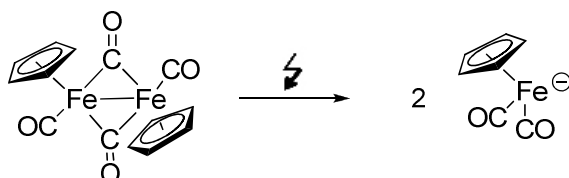
The yield of crystals or purified product is always much lower than the yield calculated out of IR and NMR data (85-95% yield). This is because the reaction is an equilibrium reaction, thus during the work up procedure Fp_2 reformed until the product is purified. So product is always lost during the work up procedure.

Another factor concerning the yield is that only very pure fractions were worked up and the product in it was isolated. Mixed fractions were not purified because of the high effort it would need to get the pure product again.

This two reasons are important to be considered concerning the product yields.

A 3.3 Electrolyses with Fp_2 in the undivided cell

A 3.3.1 Electrolysis of pure Fp_2



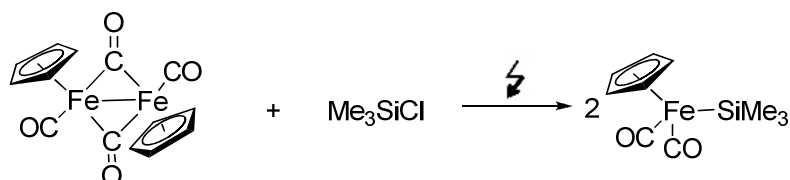
	Fp_2
m [g]	3.20
M [g/mol]	350.00
n [mmol]	9.14

The electrolysis could not be performed because after activation the resistance in the cell still was very high. Even after leaving the cell for four hours in the ultra sonic bath the total resistance did not get down. It was concluded that no electrolysis could be performed using just Fp_2 in the electrolysis cell. The starting material could not be converted under these conditions..

However after addition of a nucleophile, the reaction went on like usual.

A 3.3.2 Electrolyses of Fp_2 with mono chloro silanes

A 3.3.2.1 Formation of FpSiMe_3



	Fp_2	Me_3SiCl
m [g]	3.20	2.31
M [g/mol]	350.00	108.60
n [mmol]	9.14	21.27
ρ [g/mL]		0.856
V [mL]		2.70

The electrolysis was started at a fixed current level of 40 mA and a potential which starts at 20 V. After that the potential is slowly increasing till the resistance in the electrolysis cell was too high to run the electrolysis. Therefore the reaction was stopped for another 45 min and in between just the ultrasonic bath was running for activation. After that the potential was more or less stable at around a level of 42 V.

The electrolysis was complete after 3.6 h. That means just 14.7% of the theoretical electrolysis time (24.5 h) were needed.

After the work up procedure three different fractions (yellow, yellow-orange, orange) were collected. The solvent of the different fractions was removed and replaced by DME (1,2 dimethoxy ethane). After that the different fractions were put into the refrigerator for crystallization.

Every time when crystals were obtained, they melted away very quickly, when the temperature in the flask reached more or less room temperature. Therefore all the solvent was removed from the compound and a ductile-liquid solution was obtained. From this yellow-brownish liquid a crystal structure could be obtained using the so called OHCD technique.

In the end very pure 1.42 g of the product FpSiMe_3 could be isolated out of fraction 1. This is 31.1% of the theoretical yield. The yield corresponding to the NMR before the working up procedure was around 85-95%.

FpSiMe_3 :

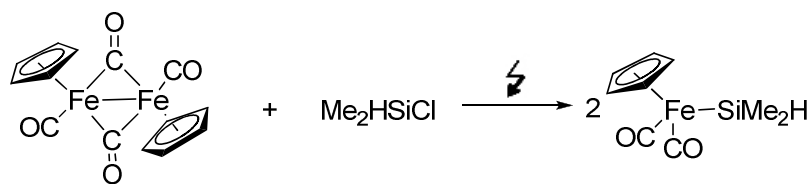
orange-brown liquid at room temperature (MW = 250.01 g/mol)

^{29}Si -NMR: 40.82 ppm (in THF, D_2O)⁶²

GC-MS data: 250 (M^+), 222 ($\text{M}^+ - \text{CO}$), 194 ($\text{M}^+ - 2\text{CO}$), 121 (194- Me_3Si), 73 (Me_3Si), 56 (Fe)

⁶² According to literature: Köhler, F. H.; Hollfelder, H.; Fischer, E. O. *J. Organomet. Chem.* **1979**, 168, 53; ^{29}Si -data in acetone- d_6 , TMS, 32°C: 40.8 ppm

A 3.3.2.2 Formation of FpSiMe₂H



	Fp ₂	Me ₂ HSiCl
m [g]	3.25	1.87
M [g/mol]	350.00	94.62
n [mmol]	9.28	19.81
ρ [g/mL]		0.852
V [mL]		2.2

The electrolysis was started but after ten minutes the resistance in the cell was too high, so that the current had to be switched off again. After two hours of activation in the ultrasonic bath the electrolysis was restarted. The current was fixed to 20 mA (\rightarrow 40V) and was stable for the next four hours during which the electrolysis was running. The IR showed that all bridging COs were gone, so the mixture was worked up. The theoretically necessary amount of time to convert all the products was calculated with 26.8 h. In the experiment just five hours (18.7% of the theoretical necessary time) were necessary for the total conversion of the product.

Column chromatography yielded two fractions (a yellow and an orange one) of the product:

Crystallization of the compound in DME at -30°C and -75°C failed. Therefore the crystal structures again were obtained by using the OHCD device technique taking the pure ductile – liquid orange-brown solution. Yield: 21%

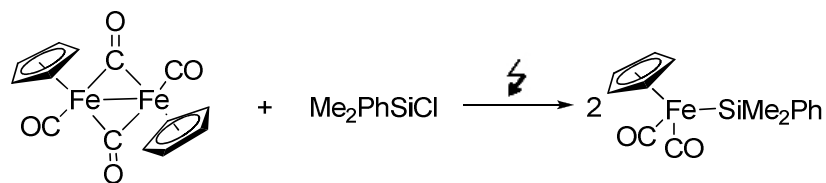
FpSiMe₂H:

brown, slightly orange liquid at room temperature (MW = 235.98 g/mol)

²⁹Si-NMR: 21.90 ppm (in THF, D₂O)

GC-MS data: 236 (M⁺), 220 (M⁺-O), 208 (M⁺-CO), 180 (M⁺-2CO), 164 (180 –MeH), 121(164-SiMe), 93 (Fe-Si), 56 (Fe)

A 3.3.2.3 Formation of FpSiMe₂Ph



	Fp ₂	Me ₂ PhSiCl
m [g]	3.2	3.46
M [g/mol]	350.00	170.71
n [mmol]	9.14	20.26
ρ [g/mL]		1.017
V [mL]		3.4

The electrolysis was started and left for 30 min at a current of 15 mA. Again the voltage slowly increased due to the rising resistance in the cell, so that the electrolysis had to be stopped after that but the ultra sonic bath was still running for activation. After one hour the electrolyses was started again at a fixed current of 15 mA. After 5 h and 15 min the electrolysis was finished. This means that the practical duration was just 5.6% of the theoretical one (93.0 h).

In this case the separation of the fractions was not so good. They were much broader than in the electrolyses performed before.

Collected were four different fractions (yellow, orange, orange and slightly brownish).

When using DME for crystallization of the products obtained in the first two fractions, small, yellow-orange crystals were generated at a temperature at -78°C. These crystals were stable at room temperature. The X-Ray structure showed that it was the product we wanted. The yield of the first fraction, from which the crystals for X-Ray were taken, was 23.4% of the theoretical one.

FpSiPhMe₂:

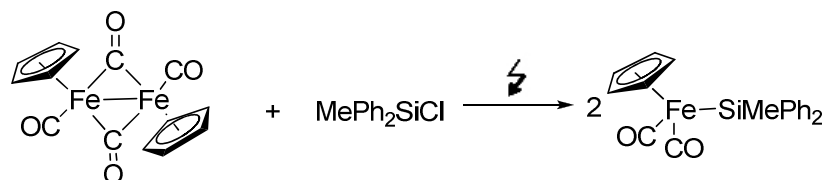
Orange crystals at room temperature (MW = 312.03 g/mol)

²⁹Si-NMR: 35.91 ppm, (in THF, D₂O)

GC-MS data: 312 (M⁺), 284 (M⁺-CO), 256 (M⁺-2CO), 178 (Me₂SiFeCp), 135 (Me₂Si), 121 (CpFe)

Melting interval: 66-68°C

A 3.3.2.4 Formation of FpSiMePh₂



	Fp ₂	MePh ₂ SiCl
m [g]	3.2	4.26
M [g/mol]	350.00	232.78
n [mmol]	9.14	18,28
ρ [g/mL]		1.107
V [mL]		3.8

It was not possible to make an NMR of the starting solution immediately, so the cell was kept under nitrogen flow during the night and the reaction was started on the next morning.

The electrolysis was started at 40 mA. The voltage stayed constant from the beginning on. A reason for that could be that the reaction mixture already had time to equilibrate with the magnesium electrode because it was left in the cell over night. After four hours the reaction was finished.

Theoretically the electrolysis should take 24.5 h., practically it took four hours to convert the starting material. So this means it took just 16.3 % of the theoretically necessary time.

After the working up procedure, two fractions were collected (yellow, orange).

From the first fraction the FpSiMePh₂ crystals could be obtained by crystallization out of toluene at -78°C. From these yellow-orange product a X-Ray structure was obtained. Yield of pure crystalline product: 27.2%.

FpSiMePh₂

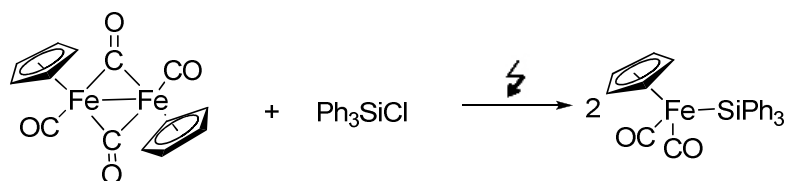
yellow - orange crystals at room temperature (MW = 374.04 g/mol)⁶³

²⁹Si-NMR: 35.91 ppm (in THF, D₂O)

GC-MS data: 374 (M⁺), 318 (M⁺-2CO), 197 (M⁺-2CO), 121 (197-CpFe), 56 (Fe)

Melting interval: 99-104°C

⁶³ According to literature: Kückmann, T. I.; Dornhaus, F.; Bolte, M.; Lerner, H.-W.; Holthausen, M. C.; Wagner, M. *Eur. J. Inorg. Chem.* **2007**, 14, 1989

A 3.3.2.5 Formation of FpSiPh_3 

	Fp_2	Ph_3SiCl
m [g]	1.8	2.95
M [g/mol]	350.00	294.85
n [mmol]	5.14	10.01

The electrolysis was started and the resistance in the cell was increasing very fast, so the current had to be switched off after five minutes, just the ultra sonic bath was still running for activation. After activation the electrolysis was started again.

Totally the electrolysis ran for 11h 44 min at an average current of 40 mA. The theoretical duration for the electrolysis at 40 mA would be 13.40 h. This means that the practical electrolysis time is 85.4% of the theoretical necessary time. This is much longer compared to the other electrolysis!

After the working up procedure two fractions were obtained (a yellow one and a yellow-greenish one).

From the first very pure fraction crystals could be obtained using toluene at -78°C , thus allowing performing X-Ray analysis. The yield of this fraction is 1.51 g (37.9%).

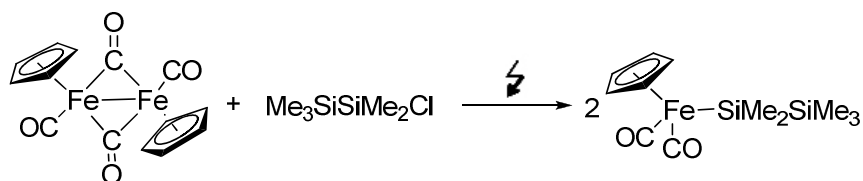
 FpSiPh_3

orange crystals at room temperature (MW = 436.06 g/mol)

$^{29}\text{Si-NMR}$: 36.31 ppm (in THF, D_2O)

GC-MS data: 436 (M^+), 408 (M^+-CO), 380 (M^+-2CO), 259 (Ph_3Si), 181 (Ph_2Si), 121 (Cp-Fe), 78 (Ph), 56 (Fe)

Melting interval: $166-168^\circ\text{C}$

A 3.3.2.6 Formation of FpSi_2Me_5 

	Fp_2	$\text{Me}_3\text{SiSiMe}_2\text{Cl}$
m [g]	1.9	1.8
M [g/mol]	350.00	166.8
n [mmol]	5.43	10.79

The electrolysis was performed at 15 mA . After 6 h the electrolysis was finished. The theoretically necessary time is 38.6 h. This means the reaction was finished in 15.5% of the theoretical duration.

After the work up procedure a solution of 1.87 g (56%) of the corresponding product out of toluene was obtained.

This solution was not only pure product therefore, it was worked up once more according to the general procedure described above. After that a clean product could be obtained. This was crystallized out of DME at -78°C .

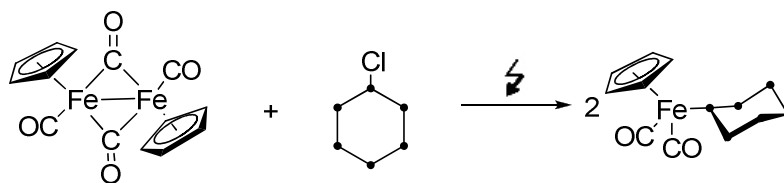
From this yellowish green crystal an X-Ray structure could be recorded (yield: 25%).

 $\text{FpSiMe}_2\text{SiMe}_3$

Yellowish green liquid at room temperature (MW = 305.13 g/mol)

^{29}Si -NMR: -11.5 ppm and 16.2 ppm for the silicon next to the iron atom (in THF, D_2O)⁶⁴

⁶⁴ according to literature: Fallmann, H. *PhD-Thesis* 2001, TU Graz

A 3.3.2.7 Formation of $\text{FpSi}_6\text{Me}_{11}$ 

	Fp_2	$\text{Si}_6\text{Me}_{11}\text{Cl}$
m [g]	1.8	3.69
M [g/mol]	350.00	369.35
n [mmol]	5.14	10.00

After starting the electrolysis in the first 20 min the potential increases so much that the reaction had to be stopped due to the high resistance in the cell. So it was left in the ultra sonic bath for activation during three hours. The same thing happened once more. So the whole procedure was repeated.

After that the electrolysis was kept at 12.5 mA for 2 h 15 min and than the current was increased. In total the electrolysis was activated for 12 h 20 min at a fixed current level of 40 mA. This means that compared to the theoretically necessary time the electrolysis needed 93.28% of the time.

After the work up procedure the following fractions were obtained (two yellow and one orange one).

Crystals were obtained out of toluene and DME at -35°C at -78°C . They were analyzed via X-Ray. Out of fraction 1 0.35 g of the product were obtained. This is a yield of 6.9 %. Out of the second fraction another 38.7% of product could be obtained.

 $\text{FpSi}_6\text{Me}_{11}$

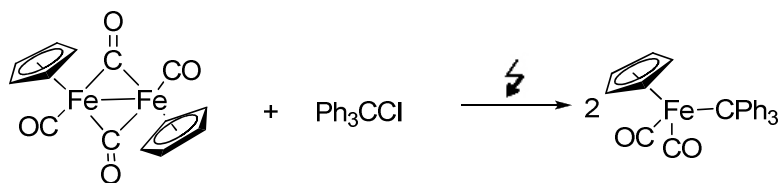
Yellow-orange crystals at room temperature (MW = 508.90 g/mol)⁶⁵

²⁹Si-NMR: -15.17 ppm and -29.77 ppm, -40.44 ppm, -43.05 ppm (in THF, D₂O)

⁶⁵ According to literature: Hoffmann, F.; Bohme, U.; Röwer, G. *Organosilicon Chem.: From Mol. to Mater.* **2005**, 6, 445

A 3.3.3 Electrolysis of Fp_2 with other group (XIV) elements

A 3.3.3.1 Electrolysis of Fp_2 with Ph_3CCl



	Fp_2	Ph_3CCl
m [g]	1.75	2.79
M [g/mol]	350.00	278.78
n [mmol]	5.00	10.00

After starting the electrolysis, the potential increases very fast, so that it had to be stopped after 5 min. Then the cell was kept in the ultrasonic bath for one hour. The electrolysis was run after that for 6 h 55 min at a level of 30 mA. This is corresponding to 34.7% of the theoretical amount.

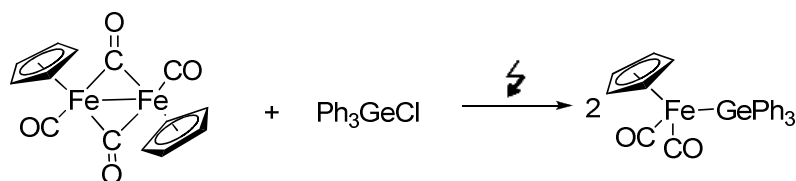
Electrolysis was stopped because the dark brown solution turned bright red.

When taking out the sample it can be seen that the sample in the IR-cell turns from red to brown. This and the really bright red color indicate, that during the electrolysis the Ph_3C anion was complete⁶⁶ indicating that the Ph_3CCl is easier to reduce than the Fp_2 . But if Fp_2 does not react no active species for Fe-element bond formation is present. Therefore the reaction leads to other products.

→ The solution was not worked up.

⁶⁶ Fernandez, I, et al ; *Chem. Eur. J.*; **2005**, 11,1495-1506; Okano, M. et al; *Electrochimica Acta*, **1995**, 40 (12), 2017-2018

A 3.3.3.2 Formation of FpGePh_3



	Fp_2	Ph_3GeCl
m [g]	1.6	3.39
M [g/mol]	350.00	339.36
n [mmol]	4.57	10.00

After activating the electrolysis the potential is slightly increasing and in one hour the voltage reaches over 80 V at a fixed current of 15 mA. That is why it had to be shut down again for another hour. After that the same thing was repeated once more. During the weekend the electrolysis solution was transferred to a prepared flask and put into a refrigerator.

After putting the solution back into the freshly prepared cell, the cell was kept in the ultrasonic bath for another hour. The potential again after two hours at 10 mA reached a high level so that the reaction had to be stopped again. In total the electrolysis ran for 2 h at 10 mA and for 40 min at 25 mA. This corresponds to 5% of the theoretically necessary amount of time (48.2 h at 10 mA)

After that the solution underwent the work up procedure.

Doing column chromatography three different fractions were collected. All of them were yellow.

With these three fractions again different crystallization methods were tried. Dichloromethane, DME, toluene and also the method with the bubbler over a schlenk flask was tried using a mixture of toluene and CH_2Cl_2 .

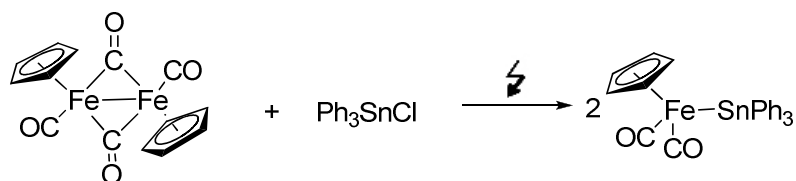
Finally the solvent, which gave crystals useful for X-Ray, was benzene. A yield of 73.5%, which corresponds to 3.24 g of the compound, could be obtained.

FpGePh_3

white-orange powder (MW = 480, 57 g/mol)

Melting interval: 158-159°C

A 3.3.3.3 Formation of FpSnPh_3



	Fp_2	Ph_3SnCl
m [g]	3.2	7.70
M [g/mol]	350.00	385.46
n [mmol]	9.14	19.98

Before starting, the electrolysis cell was kept in the ultra sonic bath for 2 h. After that the electrolysis was started with a current fixed at 40 mA. The potential was stable during the whole electrolysis, which lasted for 6.33 h at around 30 V. This time makes up 25.9% of the theoretical necessary time at 40 mA.

When the solution was taken out and put into a prepared flask, it could be seen that a grey film stayed back in the cell (tin mirror).

In this case the product already could be seen during the work up procedure. Some of the product already precipitated during the working up procedure because it is insoluble in pentane. This amount of product was diluted in toluene and added to the column. The rest of the work up procedure was performed as usual.

Different solvents, temperatures and crystallization techniques were tried to get crystals of the product, but none of these attempts worked. Finally they could be obtained out of toluene using non inert conditions.

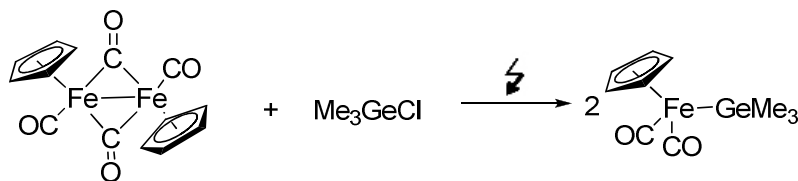
From these crystals an X-Ray could be done. The total yield of pure products obtained was 55.4% of the theoretical possible one.

FpSnPh_3

White-yellowish powder at room temperature (MW = 541.11 g/mol)

^{119}Sn -NMR: 63.28 ppm (in THF, D_2O)

Melting interval: 135-139°C

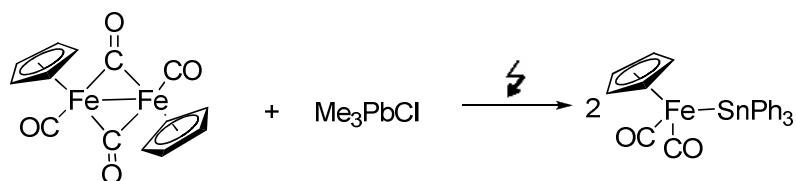
A 3.3.3.4 Electrolysis of Fp_2 with Me_3GeCl 

	Fp_2	Me_3GeCl
m [g]	2.8	2.50
M [g/mol]	350.00	153.15
n [mmol]	8.00	16.31
ρ [g/mL]		1.249
V [mL]		2.00

After starting the electrolysis the resistance in the cell increased slowly. Even after the attempt to activate the electrolysis by using the ultra sonic bath and letting it equilibrate over night, the resistance did not go down. No current flow could be obtained and therefore no electrolysis could be performed.

→ Reaction could not be started. No products could be obtained according to the unchanged IR spectra.

A 3.3.3.5 Electrolysis of Fp_2 with Me_3PbCl



	Fp_2	Me_3PbCl
m [g]	3.2	2.9
M [g/mol]	350.00	287.7
n [mmol]	9.14	10.08

The solution was electrolyzed for 7.5 h at 40 mA. This equates to 58.17% of the theoretically needed time (13.51 h).

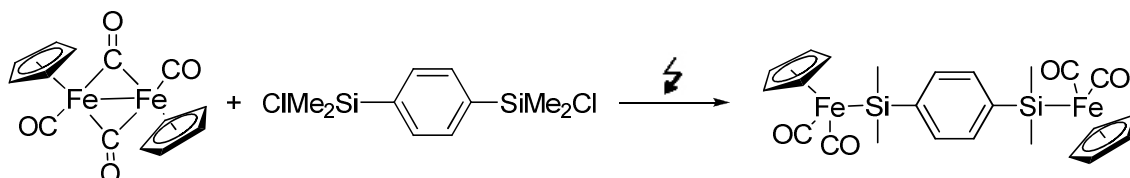
After taking out the solution of the electrolysis cell, it could be easily seen that a lot of elemental lead sticks to the wall of the cell and the magnesium electrode.

After the work up procedure an X-Ray structure of the main fraction was made. From this data it could be easily seen that the main product is ferrocene. The lead was lost during the work up procedure in form of a lead mirror, which could be seen during the proceeding of the work. E.g. when doing column chromatography much more brown- black residue sticks to the top of the column and much more brown-black substance goes into it.

→ The reaction did not show the products expected, but the main products were ferrocene and lead.

A 3.3.4 Electrolysis of Fp_2 with dichloro silanes

A 3.3.4.1 Electrolysis of Fp_2 with $\text{ClSiMe}_2\text{-Ph-SiMe}_2\text{Cl}$ (1:1)



	Fp_2	$\text{ClSiMe}_2\text{-Ph-SiMe}_2\text{Cl}$
m [g]	3.60	2.70
M [g/mol]	350.00	262.01
n [mmol]	10.28	10.30

The electrolysis begins with a very small cell resistance, but during the first 30 min it increases significantly. So the reaction had to be paused for an hour with the ultra sonic bath still running. After that it was started again at 40 mA and complete conversion of Fp_2 could be seen in the IR after 10 h and 4 min. This is 72.74% of the theoretical needed time amount.

After the work up procedure again three fractions were collected: a yellow, a slightly orange and an orange one.

It seems that the product is very sensitive to UV light, because after leaving the product over night in solution it turned from orange to slightly brownish. To get a clean product column chromatography was performed again. The product was obtained in two orange fractions.

Different solvents were used for crystallization attempts: Toluene, DME, pentane, benzene, CH_2Cl_2 , xylol and ether. The product always precipitates just as white-orange powder, which was not at all useful for X-Ray analysis. The yield obtained from the first fraction was 36.7%

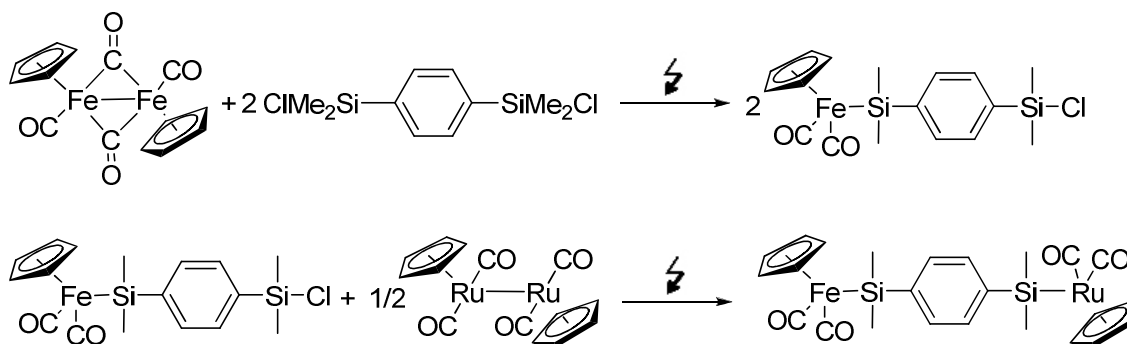
$\text{FpSiMe}_2\text{-Ph-Me}_2\text{Si-Fp}$

$^{29}\text{Si-NMR}$: 35.61 ppm (in THF, D_2O)

GC-MS: 490 (M^+-2CO), 434 (M^+-4CO), 369 (434-Cp), 313 (434-2Cp)

Melting interval: 91-95°C

A 3.3.4.2 Electrolysis of Fp_2 with $ClSiMe_2-Ph-SiMe_2Cl$ (1:2) and subsequent electrolysis with Rp_2



	Fp_2	$ClSiMe_2-Ph-SiMe_2Cl$	Rp_2
m [g]	2.63	3.93	3.33
M [g/mol]	350.00	262.01	444.14
n [mmol]	7.51	15.00	7.50

1.) Electrolysis of Fp_2 with $ClSiMe_2-Ph-SiMe_2Cl$

In the beginning of the electrolysis the resistance in the cell was too high to perform it because no current flow could be obtained. Therefore the cell was kept in the ultra sonic bath for one hour to activate the reaction. After that the electrolysis was kept at 40 mA for 2.5 h (12.4% of calculated time). Then-the reaction was finished and no bridging CO could be seen in IR anymore.

2.) Electrolysis of Rp_2 with $Fp-SiMe_2-Ph-SiMe_2Cl$

Rp_2 , diluted in ~ 10 mL THF, was added directly into the reaction mixture of the first step. After three hours at fixed 40 mA the electrolyses was stopped. This is equal to a percentage of 29.85% of the theoretically necessary electrolyses time.

After work up and purification the one yellow fraction obtained was analyzed via GC-MS. According to GC-MS the mixture contains $Fp-SiMe_2-Ph-SiMe_2-Fp$ and $Fp-SiMe_2-Ph-SiMe_2Rp$ in a ratio of 9:1. No clean product of the ruthenium compound could be obtained.

Part A: Synthesis and Calculations

FpSiMe₂-Ph-Me₂Si-Fp

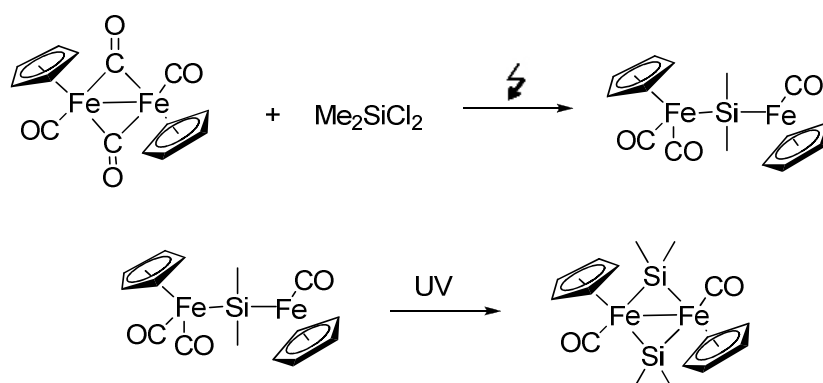
²⁹Si-NMR: 35.61 ppm (in THF, D₂O)

GC-MS: 490 (M⁺-2CO), 434 (M⁺-4CO), 369 (434-Cp), 313 (434-2Cp)

Melting interval: 91-95°C

FpSiMe₂-Ph-Me₂Si-Rp

GC-MS: 535 (M⁺-2CO), 518 (M⁺-2CO,-O), 490 (M⁺-3CO,-O)

A 3.3.4.3 Electrolysis of Fp_2 with Me_2SiCl_2 

	Fp_2	Me_2SiCl_2
m [g]	1.60	0.64
M [g/mol]	350.00	129.06
n [mmol]	4.57	4.97
ρ [g/mL]		1.07
V [mL]		0.60

In the first 20 min after starting the electrolysis the resistance in the cell strongly increases. That is why after that time the cell was kept for an hour just in the ultra sonic bath without applied current. When switching the reaction on again after that time, the potential was stable and the electrolysis was performed for 4h 10 min at 40 mA. This is about 66.51% of the theoretically necessary time. The product could be analyzed via NMR analysis.

Work up and column chromatography yielded two light red fractions. No orange or yellow one could be seen. After doing an X-Ray analysis of the obtained crystals the product found could be identified as $\text{Fp}_2(\text{SiMe}_2)_2$. The yield was 22%.

Intermediate: FpSiMe_2Fp

^{29}Si -NMR: 98.5 ppm (THF, D_2O)⁶⁷

 $\text{Fp}(\text{SiMe}_2)_2\text{Fp}$

Slightly red crystals

^{29}Si -NMR: 243.8, 229.5 ppm (CD_2Cl_2)⁶⁸

⁶⁷ According to the ^{29}Si -NMR database used on the institute

⁶⁸ Ueno, K.; Nagato, H.; Mamoru, S.; Hiroshi, O. *Organometallics* **1991**, 10, 959-962

A 3.4 Electrolyses of Rp_2 in the undivided cell**A 3.4.1 Electrolysis of Rp_2 with Me_3SiCl** 

	Rp_2	Me_3SiCl
m [g]	2.11	1.087
M [g/mol]	444.14	108.64
n [mmol]	4.75	10.01
ρ [g/mL]		1.0864
V [mL]		1.27

In this electrolysis the conversion could not be monitored by IR, because no bridging COs are available, but could by NMR.

The electrolysis was run for 8 h 15 min at 30 mA. The theoretically necessary time for the electrolysis would have been 16.33 h. Therefore, the experimental duration is consistent with 50.52% of the theoretical time.

In the end of the electrolysis still a bit of the starting silane was available, but the resistance in the cell dropped and therefore it was assumed that the reaction is finished. The electrolysis was stopped to avoid the generation of by-products, because a reason for the resistance going down could be that the wanted reaction was over and another compound was reacted.

After the work up procedure the following fractions were collected:

1. a yellow, slightly orange one
2. a deep orange solution
3. and a blue-grayish one (Probably this fraction contains ruthenium oxide, which has a blue color and can be easily produced during the procedure.).

There were also other by-products but they were not identified.

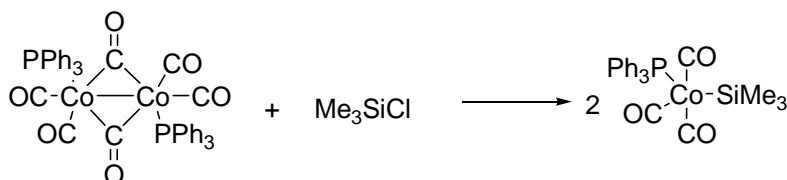
X-Ray analysis of fraction 1 was possible by the using of the OHCD device. The yield obtained of this fraction was 27%.

 $RpSiMe_3$

Brownish ductile liquid (MW = 174,252 g/mol)

^{29}Si -NMR: 26.92 ppm (in DME, D_2O)

A 3.4.2 *Electrolysis of $\text{Co}(\text{CO})_3\text{PPh}_3$ with trimethyl chloro silanes in the undivided cell*



	$\text{Co}(\text{CO})_3\text{PPh}_3$	Me_3SiCl
m [g]	2.11	0.255
M [g/mol]	444.14	108.64
n [mmol]	4.75	2.46
ρ [g/mL]		0.85
V [mL]		0.3

The resistance in the cell was not high and a current flow of 40 mA could be obtained. Electrolysis could be performed for 6 h at this current level. This is more or less the time necessary for total conversion of the starting material.

The work up procedure was performed in the same way as usual.

No silicon containing product could be obtained and the products of the different fractions could not be analyzed.

A 3.5 Electrolyses in the divided cell

The assembly of this cell as an example with the silver cathode, the H₂/Pt anode and an ion exchange membrane MA3475 is shown in Figure 39 .

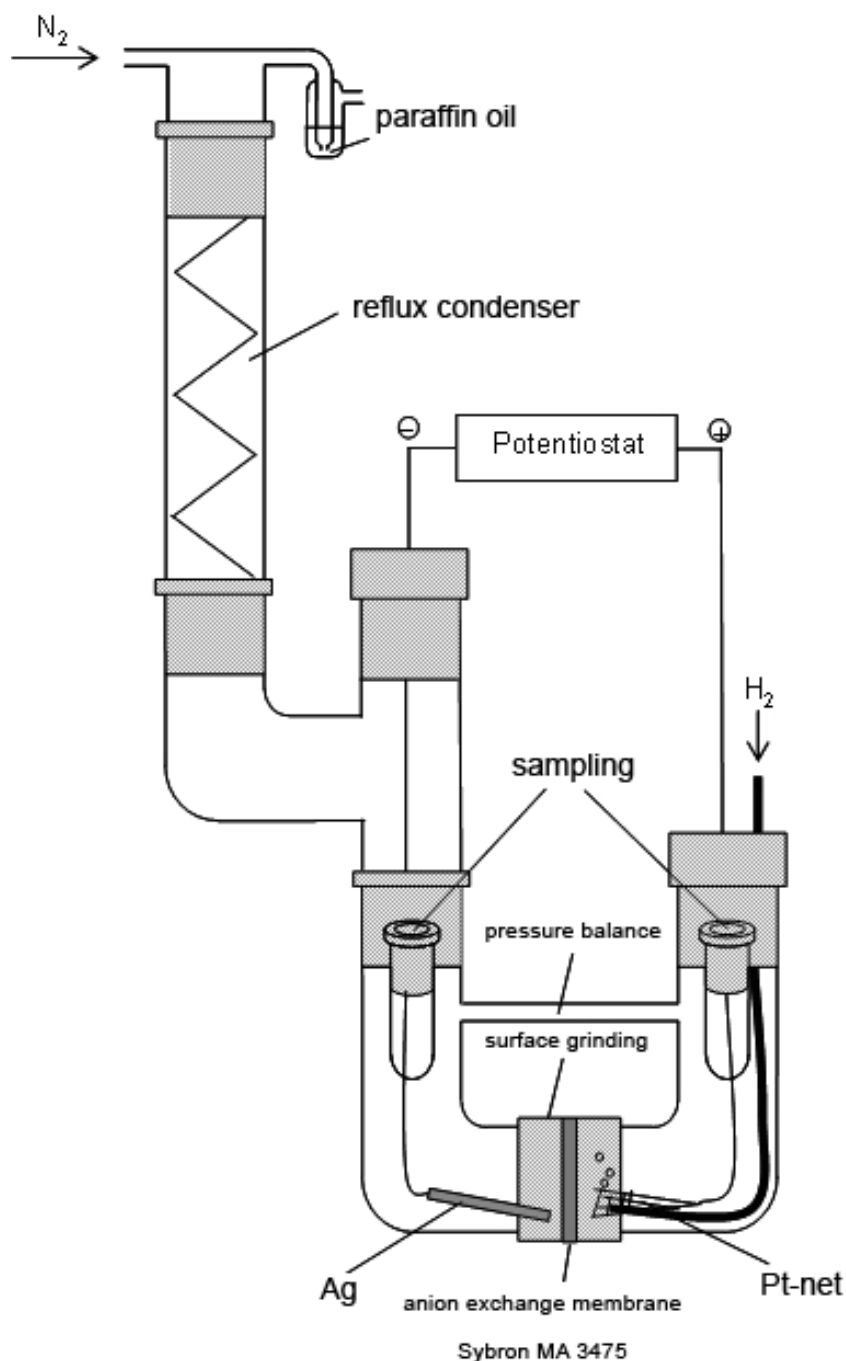


Figure 39: Divided cell with Pt/H₂-anode, silver cathode and an anion exchange membrane MA 3475⁶⁹

The cell was cooled with a water tube which was surrounding the whole cell in loops.

⁶⁹ PhD – Thesis, Stephan, J.; 2007

The membrane

The membrane must be stable in the electrolyte and should not react with the different reactants and products. It was always conditioned by putting it into the solvent at least over night, so that the membrane can swell.

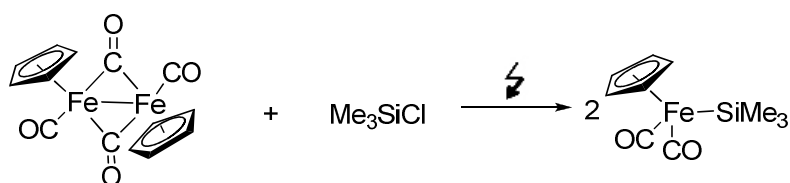
The anion exchange membrane has a chloride selectivity, which means that the chloride ions can selectively go through the membrane whereas other molecules can not pass. Also the protons generated at the electrode when using the Pt/H₂ electrode should stay in the anodic compartment

As membrane either the MA3475 or the MA700 were used. They differ in their thickness. Both membranes are from the company LANXESS Sybron Chemicals Inc.⁷⁰

Realization and results

General procedure:

The following reaction between cyclopentadienyl iron (II) dicarbonyl dimer (Fp₂) and trimethyl chlorosilane was tried to be performed in the divided cell:



Scheme 17: Reaction of Fp₂ with trimethyl chlorosilane

The membrane for the divided cell was conditioned at least for two days in THF.

The electrolyte was prepared as described before. The trimethyl chlorosilane was also put into the solution and the whole mixture was stirred over night to make sure that the solution is dry.

On the next day the Fp₂ was added and the solution was stirred for a short time. The conditioned membrane was put into the electrolyses cell being still wet of solvent.

The solution was added under nitrogen flow either to both compartments, or just into one. This means in both compartments Fp₂ was available or in just one. If Fp₂ was just in one then in the other a solution without Fp₂, but prepared the same way, was added.

Then the cooling, also the stirring of the solution and the electrolysis were started.

The electrolysis was kept at such current that the voltage always was between 40 and 70 V.

In the beginning the voltage level was watched for the first ten minutes. After that every thirty min the progress of the electrolysis was monitored via ²⁹Si-NMR or IR.

⁷⁰ 200 Birmingham Road, Birmingham, NJ 08011; alazar@sybronchemicals.com

Part A: Synthesis and Calculations

Although the parameters like solvent, membrane, electrodes and the electrolyte were varied, no results could be obtained using the divided cell. None of the reactions gave the corresponding product. Even an activation of the magnesium electrode by the use of an ultrasonic bath did not show results.

A 3.6 Calculations

A 3.6.1 Introduction

Calculations can be used to predict chemical properties of molecules, like their energy, stability of conformers, NMR, IR and UV spectra. These calculated data can then be used for a comparison with experimentally obtained data.

DFT (density functional theory) calculations were used to calculate the properties of the investigated molecules. Basis of this theory is that the electronic energy of the ground state of a system is defined through the electron density. The electron density is just dependent on the coordinates but not on the number of electrons. Calculations with this method are usually faster than e.g. Hartree Fock ones.

Although DFT is from its principal an ab initio method, the unknown form of the correct density functional leads to the use of approximate ones. These are often constructed using empirical data making DFT a semiempirical method.⁷¹

The available exchange-correlation functionals can be described by different approaches. One of them is the Local Density Method (LDA), in which the density is considered as an electron gas, other ones are gradient corrected methods GGA. In the GGA methods the electron gas is considered as inhomogenous and therefore the electron exchange functional is not only dependent on the electron density but also on the derivative of the density. One of these functionals is the Becke-Lee-Young-Paar B-LYP⁷². Another way to calculate the electron densities are hybrid functionals like B3LYP⁷³, which was mainly used in this work.

For the calculations it is important, which basis functions are being used. The basis set is a combination of mathematical functions, from which the wave function is constructed⁷⁴. A linear combination of the base functions describes the spin orbitals. By that the progress of the electron density can be described.

The basis set consists of different basis functions. For a complete basis an infinite number of basis functions would be necessary. Two main types of them exist: slater type orbitals (STO) and gaussian type (GTO) ones.

A single valence basis set is one, in which one basis function is defined for each type of orbital. This means e.g. for hydrogen there is only a 1s function.

A way to increase the flexibility is the decontraction of the basis set like STO-3G, in which each basis function is a sum of three Gaussians.

⁷¹ Young, D. C. *Computational Chemistry*, Wiley, New York **2001**, 43

⁷² Lee, C.; Yang, W.; Paar, R. G. *Phys. Rev. B* **1988**, 37, 785

⁷³ Becke, A. D. *J. Chem. Phys.* **1993**, 98, 5648

⁷⁴ Cramer, C. J. *Essentials of Computational Chemistry*, Wiley, England, **2002**, 154

Part A: Synthesis and Calculations

Split valence basis sets, like the one used, treat the inner orbitals different to the outer - valence ones like e.g. the 6-31G. The inner orbitals do not have such small contractions as the outer ones and therefore the outer ones are more flexible for the description of chemical bondings. For this basis set this means that 9 basis functions and 22 primitive Gauss functions are defined.

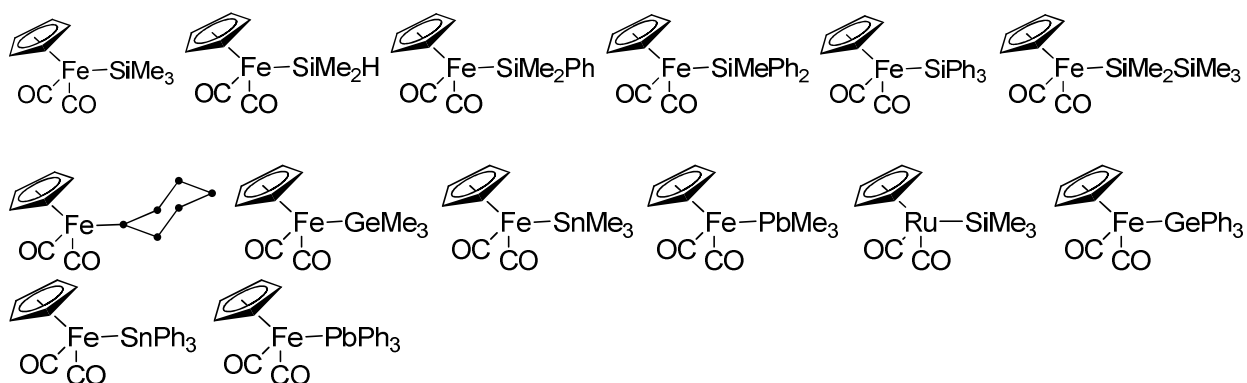
Another thing, which leads to better description are polarization or diffuse functions.

In this work mainly split valence triple zeta basis sets were used with two polarization functions.

A 3.6.2 Experimental Part

1.) Geometry and frequency calculations

The following molecules were calculated:



The program Gaussian03 was used for all the calculations⁷⁵.

⁷⁵ Gaussian 03, Revision C.02,
M. J. Frisch, G. W. Trucks, H. B. Schlegel, G. E. Scuseria,
M. A. Robb, J. R. Cheeseman, J. A. Montgomery, Jr., T. Vreven,
K. N. Kudin, J. C. Burant, J. M. Millam, S. S. Iyengar, J. Tomasi,
V. Barone, B. Mennucci, M. Cossi, G. Scalmani, N. Rega,
G. A. Petersson, H. Nakatsuji, M. Hada, M. Ehara, K. Toyota,
R. Fukuda, J. Hasegawa, M. Ishida, T. Nakajima, Y. Honda, O. Kitao,
H. Nakai, M. Klene, X. Li, J. E. Knox, H. P. Hratchian, J. B. Cross,
C. Adamo, J. Jaramillo, R. Gomperts, R. E. Stratmann, O. Yazyev,
A. J. Austin, R. Cammi, C. Pomelli, J. W. Ochterski, P. Y. Ayala,
K. Morokuma, G. A. Voth, P. Salvador, J. J. Dannenberg,
V. G. Zakrzewski, S. Dapprich, A. D. Daniels, M. C. Strain,
O. Farkas, D. K. Malick, A. D. Rabuck, K. Raghavachari,
J. B. Foresman, J. V. Ortiz, Q. Cui, A. G. Baboul, S. Clifford,
J. Cioslowski, B. B. Stefanov, G. Liu, A. Liashenko, P. Piskorz,
I. Komaromi, R. L. Martin, D. J. Fox, T. Keith, M. A. Al-Laham,
C. Y. Peng, A. Nanayakkara, M. Challacombe, P. M. W. Gill,
B. Johnson, W. Chen, M. W. Wong, C. Gonzalez, and J. A. Pople,
Gaussian, Inc., Wallingford CT, 2004.

Part A: Synthesis and Calculations

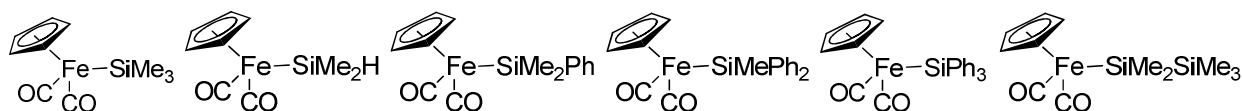
At first all the geometries were optimized with B3LYP/3-21G**, but no suitable geometries could be obtained. After that the optimization was performed with B3LYP/6-311G**. With this basis set a useful geometry could be obtained.

For the optimized geometries frequency calculations were performed. They are very used to verify that the geometry really is a minimum on the potential energy surface. For minima all frequencies have to be real.

2.) ²⁹Si-NMR calculations

Based on the optimized structures NMR calculations were done using the same level of theory namely B3LYP/6-311G**.

The calculations were done for the following molecules:



TMS, tetramethylsilane, was used as reference. As result for the TMS a magnetic shielding σ of 340.66 ppm was obtained. The chemical shift of the respective compound is obtained by the following equation:

$$\delta_{comp.} = \sigma_{ref} - \sigma_{comp.}$$

$\delta_{comp.}$... chemical shift of the compound [ppm]

σ_{ref} ... magnetic shielding of the reference [ppm]

$\sigma_{comp.}$... magnetic shielding of the compound [ppm]

The comparison between the experimental and the calculated NMR chemical shifts allowed the identification of the products.

To improve the NMR results calculations were also performed with mPW1PW91/6-311G** and with IGLOII for the atoms: Si, O, C and H. The last basis set is not available for iron therefore another triple zeta basis set was used for Fe.

3.) UV calculations

Based on the optimized geometries the UV calculations were performed with TurboMole and compared to the measured spectra.⁷⁶

All the molecules, for which geometry optimization was done, were used for the UV calculations.

⁷⁶ TURBOMOLE V6.2 2010, a development of University of Karlsruhe and Forschungszentrum Karlsruhe GmbH, 1989-2007, TURBOMOLE GmbH, since 2007; available from <http://www.turbomole.com>.

Part B: Application of the synthesized compounds as coating materials

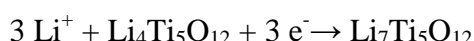
B 1 Coating of lithium electrodes: Introduction and Motivation

Due to the extensive demand of efficient energy storages for renewable energies and for vehicles, there is high need in the research of lithium ion batteries, especially because of the high safety concerns in the application of these devices⁷⁷.

Metallic lithium anodes are of special interest because they have several advantages compared to graphitic electrodes used in commercially available batteries⁷⁸. This type of anodes has a very negative redox potential (viz., -3.03 V) combined with a very low atomic weight (6.94 g/mol) and large specific capacity (viz., 3.86 Ah/g)^{79,80}. The highest energy density of a battery can be achieved with an active metal anode, which has a low potential, and a high voltage red-ox cathode, therefore lithium is the first choice for such batteries⁸¹.

As cathode material we took a material which is normally used as an anode, lithium titanate $\text{Li}_4\text{Ti}_5\text{O}_{12}$. The lattice parameters of this material nearly do not change when lithium ions are inserted or extracted, although it displays high lithium ion mobility. It does not show the problem of the reactivity with the electrolyte, is very stable, has an excellent cycling reversibility and allows high charge rates. Additionally it has little irreversible capacity and the flat voltage plateaus.⁸² But the problem, when using it as an anode, is the high working potential of 1.55 V vs. Li^+/Li , which requires especially high potential positive electrodes (see footnote 81) and the electronic conductivity is not high.

Insertion of lithium ions into the spinel structure of $\text{Li}_4\text{Ti}_5\text{O}_{12}$ proceeds according to the following reaction⁸³:



As electrolyte a mixture of 1.2 M LiPF_6 ethylene carbonate/ethyl methyl carbonate (EC/EMC) were used. Mixtures of organic aprotic solvents, (mostly organic carbonates) with lithium salts are used as electrolyte solution, although these tend to have thermodynamic stabilities below the potential window in which the cells operate. Therefore, the electrolyte is oxidized/reduced at the corresponding electrode. This decomposition mainly, but not exclusively, takes part in the first

⁷⁷ Dedryvére, R.; Foix, D.; Franger, S.; Patoux, S.; Daniel, L.; Gonbeau, D.; *J Phys. Chem. C*, **2010** 113, 10999-11008

⁷⁸ Tarascon, J. M.; Armand, M.; *Nature (London)*; **2001**, 414, 359; Vincent, C.A.; *Solid State Ionics*; **2008**, 155, A806

⁷⁹ Winter, M.; Besenhard, J. O.; Spahr, M. E.; Novak, P.; *Adv. Mater.*, **1998**, 10 (10), 725-763

⁸⁰ Munichandraiah, N.; Scanlon, L. G.; Marsh, R. A.; *J Power Sources*; **1998**, 72, 203-210

⁸¹ Aurbach, D. *J. Power Sources*, **2000**, 89, 206-218

⁸² Prakash, A. S.; Manikandan, P.; Ramesha, K.; Sathiyar, M.; Tarascon, J.-M.; Shukla, A. K.; *Chem. Mater.*; **2010**, 22, 2857-2863

⁸³ Thackeray, M. M.; *J. Electrochem. Soc.* 142, 8, 2558-2563

Part B: Application as coating materials in batteries

charging cycle.⁸⁴ The decomposition products form a film on the electrodes surface which ideally, passivates the surface against further reactions, shows high lithium ion-, and no electronic conductivity. This film is called SEI (solid electrolyte interface)⁸⁵ and it is considered necessary for the correct working of the cell, when using aprotic organic media.⁸⁶ On the contrary Brummer⁸⁷ and Newmann proposed that the passivating film offers only limited cycle life for secondary batteries. In the case of alkali metals in non-aqueous systems, a competition between an SEI generated by redox chemistry of the metal with the electrolyte solution⁸⁸ and SEI formed by electrochemical decomposition of the electrolyte is always present during operation of the battery. The “redox” SEI is formed immediately when the metal gets in contact with the solution by thermodynamically favorable reactions. Regardless of the mechanism of formation (redox chemistry or electrochemistry), there is consensus among researchers that the SEI consists mostly of different inorganic lithium salts, and organic residues of electrolyte decomposition.

In spite of the several advantages of metallic lithium anodes described above, they are not commonly used in commercial rechargeable batteries due to safety and cycle life concerns associated with changes in the surface composition and morphology during prolonged battery cycling. Most of these changes are commonly associated with dendritic or mossy growth resulting from uneven surface current distributions during repeated stripping and plating of lithium, and the concomitant dissolution and re-growth of the SEI layer.¹⁴

Different ways to handle this problem are available:

- The usage of insertion electrodes instead of pure metal can avoid the problem because under normal operating conditions these materials do not exhibit dendritic growth. For example, materials such as spinel materials or intercalation compounds.⁸⁹ These materials however, have much lower specific capacities than lithium.
- The usage of polymer electrolytes instead of liquid ones. Here the limitation is the temperature because these materials can only be used at high temperatures above 80°C because of the low conductivity at room temperature.⁹⁰ This attempt also does not fully quench the generation of dendrites.
- Another approach is to use additives like fumed silica particles to immobilize the liquid electrolyte.⁹¹

⁸⁴ Schranzhofer, A.; Bugajski, J.; Santner, H. J et al.; *J Power Sources*; **2006**, 153, 391-395

⁸⁵ Peled, E.; *J. Electrochem. Soc.*; **1979**, 126, 2047

⁸⁶ Peled E. in Gabano, J. P.(Ed.), *Lithium Batteries*, Academic Press, London, 1983,p. 43

⁸⁷ Brummer, S. B. in: Yeager, E. G. et al. (Eds.) Proc. Workshop on Lithium Non-aqueous Battery, Electrochemistry, The Electrochemical Society, NY, Vol. 80-87, 1980, p 130; Newmann in the same Journal p. 143

⁸⁸ Peled, E. *J. Electrochem. Soc.*: ELECTROCHEMICAL SCIENCE AND TECHNOLOGY **1979**, 126,12

⁸⁹ See e.g. Orsini, F. et al. *J. Power Sources* **1999**, 81-82, 918

⁹⁰ See e.g Orsini, F. et al. *J. Power Sources* **1998**, 76, 19

⁹¹ Walls, H. J. et al *J. Power Sources*, **2000**, 89, 156; Zhou, J. Fedkiw, P. S.; Khan, S. A. *J. Electrochem. Soc.* **2002**, 149, A1121; Li, Y. X.; Fedkiw, P. S. Khan, S. A. *Electrochim Acta*, 2002, 47, 3853; Zhang, X.-W.; Li Y.; Khan, S. A.; Fedkiw, P. S. *J. Electrochem. Soc.* **2004**, 151, 8, A1257-A1263

Part B: Application as coating materials in batteries

- Functionalization of the lithium anode with different materials. In this sense, developing a more uniform and stable surface layer on metallic lithium electrodes might serve to alleviate or eliminate the safety issues related to surface changes, and to extend the life of rechargeable batteries made with this type of electrodes.

B 2 Experimental part

Used Chemicals: All chemicals were used as purchased without further purification. The electrolyte (1.2 M LiPF_6 in ethylene carbonate/ethyl methyl carbonate 30/70w%) was purchased from UBE Corporation. The coin cells were assembled from Hohsen 2032 cell hardware. Metallic lithium (FMC Lithium) was used as anode and as cathode $\text{Li}_4\text{Ti}_5\text{O}_{12}$ (84%), from Ishihara company with 8% PVDF KF 9130, 4% AB carbonate and 4% SF6-6 with a total thickness of 178 μm (7 mil), and a diameter of 9/16 inch on copper foil. The separator was a Celgard 2325 one with a diameter of 5/8 inch.

Impedance spectra were recorded using a Solatron Analytical Frequency Response Analyzer at constant potential with an AC amplitude of 10 mV, and between a frequency of 10000 Hz to 0.05 Hz. The 10 mV perturbation signal was supplied by a Solatron Analytical cell test system, software Multistat version 1.2c for windows 2000/XP/Vista.

The cells were cycled galvanostatically (Maccor Cycler, Series, 4000 with MACCOR Inc. software), between 1-2 V vs. Li/Li^+ .

The lithium anodes were coated with the different cyclopentadienyl iron (II) dicarbonyl-compounds (Fp-compound; Rp is the corresponding ruthenium compound) synthesized in Part A of this work. Therefore the electrode was dipped into a solution of the compound dissolved in EMC. The solution had always the same concentration (0.0127 g/mL) no matter which compound was used. The dipping time was measured exactly and it was the same for each compound. From each compound one electrode was dipped into the solution for 1, 5, 10, 15 and 30 min. After the dipping the electrodes were rinsed with some drops of EMC and dried in the atmosphere of the glovebox before using them in the coin cells.

The compounds were synthesized following the procedure explained in part A of this thesis.

The following compounds were used as coating materials for the lithium electrode and their behavior will be described:

FpSiPh_3
 FpSiMe_2H
 RpSiMe_3
 FpSiMe_3

The coins were all assembled following this order:

Can
Gasket
Spacer

Part B: Application as coating materials in batteries

Cathode

Electrolyte (LiPF₆ in EC/EMC 30:70)

2 Separators

Lithium anode

Spacer

Ring and

Cap

The cathodes were dried in a vacuum oven at 70°C in the glove box for at least two to three hours. All cells were assembled in the glove box.

The dependency on the dipping time and the ageing time was measured via impedance spectroscopy. Impedance was done after 1h, 2 h, 24 h, 48 h, and 168 h for each coin cell. The cycling behavior is also an important factor and it was measured for each coin cell 148 h after the assembling (300 cycles, 1.0-2.0V, at 4.0 mA, rest 15 seconds, charge to 0.0001 Ah). Afterwards the impedance spectra were recorded again.

B 3 Results and Discussion

In this work the effect on functionalizing lithium anodes with different coating generated from Fp-compounds was investigated. As described previously, metallic lithium electrodes were dipped in EMC solutions containing the different compounds. Due to its low redox potential the surface of metallic lithium is highly nucleophilic and reacts readily with a variety of organic compounds.

During the coating of the lithium no visible changes of the electrode occurred. There was no obvious reaction when the lithium got into contact with the solution of the compounds like bubbling or heat formation. Also for the samples after 30 min of dipping in most of the cases no color change on the surface took place. Only the triphenylated compounds, FpSiPh₃ and FpSnPh₃, showed a slight yellowish color on the surface of the lithium.

The dipping into the different compounds leads to two possible coatings.

Either it can just be a layer on the surface or the lithium reacts with the compound. Powder X-Ray diffraction of one surface showed that both silicon and iron are still available after the coating. It seems that the main phase is Li₃Si.

Lithium normally reacts as a strong nucleophile. This suggests that a reaction took place with the different compounds. Most probably the lithium reacts with the silicon atom in a kind of transmetallation.

After functionalization, the Li electrodes were rinsed with EMC and dried inside the glove box, and used to assemble coin cells as described above in the experimental section

The first thing to be investigated was the cycling behavior of the cell. With these measurements it should be shown if the cycling stability of the cell increases when coating the anode compared to pure lithium as electrode material.

The second important thing was the impedance behavior of the coin cells with the coated anodes in comparison to the pure lithium. Also it should be investigated if the ageing influences the stability of the surface coatings, which can be qualitatively determined from changes in the impedance spectra. Also the difference between the coating materials in their behavior should be investigated.

B 3.1 Cycling behavior

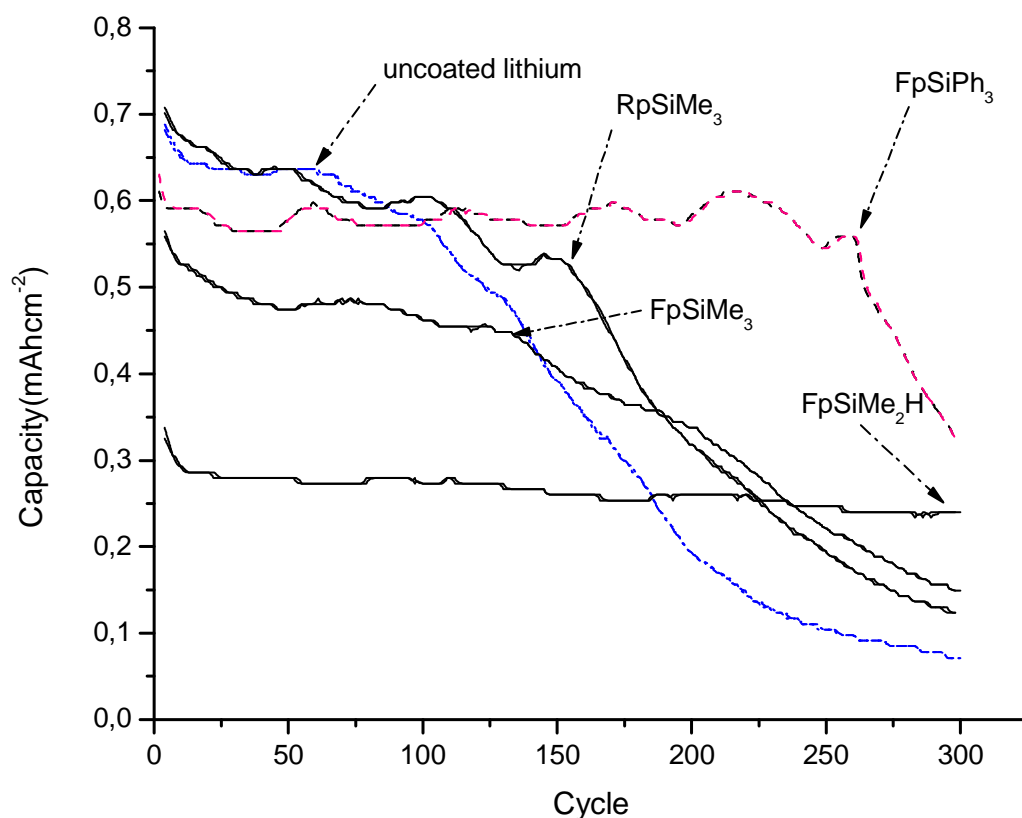


Figure 40: Cycling behavior of various coatings with a dipping time of 10 minutes.

Figure 40 shows the graph of the capacity (i.e. the amount of energy obtained from the cell) versus the cycle life for different FpSiR_3 respectively RpSiMe_3 -functionalized lithium electrodes, each with a dipping time of 10 minutes. As previously stated, all the components in our test cells have been chosen because of optimal performance under the conditions of study. Therefore, the electrochemical behavior of the cell can be directly correlated to the metallic lithium electrode, and/or the effect of the surface coating.

The point at which the slope each of the line changes in a more pronounced way is the point at which the cell starts failing, (i.e. delivering significantly less energy than during the first few cycles.) This point is indicated with the dashed arrows in Figure 40, (from now on I will call this point “failure point”.) From this figure we can see that under this cycling conditions (room temperature, and cycling current of 2.6 mAcm^{-2} , with a rest period of 15 seconds between cycles), the failure point for the uncoated lithium electrode is around 55 cycles.

It can be seen that coating the sample increases the cycle life as the failure point shifts to higher cycle numbers: uncoated lithium (~65 cycles), FpSiMe_3 (~130 cycles), RpSiMe_3 (~155 cycles), FpSiPh_3 (~260 cycles), while FpSiMe_2H did not show a failure point.

Part B: Application as coating materials in batteries

The coatings that significantly extended the cycle life of the lithium electrode were the ones obtained from FpSiPh_3 and FpSiMe_2H . However, the FpSiMe_2H showed less than half the average useful capacity of the original lithium electrode (0.28 mAhcm^{-2} vs 0.65 mAhcm^{-2} , respectively). Therefore, even the longer cycling stability is not useful.

On the other hand the electrode treated with RpSiPh_3 showed an average capacity of approximately 0.60 mAhcm^{-2} , (i.e. 92% of capacity when compared to uncoated lithium), with four times the cycle life (a 400% increase). These encouraging results motivated a further study of this type of coating.

Another important thing to mention is that the big changes in capacities for the different coating materials may be due to coating thickness.

The next figure shows a comparison between the different coating/dipping times for the FpSiPh_3 in their cycling behavior. The best performance is achieved for the coating after 10 min in the solution. All the other dipping times do not show significantly better results compared to the uncoated lithium as anode.

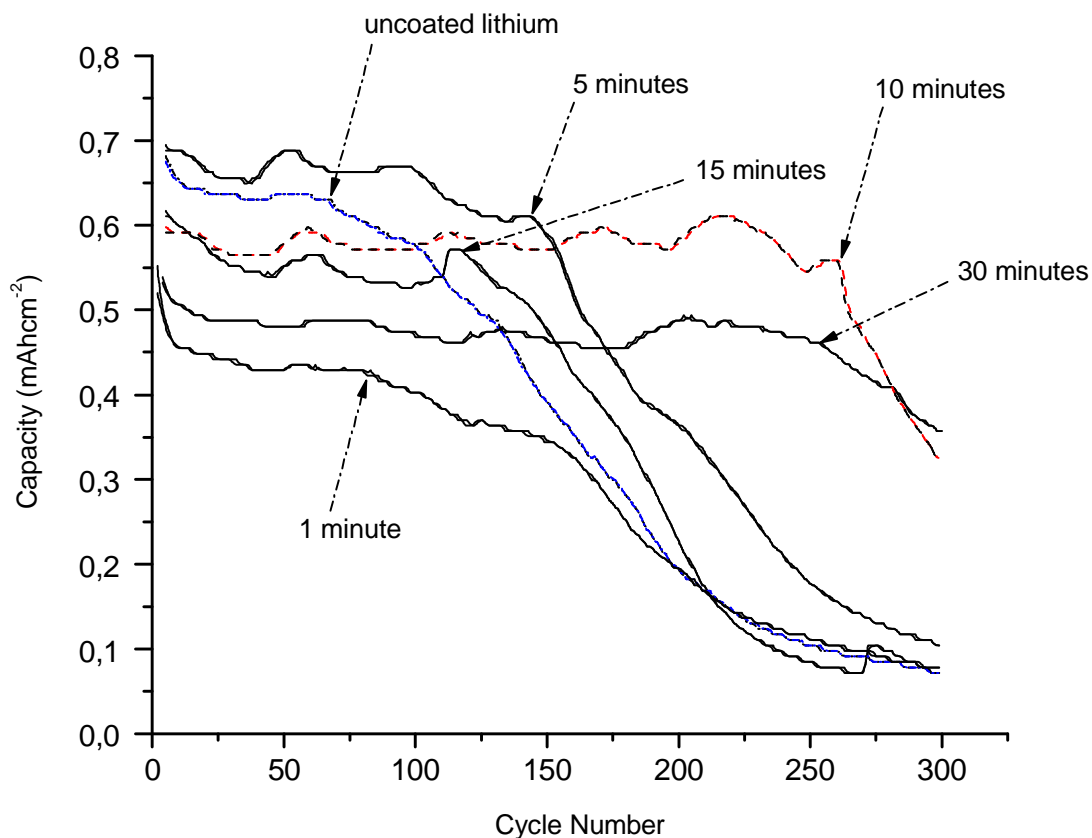


Figure 4: Cycle life of Ph_3SiFp coatings with different dipping times compared to the uncoated lithium.

The figure shows the cycling behavior of the cells containing electrodes coated with FpSiPh_3 . The comparison between the different dipping times is shown for the following samples: FpSiPh_3 after 1, 5, 10, 15 and 30 min in the solution.

Part B: Application as coating materials in batteries

Comparing the samples to uncoated lithium the capacity retention is important. Uncoated lithium has a strong decrease of capacity after around 65 cycles. At this number the failure point takes place and the slope changes. After that the capacity starts to decrease. For the other samples this point is at higher cycle numbers. The best result was obtained for the coating after 10 min. In this case the failure point is at around 260 cycles. For the others this point is at: 75 cycles for the sample dipped in the solution for one minute, around 150 for the one coated for 5 min, 120 for the functionalization after 15 minutes and also around 255 cycles for the one after 30 min. This means that the coating of the electrode has a positive influence on the cycling stability. For all functionalized electrodes the capacity retention takes place later than for the uncoated lithium.

Concerning the start capacity the sample after one minute of functionalization shows the lowest starting value. Its capacity is just 0.55 mAhcm^{-2} and even decreases after around ten cycles to 0.45 mAhcm^{-2} . This sample does not follow the general trend, because for all the other samples the starting capacity decreases by the duration of dipping. The highest one has the sample after 5 min (0.7 mAhcm^{-2}), then the one after ten (0.6 mAhcm^{-2}), followed by 15 (0.62 mAhcm^{-2}) but it decreases in the first 50 cycles to an average of around 0.58 mAhcm^{-2}) and 30 minutes (0.55 mAhcm^{-2}).

This means that the starting capacity is decreasing with the duration of the functionalization. A possible explanation for that could be that the longer reaction time leads to the formation of thicker films on the surface of the electrodes. Therefore it is possible that the surface is somehow blocked for the passing of lithium ions through this film.

B 4 Impedance measurements

An important thing to investigate was the impedance behavior of the different coatings. With these spectra various aspects of the coatings can be investigated.

For example, the stability of the coating towards immersion in electrolyte (important for the shelf life of the cell) and towards cycling, and also information that can help understand how the electrical properties of the coatings determine the electrochemical performance observed during cycling.

B 4.1 Definition^{92,93}:

The impedance is the ac equivalent to the dc electrical resistance; therefore the impedance describes the ability of an ac circuit to impede the flow of electrons.

In the dc (direct current) theory the electrical resistance is defined by the well known Ohm's law:

$$R = \frac{E}{I} \quad (14)$$

R ... electrical resistance [Ohm = Ω]

E ... potential [V]

I ... current [A]

This equation can only be applied for the one circuit element, which interferes with the electron flow in a dc circuit: the ideal resistor, which has the following properties:

- The Ohm's law is fulfilled for all current and voltage levels.
- The resistance is not dependent on the frequency.
- The current and the voltage are in phase.

The same equation can be expressed in the ac (alternation current - the current changes its polarization periodically; the frequency is not zero) theory:

$$Z = \frac{E}{I} \quad (15)$$

⁹² Application Note – Gamry Instruments (734 Louis Drive Warminster, PA 18974 USA)

⁹³ Princeton Applied Research – Basics of Electrochemical Impedance Spectroscopy – Application Note AC-1

Part B: Application as coating materials in batteries

Z ... impedance [Ohm = Ω]

E ... potential [V]

I ... current [A]

In this equation Z stands for the impedance measured in Ohms. Compared to the resistance, the impedance is not limited by the restrictions written above. This means that there are more circuit elements for which this equation can be applied: the resistor, the capacitor and the inductor.

These three circuit elements have different influence on the impedance. Capacitors and inductors affect both the magnitude of an alternating current and also the phase between the two waves, which is the time dependency.

In this treatment the current can be expressed as a vector with x, y coordinates in polar form or as a complex number with a real and an imaginary part:

$$I_{total} = I_{real} + jI_{imag} \quad (17)$$

with $j = \sqrt{-1}$

I_{total} ... total current [A]

I_{real} ... real current component [A]

I_{imag} ... imaginary current component [A]

Using a reference waveform (in phase with the real waveform and 90° out of phase with the imaginary waveform) allows to manipulate the vector for current and voltage as vectors with respect to the same coordinates. This means when the voltage is also expressed as a vector, then the impedance can be written as:

$$Z_{total} = \frac{E_{real} + j E_{imag}}{I_{real} + jI_{imag}} \quad (18)$$

Z_{total} ... total impedance [Ohm]

E_{total} ... total voltage [V]

E_{real} ... real voltage component [V]

E_{imag} ... imaginary voltage component [V]

I_{total} ... total current [A]

I_{real} ... real current component [A]

I_{imag} ... imaginary current component [A]

Therefore, the vector expression for the impedance is:

Part B: Application as coating materials in batteries

$$Z_{total} = Z_{real} + jZ_{imag} \quad (19)$$

Z_{total} ... total impedance [Ohm]

Z_{real} ... real impedance component [Ohm]

Z_{imag} ... imaginary impedance component [Ohm]

And the absolute magnitude for the impedance is:

$$|Z| = \sqrt{Z_{real}^2 + Z_{imag}^2} \quad (20)$$

Z_{total} ... total impedance [Ohm]

Z_{real} ... real impedance component [Ohm]

Z_{imag} ... imaginary impedance component [Ohm]

The phase angel can be defined as:

$$\tan \Theta = \frac{Z_{imag}}{Z_{real}} \quad (21)$$

Θ ... phase angel ($^{\circ}$)

Z_{real} ... real impedance component [Ohm]

Z_{imag} ... imaginary impedance component [Ohm]

The measured impedance spectrum is mostly analyzed via fitting of the spectrum by using electrical circuit elements. These are: resistor, inductor and capacitor. The resistor has no imaginary component and therefore the impedance is equal to the resistance. This means that current and voltage are in phase. Resistive components originate from the current collectors, the bulk of the electrode material, the electrolyte, electron transfer at the electrode/electrolyte interface etc.⁹⁴. Like the capacitor the inductor is also frequency dependent and so their impedance is not equal to the resistance, because they have an imaginary component. The inductive component in a cell is due to the porosity of the electrode.

The impedance of an inductor is:

$$Z = j\omega L \quad (22)$$

with $j = \sqrt{-1}$ and $\omega = 2\pi f$

⁹⁴ Rodriques, S.; Munichandraiah, N.; Shukla, A. K.; *J. Power Sources*, **2000**, 87, 12-20

Part B: Application as coating materials in batteries

Z ... impedance [Ohm]

L ... self-inductance [H]

f ... frequency [Hz]

For the capacitor (capacitive compounds are due to the double layer) the following equation is valid:

$$Z = \frac{1}{\omega C} \quad (23)$$

with $\omega=2\pi f$

Z ... impedance [Ohm]

C ... capacity [F]

f ... frequency [Hz]

A resistance is said to be capacitive, when most of its opposition comes from the capacitive parts, which means that the current is leading the voltage in phase. When it is the other way around it is said to be inductive.

Electrochemical systems nearly always can be represented as consisting of more than one circuit element. They can either be in series (than the total impedance is the sum of the single ones added together) or parallel (than the reciprocal values of the impedances added up give the total impedance).

A typical example for that is the so called simplified Randles cell:

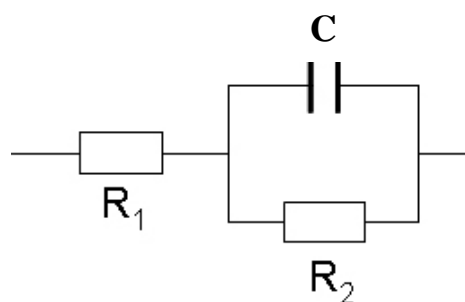


Figure 41: Randles cell

In this picture R_1 represents the solution resistance (an uncompensated resistance), R_2 represents polarization resistance and the capacity C represents double layer capacitance at an electrochemically active interphase.

One of the most used formats for data presentation is the so called Nyquist plot. In which the imaginary component of the impedance is plotted vs. the real component. For the Randles cell shown above this leads to a graph like that shown on Figure 42.

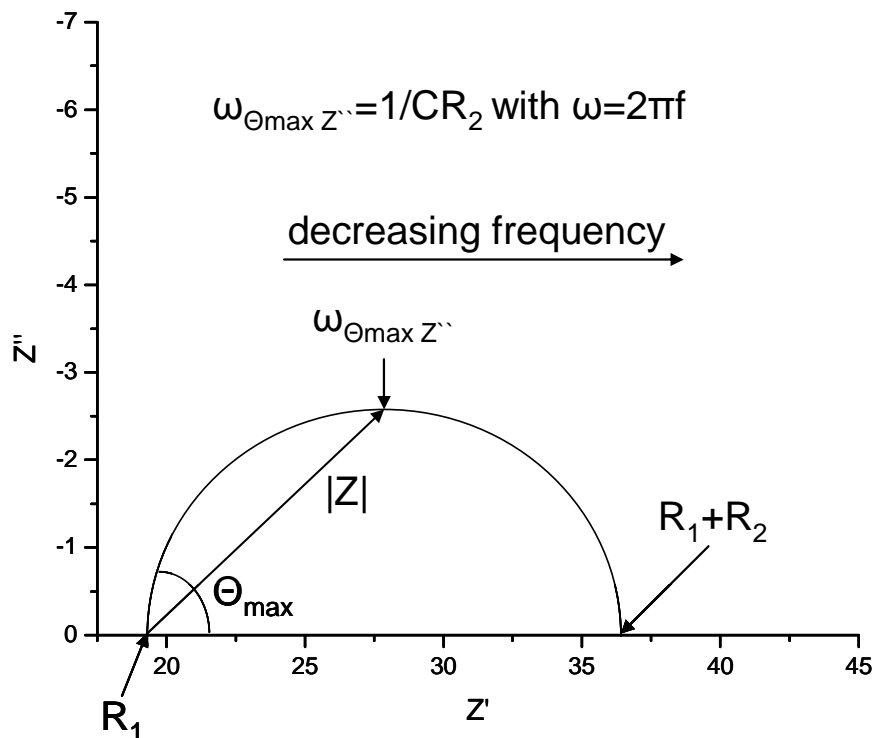


Figure 42: Nyquist plot of a Randles cell

Several important features of the Nyquist plot are highlighted in Figure 42, and wealth of qualitative and quantitative information can be obtained from analysis of these features. The general impedance of the cell (i.e. the sum of the impedance of all components in the cell, e.g. current collectors, separators, electrolyte, etc.) can be evaluated from the point (R_1) at which the highest frequency arch in the spectra intersects the real axis. The low frequency point $R_1 + R_2$ usually connects the arch (or arches) that arise as response for interfacial electron transfer to the Warburg tail, which correspond to diffusion processes, and thus provide useful kinetic information about the processes happening in the cell. Additionally, the impedance of interfacial processes can be judged from the point $\omega_{\Theta_{max} Z''}$ ($Z'' = Z_{img}$).

Another important way to present the data is the Bode plot (not shown). This is the combination of the absolute impedance $|Z|$ and the phase shift Θ vs. the frequency. With this plot the frequency dependence can be easily determined.

Part B: Application as coating materials in batteries

In general, it can be said that according to the different time constants, mass transport effects influence the graph more at lower frequencies whereas charge transfer kinetics and double layer effects have more influence on the higher frequencies⁹⁵.

In a Nyquist plot, diffusive mass transport effects appear as the so-called Warburg element. The equation for the ‘infinite’ Warburg impedance (infinite thickness of the diffusion layer, reversible system under pure diffusion control) is given by:

$$Z_w = \frac{s\sqrt{2}}{\sqrt{\omega}} \quad (24)$$

with $\omega=2\pi f$

Z_w ... Warburg impedance [Ohm]

s ... Warburg coefficient

f ... frequency [Hz]

The Warburg impedance depends on the perturbation frequency. For high frequencies Z_w is small because the diffusing molecules do not have to move long distances. The opposite is the case for low frequencies and therefore the Warburg impedance is high for lower frequencies. In the Nyquist plot it appears as a straight line with a slope of 45°.

The value of the Warburg coefficient can be obtained out of the Warburg plot. This is the real component of the impedance vs. $1/\sqrt{\omega}$.

B 4.2 Application

Impedance spectroscopy can be used for many different applications shown in the table below.⁹⁶ Further advantages concerning the application in batteries are taken from the Solartron analytical technical report⁹⁷.

Research Area	Application
Corrosion	<ul style="list-style-type: none">• Rate determinations• Inhibitor and coatings• Passive layer investigations
Coatings Evaluation	<ul style="list-style-type: none">• Dielectric measurements• Corrosion protection

⁹⁵ Orazem, M. E.; Agarwal, P.; Garcia-Rubio, L. H.; *J. Electroanalytical Chem.*, **1994**, 378, 51-62

⁹⁶ Application Note – Gamry Instruments (734 Louis Drive Warminster, PA 18974 USA)

⁹⁷ Solartron analytical, Electrochemical Impedance Spectroscopy for Battery Research and Development, Technical Report 31, 1996 (Victoria Road, Farnborough)

Research Area	Application
Batteries	<ul style="list-style-type: none">• State-of-charge• Materials selection• Electrode design• Reaction mechanism• Change of active surface area during operation• Separator evaluation• Passivating film behavior• Separation and comparison of each electrodes kinetics• Electrode corrosion
Electrodeposition	<ul style="list-style-type: none">• Bath formulation• Surface pretreatment• Deposition mechanism• Deposit characterization
Electro-Organic Syntheses	<ul style="list-style-type: none">• Adsorption/Desorption• Reaction mechanism
Semiconductors	<ul style="list-style-type: none">• Photovoltaic work• Dopant distributions

With EIS the electrochemical and electrical properties of interfaces can be tested. It allows the monitoring of changes in the surface of e.g. electrodes or coatings.

In our case we used EIS to see if the electrodes surface had different electrical and electrochemical properties after the functionalization of the pure lithium with Fp-compounds. It also allowed us to see if the coating changes during the ageing of the cell and after cycling.

The problem concerning impedance measurements is not the measurement of the spectrum itself but the data analysis. Suitable models based on the physical and chemical background have to be found and applied and data and error analysis has to be done⁹⁸.

⁹⁸ Orazem, M. E.; Agarwal, P.; Garcia-Rubio, L. H.; *J. Electroanalytical Chem.*, **1994**, 378, 51-62; Orazem, M. E.; Tribollet, B.; *Electrochimica Acta*, **2008**, 53, 7360-7366

B 4.2.1 Influence of the different coating compounds

In the following figure the difference between the impedance behavior of the different compounds, with which the electrodes were coated, is shown. All the coatings were made by dipping the electrodes in the solution for ten minutes. The spectra were recorded after 168 h respectively 200 h of ageing of the cell.

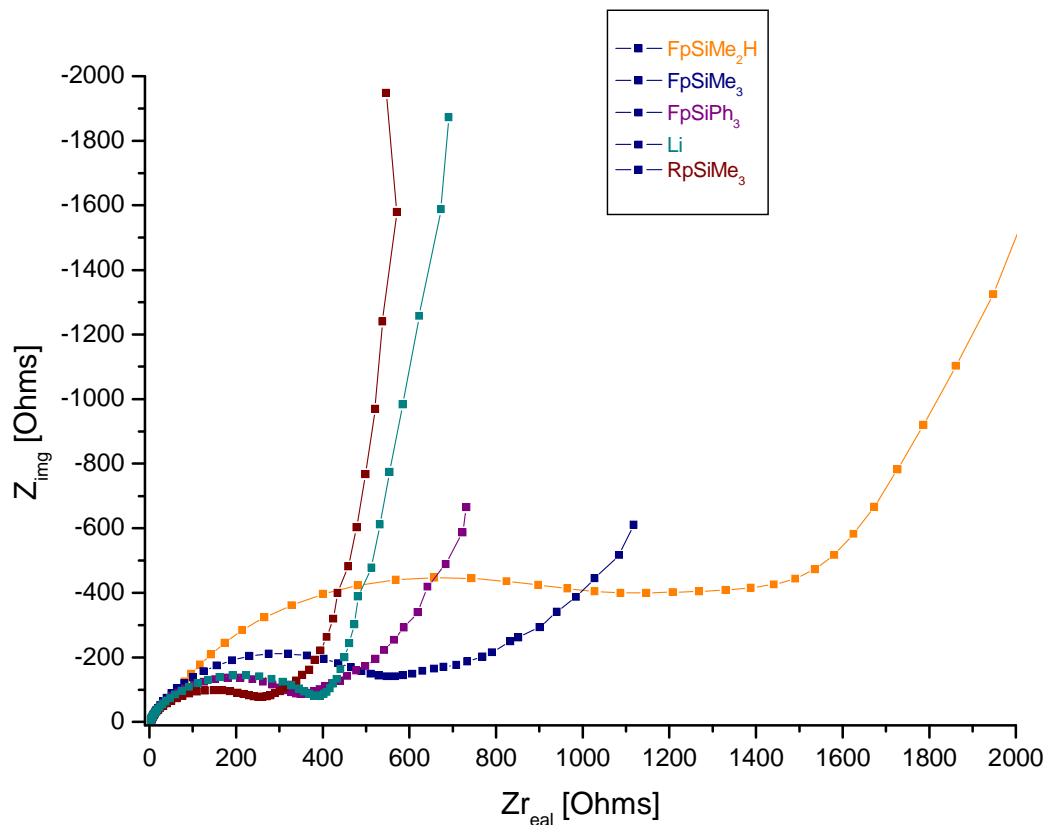


Figure 5: Comparison between the different coating compounds after 10 minutes of dipping. The impedance spectrum was measured after 168 h for the Fp-compounds respectively 200 h for lithium of ageing.

Part B: Application as coating materials in batteries

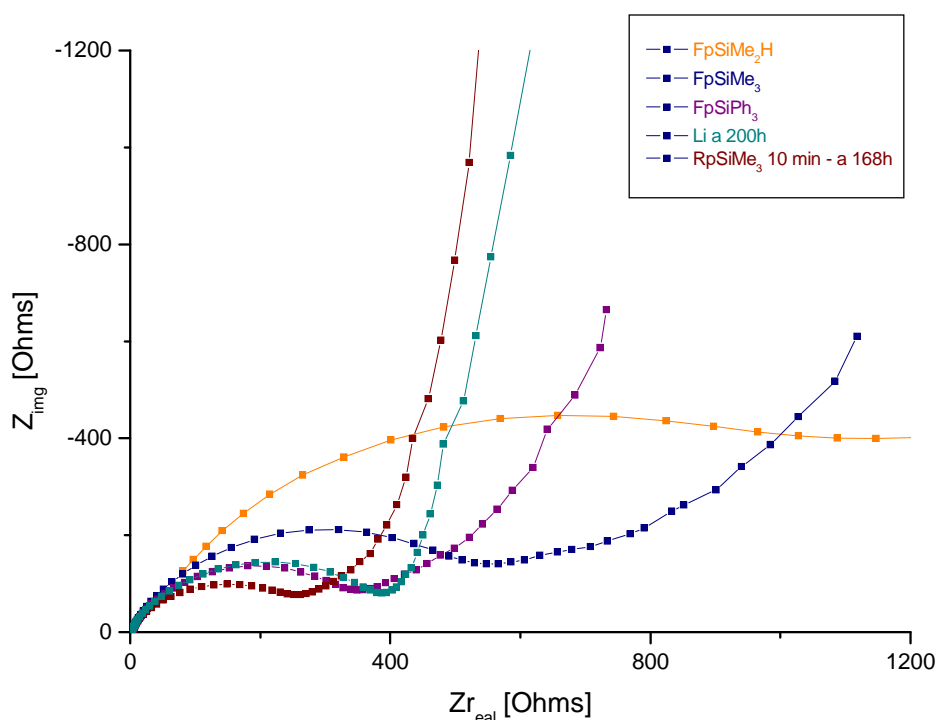


Figure 43: Zoom into the Figure shown before

It seems that after 168 h respectively 200 h there is no general trend which shows the influence of the size of the substituents. The highest impedance shows the compound FpSiMe_2H , the one molecule with the smallest rests on the silicon, as can be seen by the higher magnitude of the high frequency arch in the impedance spectrum.

This offers some explanation of the cycling behavior of the electrode containing this coating; the significantly lower cell capacity can be attributed to the high impedance of the coating, and the extension of the cycle life is not a result of protection but of slower interfacial kinetics for the coated electrode.

It can also be seen that the ruthenium compound has a lower impedance than the corresponding iron compound, which also explains why the ruthenium compound has similar average capacity to uncoated lithium, while the corresponding iron compound has only about 75% of the average useful capacity of the uncoated lithium (Figure 40).

The FpSiPh_3 coating, which significantly extended the cycle life of the battery, shows slightly less impedance than the uncoated lithium electrode, as evidenced by the high frequency arches in both spectra. The most notable difference is in the length of the Warburg tail, which is shorter for the FpSiPh_3 -coated electrode, which indicates an enhancement in mass transport in the cell. This is possibly due to dissolution of ionic species into the electrolyte, making it more conductive.

B 4.2.2 Dependency on dipping time

Figure 44 shows the impedance spectra for the FpSiPh_3 -coated samples with different dipping times. The duration of functionalization does not seem to have a strong influence in the interfacial charge transfer, in most cases, but on the magnitude of the high frequency arch.

Only in the case of the 1 minute dipping time there is a dramatic increase in impedance, which is consistent with the low cycling capacity shown by the cells made with this electrode (Figure 43). This result suggests that there may be a difference in the chemical composition of the coating done for the shorter time which results in a more insulating interphase.

The most significant aspect in the other coatings is in the length of the Warburg tail which has length order from shortest to longest: 15 min dip < 10 min < 5 min < 30 min < uncoated electrode < 1 min. Although there is no general trend for all the dipping times that can be directly correlated to the cycling performance, there are a few valid comparisons that can be made.

The coatings generated by 30 minutes dipping and 10 minutes both show failure points around 260 cycles, however the 30 minute coating shows significantly less useful capacity.

When comparing the length of the Warburg tail of uncoated lithium, 30 minute coating, and 10 minute coating it can be seen that this tail is significantly shorter in the 10 minute-coated sample, which again indicates the effect of enhanced mass transport in cells containing this coating.

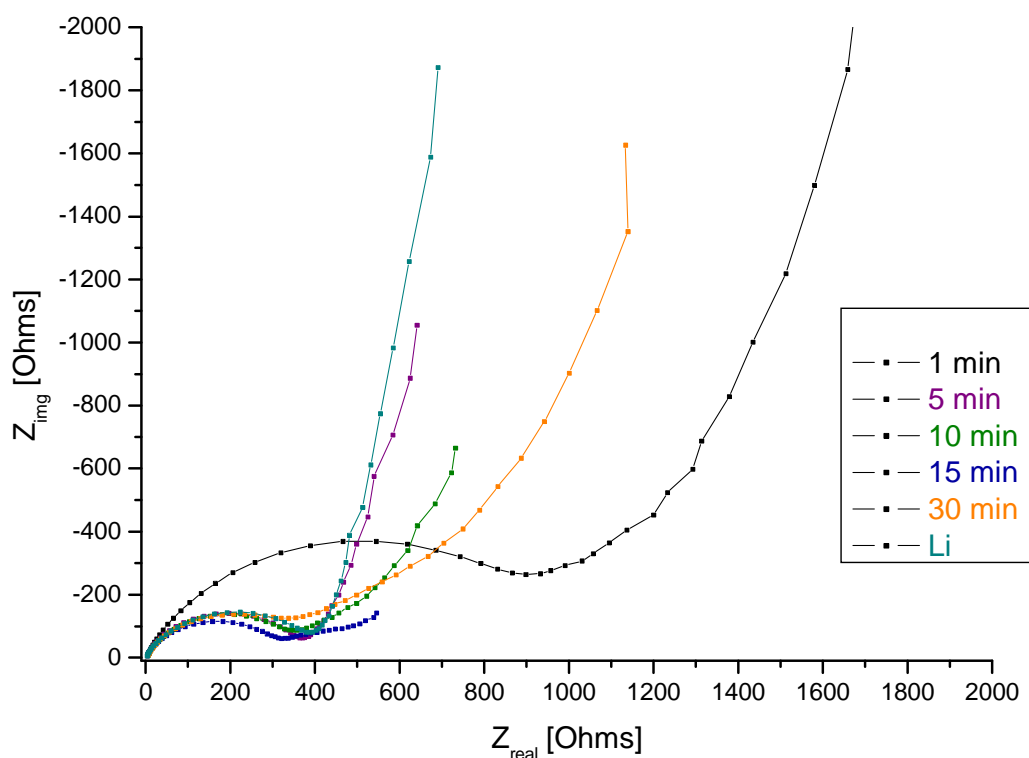


Figure 44: Impedance for FpSiPh_3 after different dipping times at an ageing duration of 168 h respectively 200 h for lithium and the sample after 30 min of dipping

The highest impedance was measured for the sample after 1 min dipping after an ageing duration of 168h. All the other samples have nearly the same impedance but they differ again in the slope of the Warburg impedance.

B 4.2.3 Dependency on Ageing Time

The impedance behavior depending on the ageing time is for all different coating samples nearly the same. In general it can be said that the impedance part influenced by mass transfer at lower frequencies is getting bigger by the time. The part caused by the Warburg impedance, which is due to diffusion controlled reactions,⁹⁹ decreases slightly by the ageing.

As an example the ageing for the coating compound FpSiPh_3 after 10 min dipping in the solution is shown.

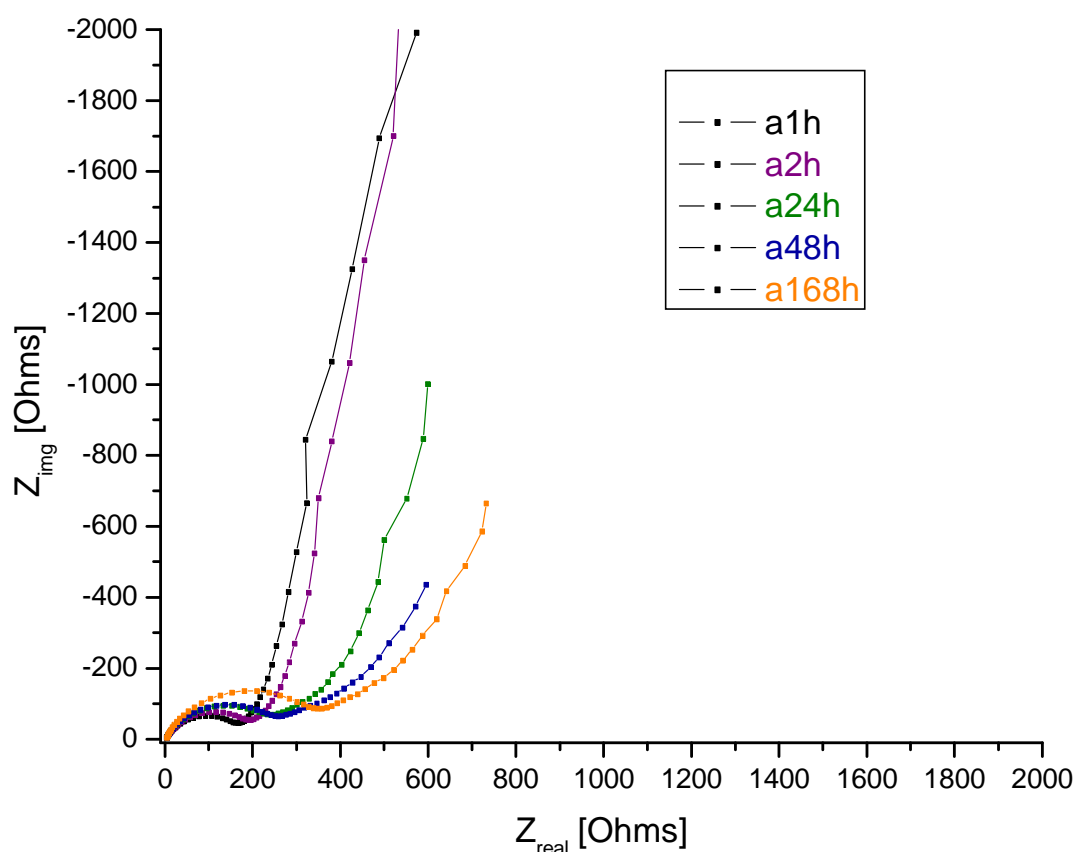


Figure 45: Dependency on the ageing time after 1, 2, 24, 48, 168 h of storage for the coin cell with the FpSiPh_3 coated anode after 10 min of dipping

⁹⁹ Orazem, M. E.; Agarwal, P.; Garcia-Rubio, L. H. *J. Electroanalytical Chem.* **1994**, 378, 51-62

Part B: Application as coating materials in batteries

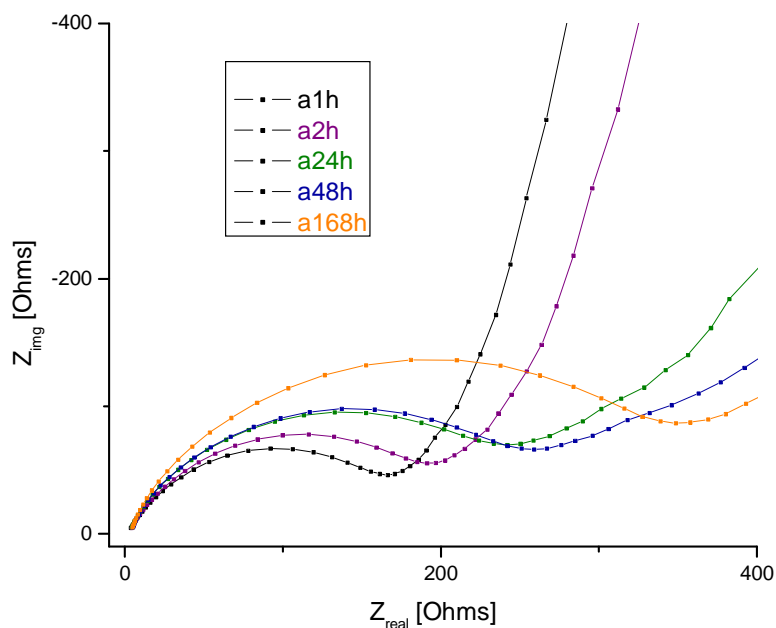


Figure 46: Zoom into Figure 45

It is obvious, that the surface gets more resistive by the time. This means the cell is not highly stable during storage.

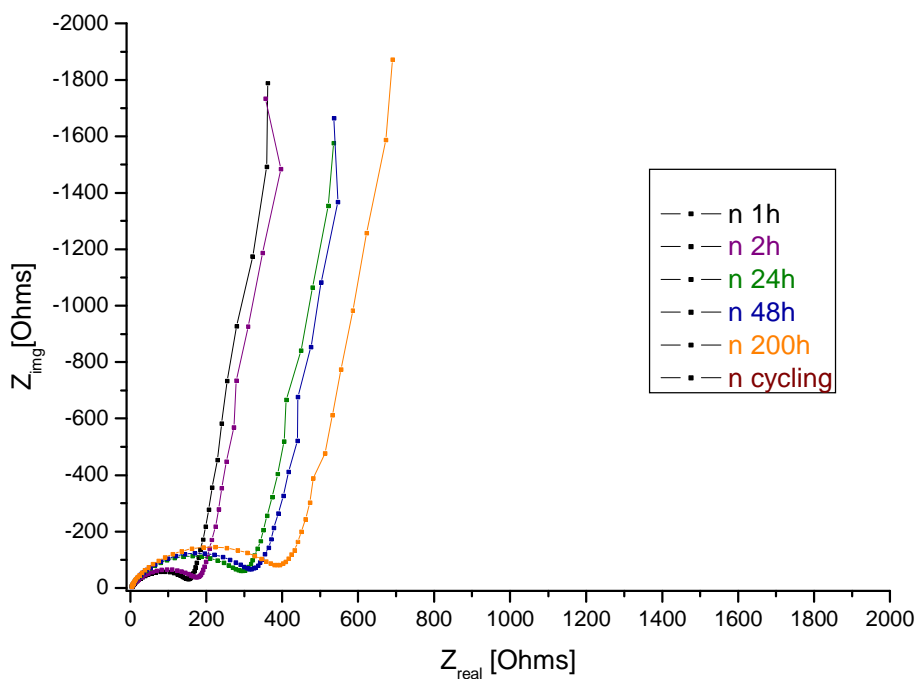


Figure 47: Ageing behavior of pure lithium as electrode material after 1, 2, 24, 48, 200 h and after cycling

Part B: Application as coating materials in batteries

It can be seen that the lithium coin cell also ages and is not stable during the time, when the material was measured. The difference to the coated electrodes is that here the slope of the Warburg impedance seems to stay the same.

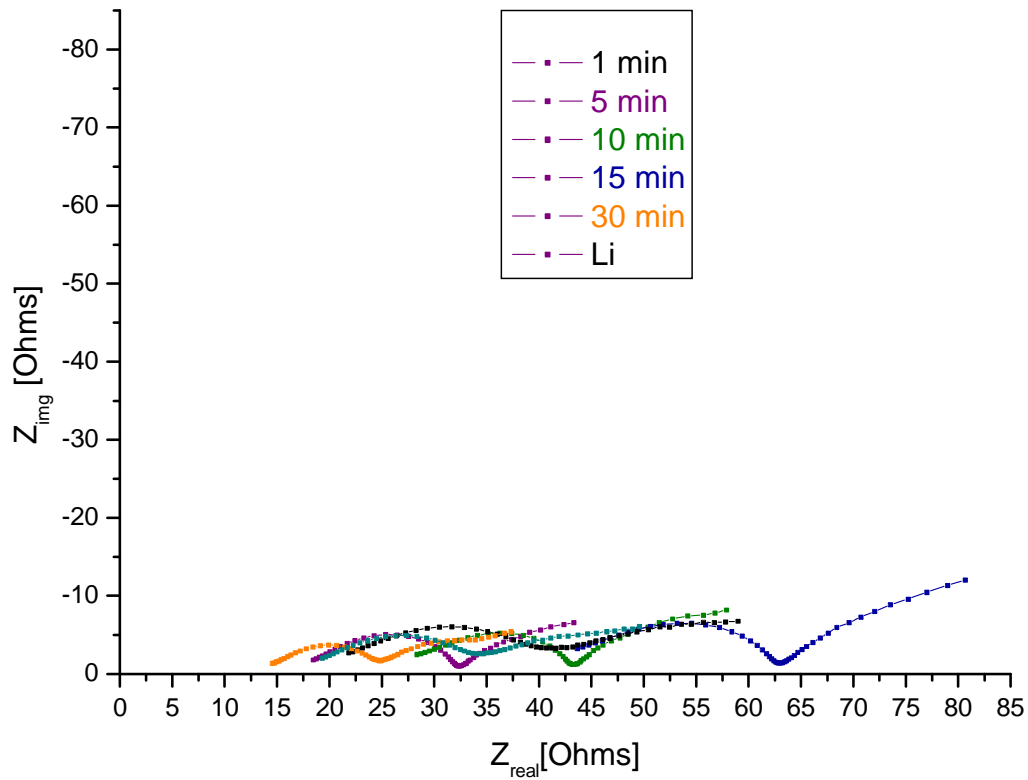


Figure 48: Impedance after cycling for all the FpPh_3Si samples (different dipping times) and pure lithium

Part B: Application as coating materials in batteries

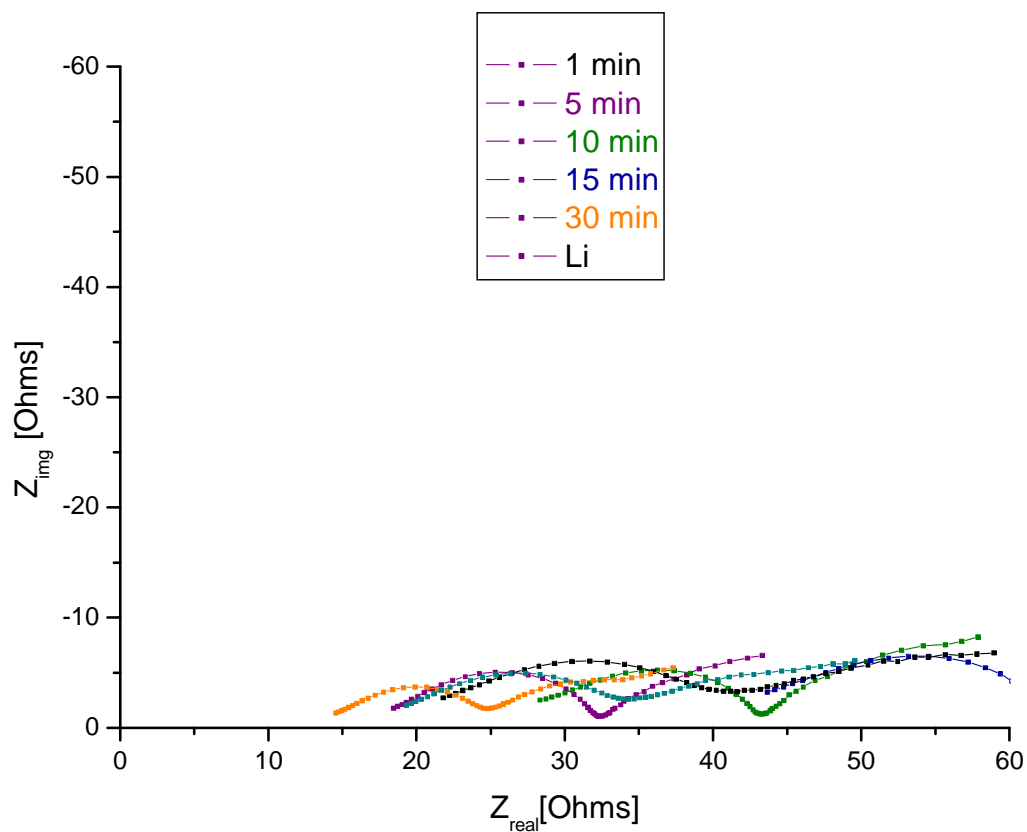


Figure 49: Zoom into Figure 48

The impedance after cycling is significantly lower than all the others before cycling. This could be explained by the bigger surface of the electrode.

No general dependency on the dipping time can be found.

All the other data for the other compounds can be found in the appendix – Part C 3.

B 4.3 Conclusion

We have discussed the effect of coating with cyclopentadienyl iron dicarbonyl compounds on the electrochemical behavior of metallic lithium electrodes. It was shown that the triphenylsilyl coating provides a significant enhancement in the cycle life of this type of electrodes with little loss of useful capacity.

The electrochemical properties of the coatings were investigated by Electrochemical Impedance Spectroscopy (EIS) and it was found that: The surface of the electrodes is becoming more resistive with time (ageing). This indicates that it is not stable during storage and more investigations are necessary to find out, what exactly happens during coating. An optimization of this kind of coatings has still to be performed.

The impedance results show that the coatings have an influence on the surface because the Warburg impedance changes compared to pure lithium.

Nevertheless it could be shown that FpSiPh_3 as coating material nearly doubles the life of the battery. This is a really interesting result that justifies further investigations on this topic. Furthermore, we have demonstrated that the cyclopentadienyl iron dicarbonyl substituted compounds are not only fundamentally interesting, but can be useful in improving current technologies for electrochemical energy storage.

Abbreviations

Cp	...	cyclopentadienyl
DME	...	1,2 dimethoxy ethane
Fp	...	cyclopentadienyl iron dicarbonyl
Fp ₂	...	cyclopentadienyl iron (II) dicarbonyl dimer
GC-MS	...	gas chromatography with coupled mass spectrometer
IR	...	infrared
MW	...	molecular weight
NMR	...	nuclear magnetic resonance
Rp	...	cyclopentadienyl ruthenium dicarbonyl
Rp ₂	...	cyclopentadienyl ruthenium dicarbonyl dimer
THF	...	tetrahydrofuran
m	...	mass [g]
M	...	molar mass [g/mol]
V	...	volume [mL]
ρ	...	density [g/mL]
n	...	amount of substance [mmol]